Avian Influenza Epidemic Recurrence and Approximate Stochastic Models

by

May Anne Estrera Mata

B.Sc., University of the Philippines Mindanao, 2007
M.Sc., University of Washington, 2011

A THESIS SUBMITTED IN PARTIAL FULFILLMENT OF
THE REQUIREMENTS FOR THE DEGREE OF

DOCTOR OF PHILOSOPHY

in

THE COLLEGE OF GRADUATE STUDIES

(Interdisciplinary Studies)

THE UNIVERSITY OF BRITISH COLUMBIA

(Okanagan)

April 2017

Thesis Committee

The undersigned certify that they have read, and recommend to the College of Graduate Studies for acceptance, a thesis entitled: Avian Influenza Epidemic Recurrence and Approximate Stochastic Models submitted by May Anne Estrera Mata in partial fulfilment of the requirements of the degree of Doctor of Philosophy

Rebecca C. Tyson, Unit 5 (Mathematics), The University of British Columbia
Supervisor, Associate Professor

Priscilla E. Greenwood, Department of Mathematics, The University of British Columbia
Co-supervisor, Professor Emeritus

Robert G. Lalonde, Unit 2 (Biology), The University of British Columbia
Supervisory Committee Member, Associate Professor

David B. Jack, Unit 3 (Chemistry), The University of British Columbia
University Examiner, Associate Professor

Sebastian J. Schreiber, Department of Evolution and Ecology, University of California
External Examiner, Professor

April 24, 2017
(Date Submitted to Grad Studies)

Abstract

This thesis is mainly concerned with avian flu epidemic recurrence, its current paradigm, and further mathematical research. Generally, this thesis aims to characterise the recurrent pattern of epidemics simulated by stochastic avian flu models using mathematical techniques. Of particular interest here are the stochastic fluctuations observed in recurrent epidemics. This thesis has two main parts.

The first part presents a thorough analysis of a simple stochastic avian flu model to provide insight into the role of different transmission routes in its recurrent dynamics. Recent modelling work on avian influenza in wild bird population takes into account demographic stochasticity and highlights the importance of environmental transmission in determining the outbreak periodicity, but only for a weak between-host transmission rates. A new analytic approach is used here to determine the relative contribution of environmental and direct transmission routes to the features of recurrent epidemics. Using an approximation method to describe noise-sustained oscillations, the recurrent epidemics simulated by the stochastic model is identified to be governed by the product of rotation and a slow-varying standard mean-reverting stochastic process, in a limiting sense. By analytically computing the intrinsic frequency and theoretical power spectral density, it can be shown that the outbreak periodicity can be explained by both types of transmission, and even by either one in the absence of the other.

The final part of this thesis presents a novel approach to understanding the role of parametric (e.g. seasonal) forcing and stochasticity in the stochastic fluctuations around a cyclic solution. An approximate description about these stochastic fluctuations is developed, which paves the way for a new mathematical tool to be used for analysing oscillations generated from the interactions of non-linear terms and stochasticity. The theory developed here is used to explore a stochastic avian flu model with seasonally forced environmental transmission which may be applicable to other stochastic system with seasonal forcing.

This thesis highlights the importance of approximation theory to analyse complex stochastic systems such as avian flu epidemic recurrence.

Preface

i The author of this thesis owns certain copyright or related rights in it (the Copyright) and she has given The University of British Columbia Okanagan certain rights to use such Copyright, including for administrative purposes.

ii The main content of this thesis manuscript is an original, unpublished, and independent work of the author.

iii Chapter 2 is written with the help of different review papers on avian influenza that the author of this thesis collected, synthesised, and summarised.

iv Article versions of Chapter 3 and 4 are prepared for submission to ISI-indexed (or Scopus-indexed) journals.

Table of Contents

Thesis Committee . . . . . **ii**

Abstract . . . . . **iii**

Preface . . . . . **iv**

Table of Contents . . . . . **v**

List of Tables . . . . . **viii**

List of Figures . . . . . **ix**

Acknowledgements . . . . . **xiii**

Dedication . . . . . **xv**

Chapter 1: Introduction **1**
1.1 Epidemic recurrence 2
1.2 Modelling epidemic recurrence 4
1.2.1 Damped oscillations 4
1.2.2 Noise-sustained oscillations 5
1.2.3 Parametric forcing: Forced limit cycle 6
1.2.4 Parametric forcing with noise 7
1.3 Mathematical theories and methodology used in this thesis . 9
1.4 Thesis structure and contribution 10

Chapter 2: The Epidemiology, Ecology, And Epidemic Recurrence Of Avian Influenza: An Overview **12**
2.1 Avian influenza (AI) 12
2.2 Avian influenza virus (AIV) 12

2.3 AIV ecology in wild birds 13
2.4 Transmission of AIVs to and between birds 14
2.5 AI epidemic recurrence 15
2.5.1 LPAI outbreaks 15
2.5.2 HPAI outbreaks 17
2.5.3 Modelling efforts 18
2.6 Discussion 19

Chapter 3: The Role Of Direct and Environmental Transmission In Stochastic Avian Flu Epidemic Recurrence 21
3.1 Background 21
3.2 The stochastic avian influenza model 23
3.2.1 Model description 23
3.2.2 Parameter values 28
3.2.3 Preliminary analysis of the model 30
3.3 Analytic methods 33
3.3.1 Approximate solutions 33
3.3.2 Power spectral density 34
3.3.3 The intrinsic frequency and the decay rate of the deterministic dynamics 34
3.3.4 Numerical tools and functions 35
3.4 Results 35
3.4.1 An approximate avian flu epidemic process 35
3.4.2 The relative contribution of the different transmission routes 39
3.5 Discussion 46

Chapter 4: Sustained Oscillations in Stochastic Models With Periodic Parametric Forcing 49
4.1 Motivation 49
4.2 A periodically parametrically forced (PPF) Markov model . . 52
4.2.1 Description 52
4.2.2 Stochastic fluctuations around the limit cycle solution 54
4.3 The approximation 56
4.3.1 Transformations 56
4.3.2 Result 61
4.4 Example: Driven harmonic oscillator with 1D noise 64
4.4.1 Power spectral density (PSD) 65
4.4.2 Amplitude and phase as stochastic processes 67
4.5 Application: an avian flu model 70

4.5.1 Stochastic avian flu model with seasonal forcing . . . 70
4.5.2 Deterministic dynamics . . . 72
4.5.3 Stochastic fluctuation around the limit cycle and its approximation . . . 75
4.6 Discussion . . . 77

Chapter 5: Conclusions and Future Work . . . 81
5.1 Factors influencing epidemic recurrence . . . 82
5.2 The stochastic fluctuations around a deterministic skeleton . 83
5.3 Avian flu in a stochastic and seasonally forced environment . 84
5.4 Open questions . . . 86

Bibliography . . . 88

Appendices . . . 110
Appendices A: Supplementary materials for Chapter 3 . . . 111
A.1 Derivation of the avian flu SDE system . . . 111
A.2 Stochastic linearization . . . 113
A.3 Approximate solution for linear diffusion equations in three dimensions . . . 115
A.4 Additional insight from the approximation on the interaction of disease components . . . 118
A.5 The subspace where the cycling takes place . . . 121
A.6 Derivation of the explicit form of the mean-field eigenvalues . 121
Appendices B: Supplementary materials for Chapter 4 . . . 125
B.1 Floquet Theory . . . 125
B.2 Itô formula for multi-dimensional process . . . 126

List of Tables

Table 3.1 Descriptions of the parameters in the avian flu model and the values used in stochastic simulations. The range of values for β in bold-faced is the set of values that were used in [1]. 29

Table 4.1 Descriptions of the parameters in the avian flu model and the values used in stochastic simulations of (4.78). 74

List of Figures

Figure 1.1 Observed recurrence in epidemics for infectious diseases:(a) Reported incidence of measles in Copenhagen from 1920-1990 [2], (b) monthly cholera mortality from 1893-1940 in India [3, 4], and (c) annual prevalence of avian influenza from 1975-2000 in North American wild birds (in green square) and shorebirds (red circle) [1]. Figures are adopted from cited sources. 3

Figure 1.2 Whooping cough cases from actual data and SEIR models with seasonal forcing. The plots are adapted from [5]. 8

Figure 3.1 A schematic diagram of the host-pathogen model for avian influenza adapted from Wang et al. [1]. The host population has three compartments corresponding to susceptible, infected, and removed individuals. The solid arrows represent movement of individuals from one compartment to another as a result of birth, death, infection, and recovery processes. The dashed arrows represent the increase or decrease in the number of infected individuals due to the interaction (squiggly arrow) of the susceptible host with the avian influenza virus present in the environment. . . . 25

Figure 3.2 The real (solid curves) and imaginary (dash-dot curves) parts of the eigenvalues of $\mathbf{A}_0$ in (3.10) associated with the stability of the endemic steady-state (3.8) plotted against $\mathcal{R}_0$ in the case where $\beta = 0.05$. There are three real eigenvalues when $\mathcal{R}_0 < 1$, of which two are negative (thick solid lines). For $\mathcal{R}_0 > 1$, we have a complex-conjugate pair of eigenvalues with negative real parts (thick solid lines) and another negative eigenvalue (thin solid line). The imaginary parts of the complex eigenvalues are shown by the dotted lines. Other parameter values are shown in Table 3.1. 31

Figure 3.3 Simulation of the stochastic model (3.2) and its corresponding deterministic solution for $\beta = 0.05$ with (a) $\mathcal{R}_0 = 1.2$ and (b) $\mathcal{R}_0 = 2.5$, and for $\mathcal{R}_0 = 2.5$ with (c) $\beta = 0$ ($\rho = 0.4205$) and (d) $\rho = 0$ ($\beta = 14.5$). 32

Figure 3.4 Comparisons between the theoretical PSD of the exact process $\boldsymbol{\xi}(t)$ (solid line) satisfying (3.21) and the approximate process $\boldsymbol{\xi}^{app}(t)$(dashed line) given by (3.25), for the fluctuations of the susceptible, infectious, and the virus populations. Default parameter values are in Table 3.1 with $\beta = 0.05$ and $\rho = 0.4$. 37

Figure 3.5 A stochastic realization of the population fluctuations by simulating (3.21) (solid line) and (3.25) (dashed line) and their corresponding stationary standard deviations, i.e. typical amplitudes (in horizontal lines) computed using (3.28). 38

Figure 3.6 (a,b) Plot of the ratio λ/ω as a function of β and ρ. The triangular white region in the lower left is where no recurrence is observed. Panel (a) considers $0 \leq \beta \leq 50$ and $0 \leq \rho \leq 1$ while Panel (b) considers $0 \leq \beta \leq 300$ and $0 \leq \rho \leq 3$. The grey region in both panels is where $\lambda/\omega \leq 0.35$. In Panel (b), the black curve corresponds to $\lambda/\omega = 1$. (c) Plot of the basic reproduction number $\mathcal{R}_0$ as a function of β and ρ. The darker (blue online) shade indicates that no epidemic can be observed in the model for this parameter region. Parameter values and ranges from the literature are in Table 3.1. 40

Figure 3.7 Plots of (a) the intrinsic frequency ω and (b) the steady-state proportions of the susceptible and infectious populations as functions of the direct transmission rate β (left) and the environmental transmission rate ρ (right). The dark region in (a) is where the 2 to 8 year recurrence period is observed. Parameter values are in Table 3.1. 42

Figure 3.8 *Top panels:* Theoretical PSDs of the infectious population fluctuations $\xi_I(t)$ for (a) $\rho = 0.22, 1.1, 2.2$ when $\beta = 0$ and (b) $\beta = 7.5, 37.5, 75$ when $\rho = 0$. The linewidth of the PSD curves increases with the transmission parameter values. *Bottom panels:* Approximate dominant outbreak period, $2\pi/\omega$ with formula (A.42), as a function of (c) ρ when $\beta = 0$ and (d) β when $\rho = 0$. The square markers in (c) and (d) are located at $\rho = 0.22, 1.1, 2.2$ and $\beta = 7.5, 37.5, 7.5$, respectively. The black dots represent the exact dominant outbreak period obtained using the theoretical PSDs in the top panels. The black dots and square markers are indistinguishable from each other. The horizontal lines in (c) and (d) indicate the 2 to 8 year periods observed in actual prevalence data (See [1]). The corresponding R_0 values are also shown. Default values for all other parameters are given in Table 3.1. 44

Figure 3.9 Typical amplitude (intensity) of the fluctuations in the proportion of (a) susceptible, (b) infectious, and (c) virus populations, measured by their stationary standard deviations (3.29) as a function of the environmental transmission rate ρ and β. All other parameters are at the default values in Table 3.1. . . . 46

Figure 4.1 Numerical PSDs of the approximate (solid curves) and exact (dashed curves) solutions of (4.62), given (a,b) damped and (c,d) undamped regimes as defined in Section 4.4.1, obtained using forcing amplitudes (a,b) $b = 0.01$ and (c,d) $b = 0.5$ for noise levels $\sigma_0 = 1$ (gray curves) and $\sigma_0 = 5$ (black curves). Other parameters are held fixed, namely $a = 1, b_0 = 2, k_0 = 0.1$ for underdamped case, and $k_0 = 0$ for the undamped case. 66

Figure 4.2 Deterministic dynamics when (a) $b = 0$ and (b) $b = 1$. The initial condition is indicated by a black arrow. The initial conditions used are: $(\phi_1, \phi_2, \psi) = (0.3295, 0.0298, 0.6935)$. 73
Figure 4.3 Limit cycle generated from the solution of (4.82) for different values of the forcing amplitude b. 73
Figure 4.4 Computed values of (a) $\mathbf{A}_{11}(t)$ and (b) $\mathbf{C}_{11}(t)$ in (4.83)-(4.85). The parameter values used are in Table 4.1. Each function has a periodic behaviour with period equal to 1, the period of the limit cycle and the forcing frequency. 76

Figure A.1 (Colour online) A sample path of the approximate fluctuations given by (3.25) when the first term is (a) not set to zero and (b) set to zero. The grey region is the plane (A.31) that lies in the subspace spanned by the eigenvectors of $-0.3091 \pm 0.8377i$. 119
Figure A.2 (Colour online) Plot of ζ (left panel) and λ (right panel) as functions of β and ρ. The white region is where $R_0 < 1$, i.e. noise-sustained oscillations cannot be observed here. Default parameter values are in Table 3.1. 120

Acknowledgements

There are so many people to acknowledge for their moral, emotional, and academic support in my doctoral study. Since they are too many to mention, I hereby only recognise the most important contributors of this great work. I wish to thank the following people whom I have close contact with during my PhD study here in Canada.

First of all, I would like to express my sincerest gratitude to my wonderful supervisors, Rebecca Tyson and Cindy Greenwood. The positive energy of my academic mentor Rebecca is contagious and I will forever treasure her motherly care for me in this PhD journey. All pieces of advise and encouragements she shared are valuable to me and her brilliant ideas especially with regards to writing this thesis were inspiring. On the other hand, this thesis was conceived from a small summer project that was suggested by Cindy before I left UBC Vancouver. I am very grateful that Cindy challenged my thoughts and trained me to become a probabilist. Her mentoring style taught me to be stronger than I used to be and I will always remember her words of wisdom. I also would like to thank Leah Keshet for choosing me to be part of her research group when I first applied for PhD at UBC Vancouver. Leah helped me see my research potential and the support she has given me ushered the fulfilment of this dream. Thanks to Bob Lalonde for the insightful conversation and constructive remarks on the epidemiology and ecology of avian influenza part of my thesis. I thank my thesis examiners, David Jack and Sebastian Schreiber, for their time spent to evaluate my research work.

I thank my academic brothers and sisters in the TyLab group: Jessa, Joe, Jimit, Sarah, Maria, Geoff, Charles, and Michael, for the stimulating discussions, questions, and anything-under-the-sun chitchats. To Joey and Ali for the good laughs, the late night rides, and inspiring conversations on research writing. To my colleagues in the Computational Ecology Research Group (CERG), especially to Bruno, Fabian, Matt, and Rodolphe, for the support and constructive criticisms. More than helping me with paper works, providing supplies, and scheduling my teaching duties, I thank the Unit5 Staff, Hilda and Ashlee, for their moral support.

To my folks at my home university, the University of the Philippines Mindanao (UPMin), I am very grateful for their continued support and for believing me in my pursuit to become a biomathematician. I thank the UPMin officials for granting me this special privilege of leaving the country to study and getting paid at the same time. I am grateful that they held on to my intention of returning service after my study.

To those people who showed me that there is more than a scientific life, I thank them all a ton for their support especially during the lowest point of my study. To my very supportive and amazing friends – Ellaine, Aleza, Stephanie, Aaron, and Brent – for welcoming me like family. To my spiritual mentors, Tita Liza, Tito Odi, Ate Arleen, Kuya Daniel – who had helped me walk in faith. To my Christian brothers and sisters all over the world, especially the Buhangin Community Church, the Willowpark Church and all the small groups I have attended with, for praying with me. To Simon, Jenny, Tian, and Isabell for the life-giving stories, encouragements and exhortations. To my ever-dearest friend Jen M, for the sisterly pieces of advice. To my former roommates Janine, Jocelyn, and Chalise, for the fun adventures and "Canadianizing" me. To Mr. and Mrs. Diopita for their generosity and providing me a comfortable place to stay for my last few months here in Canada.

Last but not least, thanks to my biological family especially to my mother, Mimay Luz, who stayed strong for me despite all the crises we faced and to my only sibling, Janelle, who cheered me up and helped me learn not to take life so seriously. To Kuya Telo and other online friends for the good company and for boosting my confidence. And of course, to Patrick, for his love that continually reminds me of my good qualities and inspires me to finish this degree.

Finally, I would like to thank the heroes from the Good Book who taught me these seven valuable lessons during my PhD study:

To fight the good fight of the faith, be a good steward of my intellectual gifts, conquer my fears, draw strength from the real Source, be wise as a serpent, be humble as a dove, and believe that all things work together for good for those who are called according to the LORD's purpose.

Hakavod lashem!

Dedication

Despite all stochastic perturbations,
His steadfast love remains as my deterministic skeleton.

Still in awe of His faithfulness!
Truly, He never left me behind.
Hence I offer this great work
for the glory of the Almighty, not mine.

Beloved Mayang (2017)

Chapter 1

Introduction

The ever-present outbreaks of avian influenza and its pandemic threats emphasize the importance of understanding and predicting how the disease spreads. Mathematical models are important tools in the study of disease dynamics. Theoretical epidemiological models and methods may not always be directly applicable to real-life epidemics but they provide qualitative insight into the dynamics of the spread of infection. Most of these models are mathematically intractable or difficult to analyse and so numerical simulations of these models have been used for predictions. Hence, analysis of useful disease models remains as a challenge [6]. Moreover, real-life applications of disease models demand for more advanced mathematical methods to be developed that can also be useful in other fields of study [7, 8].

The methods we developed here can be applied to study infectious diseases, such as measles, that display a recurrent pattern. All of the models we consider in this thesis are formulated as continuous-time Markov processes whose temporal evolution is described by a system of stochastic differential equations (SDEs). In the physical literature, the SDE system is typically derived through the master equation and system-size expansion [9]. Here, however, we use an alternative approach known as strong approximation theorems for Markov chains [10] to obtain the full stochastic dynamics. As with the system-size expansion, the full stochastic dynamics are decomposed into a macroscopic part (deterministic dynamics) plus a stochastic fluctuating part scaled by the square-root of the population size.

In this thesis, we are concerned with applying and developing mathematical methods to analyse disease models that simulate stochastic population fluctuations. Our study focusses primarily on understanding recurrent avian flu epidemics. While stochastic simulations can capture the qualitative epidemic pattern of recurrent diseases, there remains considerable discussion regarding the characteristics of this pattern. The novel aspect of this thesis is the development of an approximate description for the recurrent dynamics of avian influenza and the subsequent analysis of potential mechanisms that drive disease recurrence.

In this chapter, we introduce the technical terms and theoretical background which are necessary to support the content of this thesis. Specifically, we describe epidemic recurrence and its models. Moreover, we briefly discuss here the mathematical theories used in this study. Finally, we note in detail the structure of this thesis, its aims, and contributions.

1.1 Epidemic recurrence

A disease is said to display recurrent epidemics if its incidence (number of cases per unit time) fluctuates dramatically over a period of time. Recurrent epidemics have been observed in childhood diseases such as measles, whooping cough, and chicken pox. It is also observed in non-childhood diseases such as avian influenza and cholera (see Figure 1.1).

A recurrent disease can exhibit various patterns of recurrence in different locations and periods of time [11]. Measles, for instance, displays recurrent outbreaks that have been observed to transition from an annual to a biennial pattern in some locations [2], or exhibit an irregular pattern in other locations [12]. Patterns of recurrent epidemics also vary from one disease to another. In contrast with measles data from Copenhagen [2], wavelet analysis of data for avian influenza among wild birds revealed multi-year major outbreak periodicity [1, 13].

The pattern of recurrent epidemics is characterized by large-amplitude fluctuations, which are said to arise from a resonance phenomenon. Understanding the underlying mechanism of this ubiquitous feature of recurrent disease has received attention from mathematical modellers with an aim to provide additional insights into the disease transmission process. When given an epidemiological or ecological time-series with a recurrent pattern, typical questions raised are:

1. What are the periodicities?
2. Can we identify the sources of these periodicities?
3. Why does the amplitude size of the epidemics vary?

These questions have been addressed in the context of childhood diseases using traditional modelling approaches. One useful tool for distinguishing different periodicities in a time-series is the power spectrum, which shows the distribution of frequencies present in the time-series data [14, 15]. The power spectrum has been used to demonstrate that childhood diseases, e.g. measles and whooping cough, have a strong seasonal component. This tool

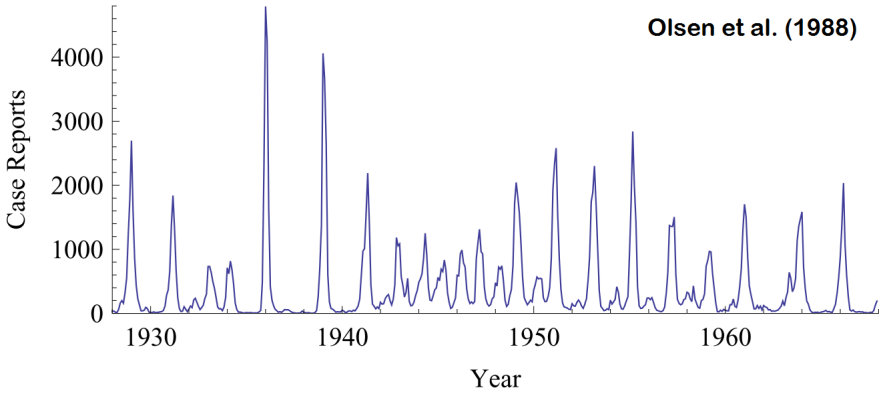

(a)

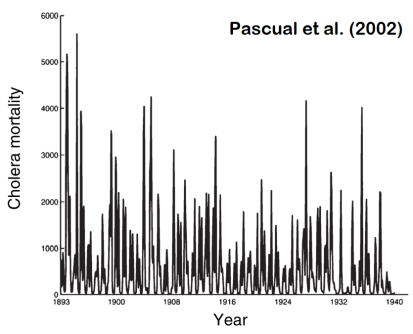

(b)

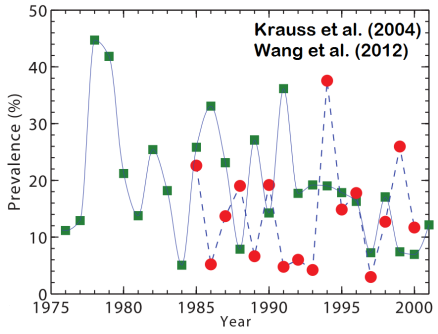

(c)

Figure 1.1: Observed recurrence in epidemics for infectious diseases:(a) Reported incidence of measles in Copenhagen from 1920-1990 [2], (b) monthly cholera mortality from 1893-1940 in India [3, 4], and (c) annual prevalence of avian influenza from 1975-2000 in North American wild birds (in green square) and shorebirds (red circle) [1]. Figures are adopted from cited sources.

has also been used to illustrate the influence of one disease parameter on the periodicity of disease outbreaks. In this thesis, we use the power spectrum to study the relationship between the approximate and exact stochastic processes describing epidemic recurrence.

1.2 Modelling epidemic recurrence

Models in the form of differential equations are widely used in the study of biological dynamics [16–19]. Epidemic recurrence, in particular, is another area in which mathematical modelling has played important role. It is noteworthy to mention that in modelling epidemic recurrence, extensive datasets are often available and can be used to validate and inform the modelling exercise. Here we discuss the existing paradigms for modelling epidemic recurrence.

1.2.1 Damped oscillations

The model developed by Kermack and McKendrick [20] set the foundation for epidemic modelling studies. Their model describes the spread of an infectious disease wherein recovered individuals gain immunity to reinfection. Fundamentally, the model considers a population that can be divided into three classes or compartments and keeps track of how the population of each class changes over time. The dynamic variables are the number of susceptible ($S(t)$), infectious ($I(t)$), and recovered ($R(t)$) individuals at time t. The susceptibles are those individuals who have not been infected by the disease while infectious individuals are those who have the disease and the ability to spread it to susceptibles. Recovered individuals, on the other hand, are those who no longer have the disease and are immune to the disease after infection. The SIR (susceptible-infected-recovered) model assumes a (homogeneous) well-mixed population and is formulated in terms of three ordinary differential equations. It was learned from the classical SIR model that an epidemic threshold exists, which is defined in terms of the basic reproductive number $\mathcal{R}_0$, i.e. the average number of secondary infections caused by one infected individual in a pool of susceptibles [20]. A disease can spread and is said to be endemic in the population when $\mathcal{R}_0 > 1$, otherwise, it dies out.

A modification of the SIR model serves as a starting point for modelling epidemic recurrence. An SIR model that gives rise to damped oscillatory behaviour, i.e. decaying oscillations, is a typical starting point for recurrent behaviour. These models has been used to investigate measles dynamics

[21]. The key point here is that the disease model exhibits an endemic equilibrium wherein infectives tend to oscillate around a mean value over time, i.e. exhibit damped oscillations, as a new supply of susceptibles enter into the system. Damped oscillations can also be observed when another population class is incorporated to the SIR model. For example, one can add an exposed class, a population of individuals that are exposed to the disease but not yet infectious. Such a model is known as an SEIR model, and is biologically meaningful for many childhood diseases [21]. Another example is a simple host-pathogen model such as the SIR-V model, where V represents the virus population. This model is used to study avian influenza (see [1] and Chapter 3).

Recurrent behaviour, however, is not entirely captured in models producing damped oscillations because, in the long-run, the infectives tend to a constant level. Sustained oscillations obtained by introduction of age structure in the population, delays and non-linear infection terms [22–25], on the other hand, are not able to predict the regularity in patterns of most epidemics. From the literature, it is apparent that there must be two main ingredients necessary to model epidemic recurrence accurately: (1) stochasticity, because the population is made up of individuals and it changes by means of random processes [26]; and (2) parametric forcing, because some parameters vary periodically over time, e.g. seasonally forced transmission rate for measles [3, 12, 27]. These two factors are well understood independently but there is a considerable question as to how they interact [5, 11, 28, 29].

1.2.2 Noise-sustained oscillations

Interacting populations, in general, behave as stochastic processes. The discrete nature of populations means that there is inherent randomness in the birth and death terms, thus introducing demographic stochasticity. In modelling epidemics, the role of stochasticity has long been recognised as a key element in the appearance of a recurrent pattern of epidemics. Bartlett [30], in his first stochastic simulations, recognised that the addition of stochastic noise to a simple deterministic model can drive recurrent dynamics. The idea here is that noise maintains oscillations by constantly perturbing the system away from its steady state [31]. A number of systems exhibit oscillations sustained by noise (or noise-sustained oscillations) [26, 32–34]. One example is the amplified biochemical oscillations studied by McKane et al. [34] where they show that noise alone can give rise to dramatic fluctuations and explain that intracellular processes may have taken

advantage of inherent stochasticity to amplify the oscillations. From a theoretical standpoint, noise-sustained oscillations are generated by a stochastic model whose deterministic version shows damped oscillatory behaviour and are quantified as coherence resonance [35].

According to Coulson et al. [5], the role of stochasticity can either be categorised as active or passive. Noise has an active role when the system produces new patterns, due to the interaction of non-linear dynamics and stochasticity, that the deterministic model alone cannot capture [28, 29]. Noise has a passive role when perturbation of the 'deterministic skeleton' is sufficient to explain the stochastic dynamics [36]. In the context of disease dynamics, the passive noise interpretation has gained weight because it seems to explain the behaviour of time-series and simulations for a broad range of diseases [5]. In fact, for systems exhibiting noise-sustained oscillations, demographic stochasticity generally has a passive role.

In epidemic modelling, the use of noise-sustained oscillations to describe disease recurrence has been observed. For example, Wang et al. [1] added stochastic noise to an SIR-V model for avian influenza and showed that the dominant outbreak period varies with the environmental transmission rate, i.e. the rate at which the virus enters the host from the environment. Modelling epidemic recurrence with this technique can be challenging, especially when one is interested in identifying the parameters that influence the periodicity and/or intensity of outbreaks in a system with more than two population classes. One of the aims of this thesis is to demonstrate the use of an approximate stochastic process to study recurrent behaviour in a population system composed of four populations.

1.2.3 Parametric forcing: Forced limit cycle

Up to this point, we have discussed models of epidemic recurrence without external parametric forcing. Here we introduce the forced limit cycle as another paradigm for a recurrent pattern in epidemics. A common source of parametric forcing is time-dependence in a model parameter. In this thesis, we define a forced limit cycle as a stable limit cycle generated by a deterministic system with time-periodic parameter. In the context of epidemiological models, forced limit cycles occur in seasonally forced systems [33, 37, 38].

The most popular approach for introducing seasonal forcing in an epidemic model is by making the transmission rate a periodic function of time. For example, in studying measles recurrence, the transmission rate is simply represented as a step function so that transmission is high during school terms and low otherwise [22, 28]. This deterministic forced epidemic model

can display a wide range of dynamic behaviour such as limit cycles and attractors with sub-harmonic frequencies depending on the magnitude of the seasonal forcing [39–41].

The seasonality of avian influenza outbreaks points to a seasonally varying transmission rate as a potential driver. This idea has been investigated by [42] who showed that a simple epidemic model with periodic transmission rate and disease-induced mortality best explained the periodicity of H5N1 avian influenza data from Food and Agriculture Organization of the United Nations [43]. As with the measles model mentioned above, this simple forced model for avian flu exhibits complex dynamics, such as period-doubling and chaos, for various forcing magnitudes.

With respect to the fluctuating avian flu epidemics seen in wild birds, this thesis explores the possibility of modelling the recurrent pattern as a forced limit cycle. One potential driver for recurrent behaviour that we investigate in this study is seasonality in the environmental transmission rate.

1.2.4 Parametric forcing with noise

It is likely that both seasonal forcing and stochasticity are important in capturing realistic epidemic dynamics. To illustrate this view, consider the different plots of whooping cough cases in Figure 1.2. Rohani et al. [29] demonstrated that although the deterministic SEIR model with seasonal forcing provides the appropriate 'deterministic skeleton' for the actual whooping cough cases reported in Birmingham, adding stochastic noise improves the model's ability to capture the observed qualitative dynamics.

Despite all known studies involving discussion of the role of stochasticity and seasonal forcing [37, 44], little is known about the stochastic dynamics of models exhibiting both limit cycle and stochasticity. This point motivates one of the main questions this thesis aims to answer: how do seasonality and stochasticity interact within the fluctuations of the system when the deterministic skeleton of the system is a robust oscillation, i.e. stable limit cycle? Can we mathematically distinguish between the fluctuations around an endemic fixed point from the fluctuations around a cyclic solution? The latter part of this thesis is devoted to answering these questions by means of analytic methods for stochastic equations.

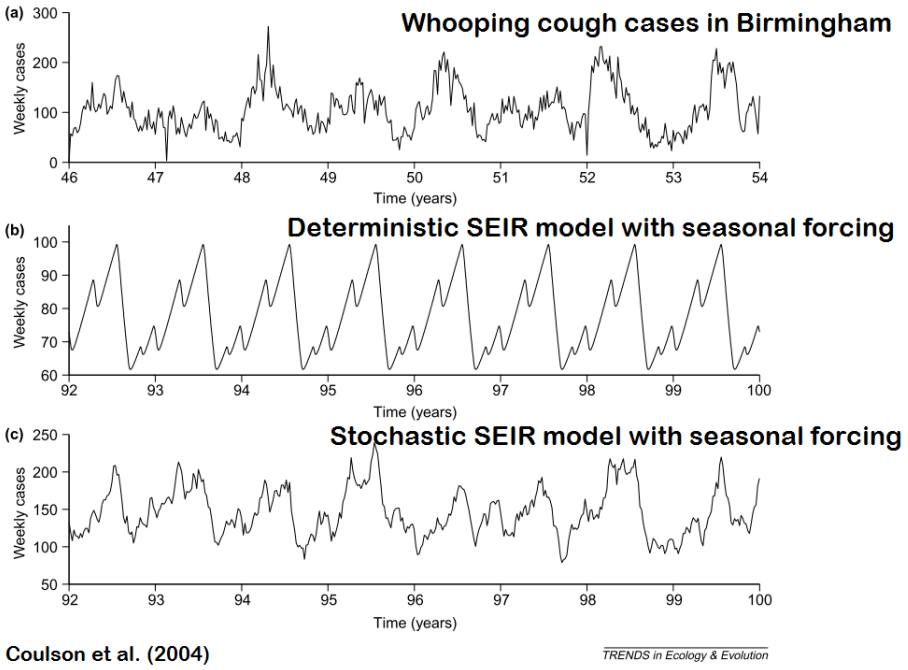

Figure 1.2: Whooping cough cases from actual data and SEIR models with seasonal forcing. The plots are adapted from [5].

1.3 Mathematical theories and methodology used in this thesis

Biological systems are characterised by changes in natural variables and so are often described in terms of differential equations. These equations are also referred to as dynamical systems. Given a dynamical system, one is interested in obtaining its solution to accurately determine the 'fate' of the system over a period of time. Most differential equations with real-life applications have solutions that are difficult or even impossible to obtain analytically. Qualitative methodologies for studying dynamical systems, such as stability and bifurcation analyses [45], are straightforward to apply in most deterministic equations. In the case when random processes are involved, the behaviour of the system is predicted by means of probability distribution and generating functions [46]. This is due to the fact that multiple runs of a stochastic model generate different realisations that show variations. Furthermore, when both randomness and external forcing are incorporated in the system, the analysis of its dynamical behaviour demands tractable mathematical techniques.

In this thesis, we focus our attention on stochastic differential equation (SDE) models to describe the epidemic recurrence observed in avian flu dynamics. These stochastic epidemic models are approximations to the Markov chain model for population growth in the epidemiological system. The SDE models are developed based on the theorem of Kurtz [10], which shows that the (density-dependent) Markov jump process, normalized by the total population size N, and the approximating diffusion process can be constructed on the same probability space. Kurtz [10] proved that the diffusion process deviates from the jump process by $\mathcal{O}(\log N/N)$ as $N \to \infty$. Application of this method to epidemic modelling is found mostly in the literature on stochastic processes [47–49]. Note that in the physical literature, the method for constructing SDE models is based on the system-size expansion [9]. This thesis, however, uses the former approach (i.e. Kurtz's method) in formulating the SDEs for avian flu epidemics, not only because it is straightforward to implement but to also introduce this method to the present body of knowledge on stochastic modelling of epidemics.

The recurrent dynamics displayed by the SDE models in this thesis are analysed by studying the equations mathematically. Here we apply the theorem of Baxendale and Greenwood [50] (the BG theorem) to study the stochastic system without external forcing by constructing an approximate process that allows us characterise the simulated avian flu recurrent epi-

demics. The power spectral density (PSD) [15] is used to check the proximity of the approximate process to the actual process, and stochastic simulations via the Euler-Maruyama scheme [51] are used to generate sample paths.

In investigating the stochatic system with external forcing, i.e. seasonal forcing, Floquet theory [52] is applied, which provides the stability information of the deterministic perturbation around a cyclic solution (e.g. limit cycle). The use of this theory is common in the physical literature that takes into consideration linear differential equation with time-periodic coefficients. Another novel aspect of this thesis is the extension of the BG theorem to develop an approximate process for fluctuations in the time course of epidemics resulting from the interaction of nonlinear dynamics and stochasticity. Moreover, we extend BG theorem to noise around the forced limit cycle. Finally, fundamental probability concepts and methodologies, e.g. Itô's formula [53], Ornstein-Uhlenbeck process [46], etc., are essential for the development of the theory.

1.4 Thesis structure and contribution

In this thesis, we study the recurrent pattern of avian flu epidemics by means of analytic techniques. We begin by gathering information about the epidemiology, ecology, and outbreak recurrence of avian influenza (Chapter 2).

In Chapter 3, we first develop an understanding about the current paradigm for modelling avian flu recurrent epidemics. This is done by analysing mathematically, i.e. using approximation technique, a host-pathogen stochastic model for avian influenza recurrent epidemics with two types of transmission modes. It is found with the aid of analysis that the periodicity of recurrence is determined by the transmission modes while the noise has a substantial contribution to the intensity of epidemics.

In Chapter 4, we develop a new approximation tool that can be used to understand epidemic recurrence modelled as stochastic perturbations around a limit cycle. Our tool is an extension of the approximate model for stochastic fluctuations around an equilibrium, i.e. the result of Baxendale and Greenwood [50]. Our approach can be applied to a general class of SDE systems - SDEs with time-dependent drift and diffusion coefficients due to periodic parametric forcing. Such systems naturally occur when one of the parameters is a periodic function of time.

Finally, the conclusion of this thesis is presented in Chapter 6. The main finding points to the deterministic mechanism playing a key role in influ-

encing avian flu epidemic recurrence described by stochastic perturbations around the deterministic dynamics (e.g. endemic equilibrium or forced limit cycle solution).

Chapter 2

The Epidemiology, Ecology, And Epidemic Recurrence Of Avian Influenza: An Overview

2.1 Avian influenza (AI)

Avian influenza (AI) also known as "bird flu" is a viral disease that commonly infects poultry and wild birds. In poultry, the disease is characterised by various symptoms such as nasal discharge, lack of energy, and diarrhea, resulting to "fowl plague" in which mortality of at least 75% has been observed [54]. In wild birds, the disease do not usually manifest symptoms [55]. More than a decade ago, AI was a disease of limited significance [56, 57] but this perspective has changed since the emergence of various virus strains (e.g. H1N1 in 1976, 1986, and 1988; H3N2 in 1993; H7N7 in 1996; H9N2 in 1998, 1999; H5N1 in 1997, 2003, and 2013; H7N9 in 2014) that are deadly to humans [58–60]. Since the disease poses threat to human health, several efforts have been made to control its spread such as culling large number of poultry and restrictions on trade of poultry products [61].

2.2 Avian influenza virus (AIV)

The causative agent of avian influenza is an influenza A virus [62] consisting of different combinations of haemaggluttinin (HA) and neuraminidase (NA) surface glycoproteins [63, 64]. A total of 16 HA subtypes (H1-H16) and nine NA subtypes (N1-N9) have been recognised [65], and each virus has one HA and one NA antigen.

The avian influenza viruses (AIVs) can be divided into two distinct groups according to their virulence in poultry, namely the low pathogenic avian influenza virus (LPAIV) and the highly pathogenic avian influenza

virus (HPAIV). The LPAIVs are commonly isolated from many species of wild birds [66] and cause little harm in the wild [55, 65]. On the other hand, HPAIVs are not maintained by wild birds [67] but have been isolated from wild population in the event when the disease has spread to domesticated birds [68, 69]. Significantly, certain LPAIV subtypes (e.g. H5 and H7) may become highly pathogenic if they are transmitted to poultry [70–72]. The ability of LPAIVs to mutate into HPAIVs [73] in poultry and the diversity of these viruses circulating in bird populations in the wild potentially makes wild birds the primary source of introduction of influenza into humans [74–76].

2.3 AIV ecology in wild birds

The AIVs found in wild birds constitute the historic source of human influenza viruses having a rich pool of diversity that may likely lead to cross-species transmission [55, 77]. A most recent example is the transmission of H7N9 AIV to humans in China (see [78] and references therein). The H7N9 virus is associated with a significant risk of mortality to humans. In the year 2014, 212 deaths were reported to the World Health Organization due to infection with H7N9 alone. Thus, it is important to have a better understanding of the ecology of AIVs in wild birds.

Influenza viruses infect a great variety of birds [66, 79, 80]. Various subtypes of AIVs are maintained in and isolated from wild bird populations from a variety of major Families. In 1961, an influenza virus was first isolated from common terns (*Sterna hirundo*) in South Africa [81]. Further monitoring suggested that ducks and geese are important natural reservoirs of AIV [82]. Sharp et al. [83] however suggested that waterfowl do not act as a reservoir for all AIVs. It is possible that AIV that ultimately gets transmitted to humans is maintained in shorebirds and gulls, where the AIV isolates predominantly have different subtypes than those isolated from ducks [84]. According to Stallknecht and Shane [82], AIVs infect 90 bird species from 22 different Families and 12 Orders. On the other hand, Olsen et al. [85] lists at least 105 wild bird species from 26 families. With the large number of recent AI outbreaks, it seems that the actual number of fully susceptible species is likely to be much greater.

The complexity of the ecology of AIV is linked to the biology of the natural host and environment. For example, it seems incidental that ducks living in freshwater habitats have relatively high prevalence rates of AIV infection [86] in contrast to shorebirds and gulls, which are salt water birds.

However, as demonstrated by Stallknecht et al. [87] some AIV isolates are more sensitive to salinity. Moreover, persistence and prevalence of AIV as outlined by Stallknecht et al. [88] can depend on three factors: (i) concentration of AIV shed at an adequate time duration, (ii) the stability of AIV in the environment, and (iii) the AIV concentration required for productive infection of the next host (infective dose).

Human intervention could play a role in the ecology of AIV. For example, the movement of infectious agents among numerous domestic avian and mammalian species due to global wildlife trade provides transmission mechanism into wild bird population when these infected species are released into the wild [89]. However, as reviewed by Reed et al. [90], human effects on bird movement patterns may have greater significance. For example, climate alterations around urban areas may distort the disease epidemiology as it affects the pattern of migration, population densities, and species interaction of many wild bird species.

2.4 Transmission of AIVs to and between birds

A potential cause of initial infection for AI outbreaks in poultry could be direct or indirect contact with infected waterfowl populations [91–93]. However, the knowledge about the transmission mechanism of AIVs between birds is insufficient. It is suggested that AIVs could be transmitted among birds via oral-oral (respiratory) route [94] or faecal-oral/faecal-cloacal route [95].

In oral-oral route, i.e. direct transmission, AIVs are transmitted through direct contact between infected and susceptible birds. Past experimental assessments on the transmissibility of AIVs in poultry suggested that direct transmission is a complex process as it depends on the virus strain, the bird species and many environmental factors [91, 96–99]. For example, HPAIVs tend to show much poorer transmission from infected to susceptible hosts in poultry than LPAIVs in both natural and experimental settings. On the other hand, low LPAIV samples from mallards may suggest that the respiratory tract plays a limited role in the replication, transmission and ecology of LPAIV in dabbling ducks [100], yet oral-oral route may be relevant for bird species in which faecal-oral transmission would prove difficult.

The fecal-oral route is identified to be the main transmission mechanism among aquatic birds. LPAIVs are thought to be transmitted via the fecal-oral route in wild bird population when infected birds shed virions in their faeces and susceptible birds ingest the virions from the contaminated aquatic

habitat [55, 87, 101–103]. The filtering or drinking of contaminated water could be a potential explanation for the high AIV prevalence among bird species aggregating in wetlands. Moreover, the prolonged infectious periods of the virus could potentially allow temporal and spatial connectivity among bird populations with their respective virus populations. In freshwater lakes, AIVs remain infectious for up to 4 days at 22 degrees Celsius and up to 6 months at the freezing point [93]. The virus stays infectious for even longer time durations in ice or frozen ground [104–107]. During the breeding season, infected birds in the Arctic region shed AI virions into the environment through faeces, which then persist in cold water, in ice or frozen ground throughout the winter. The thawed contaminated ground ice or frozen lake becomes, in the next spring, a source for re-infection among birds returning to the breeding ground [93, 108] suggesting that bird migration is associated with the persistence of AIV in wild bird populations.

Virus transmissibility may be related to the amount of virus released orally or from excretions. Several factors such as virus strain, bird species, and immune response can affect the virus shedding rate [71]. For example, it is possible that a relatively small quantity of virus is excreted during the course of HPAIVs infections, as they cause rapid deaths in poultry. The Asian H5N1 HPAIV, on the other hand, are shed at much greater concentrations and for longer durations from the respiratory tract than by the cloacal route [109, 110]. Such differences may potentially explain the efficiency of virus transmission within bird population or to domestic poultry [88].

2.5 AI epidemic recurrence

Survey-based reports suggest that AI epidemics are recurrent and are tied to the persistence and prevalence of AIV. Here we give an overview of LPAI and HPAI outbreaks that have been observed in the past as reviewed by several authors [66, 111–113]. We also summarize and highlight the existing modelling efforts that have been done to understand AI outbreaks, e.g. the role of transmission on its multi-year periodicity.

2.5.1 LPAI outbreaks

The prevalence of LPAIV in its natural reservoir, i.e. wild birds, is believed to be the source of LPAI infection in poultry. For certain subtypes of LPAIV, when the AI infection moves to poultry it can escalate to the highly pathogenic type. In this review of LPAI outbreaks in poultry, it is

important to distinguish between outbreak events caused by non-mutating and mutating subtypes as the latter type is linked to HPAI outbreaks.

H5/H7 subtypes

Prior to the discovery that certain subtypes of LPAIV, e.g. H5 or H7, can mutate to HPAIV, little attention was given on identifying LPAI outbreaks in wild bird population. In fact, the relationship between wild birds and LPAIV is assumed to be of a commensal nature [114]. LPAI outbreaks, however, occur frequently in poultry where the association is less benign.

Since 2006, H5/H7 LPAI outbreaks were observed in several parts of Europe [115–117]. Between 2002 and 2006, there were sixty LPAIV strains isolated from poultry and other captive birds in Europe, Asia, Africa and Australia [118]. Since many outbreaks may remain unnoticed, the actual number of LPAI outbreaks in poultry may be even higher [112].

A number of outbreaks can spread over large regions as a result of LPAIV circulating among poultry. From 1997 to 2001, Italy, for example, had several subtypes of LPAIV circulating in areas populated with a high density of poultry farms. In 1999 to 2000, an LPAIV (H7N1) that was endemic in poultry gave rise to the emergence of a highly pathogenic variant [119]. Although efforts have been done to eradicate H7N1 HPAIV,viruses related to H7 LPAIV appear regularly in Italy and less commonly in other European countries [115]. Similarly, in 1994-1995, another LPAIV (H5N2) causing the emergence of a HPAIV in Mexico still circulates throughout Central America.

An H7N2 LPAIV that had become endemic in poultry circulated among live bird markets and backyard smallholder flocks for 13 years in the north-east region of United States. Fortunately, the virus was finally eliminated in 2006 without evolving into HPAIV [120]. Several LPAIV subtypes have been introduced recently in poultry farms in Germany, the Netherlands, Denmark, and Belgium. For most of these outbreaks, it is assumed that LPAIVs of H7 subtypes are acquired by direct introduction from their natural reservoir, i.e. wild birds. However molecular analysis suggests that the LPAIV in poultry has become endemic [116, 121].

Non-mutating subtypes

LPAIVs that do not mutate to HPAIVs may not be a serious problem, however these viruses can still cause severe illness and so should not be deemed unimportant. Non-mutating LPAIVs continue to spread in various

parts of the world: the H3N2 in Italy [122] and China [123], H6N1 in Hong Kong [124], H6N2 in USA [125], and H9N2 in the Middle East [126]. In particular, the subtype H9N2 became very widespread and maintained in poultry throughout large parts of Asia [127]. According to many case reports based on the review by [112], H9N2 has caused high mortality rates in poultry that is comparable with HPAI outbreaks. Under experimental conditions, H9N2 do not produce severe symptoms in affected poultry but secondary infections, accompanied by bronchitis virus and *Mycoplasma gallsepticum* are always involved [128]. Since non-mutating LPAIVs pose harm to poultry and their aggravating symptoms are worrisome, such as the case of H9N2, eradication (depopulation) or control measures (vaccination) are applied to such outbreaks [116, 129].

2.5.2 HPAI outbreaks

Several descriptions of disease outbreaks or animal plagues are analogous to the present HPAIV outbreaks [130]. An HPAI outbreak was first reported by an Italian scientist Perroncito [131] who described that the infection of poultry around Torino during the Fall and Winter season of 1877-1878. Although the infected poultry initially did not show serious illness, the disease became epidemic throughout a larger area causing high mortality among poultry [113]. After few decades, the outbreak was found to likely involve the mutation of LPAIV into an HPAIV [132] as witnessed in the United States of America [133], Mexico [134], Italy [135], Chile [136] and Canada [137]. Several HPAI outbreaks have been studied from then on.

Major HPAI outbreaks occurred around the world in the early 20th century, in which poor outbreak detection and management promoted the spread and distribution of the virus. Nevertheless, it seemed that efforts were made to control (e.g. live poultry shipping restrictions, depopulation, quarantine and disinfection) some of these outbreaks [113]. In 1959, the first HPAI outbreak took place in Scotland and thereafter other outbreaks occurred in various places. These HPAI outbreaks are enlisted by Alexander and Brown [132], Koch and Elbers [138], Lupiani and Reddy [113], and World Animal Health Organization (OIE) [117].

Since about 19 years ago, the most worrisome HPAI outbreak, the Asian H5N1 HPAI, emerged and is still severely infecting poultry all around the world. It has been found that this notorious virus has managed to spill-over from poultry to the wild bird reservoir and is maintained in natural hosts despite its tendency to cause sickness and mortality in these wild birds [138–141].

Originating from Hong Kong and other parts of southern China since 2004, it seemed that the Asian H5N1 HPAIV became endemic in birds throughout south-east Asia [117]. The virus was said to spread across the Himalayas to the south and westward to Europe and Africa through migratory routes [142]. In 2006, the H5N1 virus prevalence peaked and has spread to as many as 63 countries across Asia, Europe and Africa. There is evidence that the virus continues to spread, but at a slower rate. In 2008, H5N1 HPAIVs were last detected in Germany. Two years later, the epidemic ended in Romania, Bulgaria and Russia [117]. However, Asian H5N1 HPAIV remains endemic in some Asian countries and Egypt as of 2014 [116].

2.5.3 Modelling efforts

Mathematical modelling has been shown to play an important role in understanding disease dynamics [143, 144]. For AI, models have been used to describe the disease transmission, evaluate parameters of interest and assess intervention strategies (see [145] and references therein). Other modelling work emphasizes the importance of combining modelling with experimental or survey data to generate quantitative information that is essential for designing control strategies for epidemics [146]. The probability of transmissions and incidence rates, for example, can be used to assess the role of improving bio-security [147]. Other works showing the use of models and data from other epidemics are described by Garske et al. [148], Mannelli et al. [149], McQuiston et al. [150], Sharkey et al. [151], Nishiguchi et al. [152]. As outlined by Dorjee et al. [145], AI is studied using deterministic and stochastic compartmental models [153–158], and network models [151, 159].

Past AI models focussed on investigating how the spread of AI to humans could potentially lead to pandemia [160–162]. A few models were developed involving both animals and humans linked by a pathogen. An example is the simplest model that captures the transmission pathway of H5N1 from poultry to humans [163]. However, in light of the recurrent outbreaks of LPAI and HPAI, recent models focus on capturing the pattern of AI outbreaks and identifying the drivers of the disease dynamics. The temporal pattern of AIV prevalence have been used to shed light on the outbreak periodicity of LPAI [1, 164]. These studies support the result of Rohani et al. [165] which emphasises the importance of environmental transmission, i.e. faecal-oral/faecal-cloacal route, in recovering the pattern of periodicity and persistence of AIV in waterfowls. On the other hand, seasonal patterns of infection have been detected where prevalence is highest during late Autumn

and Winter [3, 42, 76, 166–168]. The patterns are said to be associated with immune response, bird migration, and/or environmental variability. For instance, the high virus prevalence in juvenile mallards for their low immune response and the virus persistence in the environment under colder temperature contribute to a spike (or spikes) of influenza activity during winter months [169].

2.6 Discussion

Avian influenza is indeed a very complex disease in which understanding of its epidemiology, ecology, and epidemic recurrence is limited by monitoring methods, genetic sequencing technology, and other data gathering techniques. Although it is established that wild birds are the natural reservoir of AIVs, no accurate tracking survey has been done to show that LPAI-infected wild birds cause HPAI outbreak in poultry. The recent discovery of HPAIV infection in wild bird populations poses a challenge to determine whether it is likely that virus in wild birds will become endemic in the case when the virus ceases to spread in poultry. The diversity and evolution of AIV are other important research subjects. The answers to the research questions on the biology of each virus subtype and the complex nature of its replication and interaction with the host cell are useful for vaccine development and other methods to control disease spread.

Mathematical models are effective tools to mimic the complex dynamics of AI epidemics. The models can assist by evaluating current measures and mechanisms to explain outbreak pattern, investigating hypothetical scenarios, and making predictions based on empirical data. Some modelling work has addressed AI systems but more needs to be done. For example, whereas some AI outbreak recurrence models have been used to provide a persistence mechanism within host populations, these models were based on the temporal pattern of AIV prevalence data and not on the incidence of infectious cases. It may be true that recurrent prevalence produces recurrent outbreaks, however such an idea remains poorly tested. We suggest that careful attention must be given to using epidemiological terminologies when describing models. Further modelling work is needed in order to evaluate the relative contribution of other possible persistence mechanisms, as there are other factors that come into play such as spatial and age structures, host immunity and evolutionary processes of virus strain. Also other recurrence models incorporate seasonality due to environmental factors, but a major drawback is the lack of consideration for spatial features in the transmis-

sion dynamics of AI. Nevertheless, these final steps serve as a starting point to acquire further insights about AI epidemiology, ecology, and epidemic recurrence.

Chapter 3

The Role Of Direct and Environmental Transmission In Stochastic Avian Flu Epidemic Recurrence

3.1 Background

Avian influenza is an infectious disease present in poultry and wild birds, and is known to pose threats to humans [170]. The disease pathogen is the avian influenza virus (AIV) whose natural hosts include aquatic birds [83, 171] with wild ducks as its main reservoir [172]. AIV strains can be either highly pathogenic (HP) or lowly pathogenic (LP) according to their ability to infect hosts. The HPAI viruses are the most virulent and are responsible for 'fowl plague' causing mortality as high as 100% in poultry [66]. The LPAI viruses are endemic in wild bird populations [55, 85] but can easily be transmitted to domestic stock and then mutate to HPAI type [173]. Regardless of the type of virus strain, the prevalence data for avian influenza displays recurrent epidemics over time. The underlying mechanism behind this outbreak pattern is the subject of active investigation [13, 165, 174–176], and is a key consideration in the development of effective control strategies for disease mitigation.

The virus spreads to healthy individuals either (i) by contact with an infected host i.e. through inter-host (direct) transmission, or (ii) by hosts acquiring the virus from the environment through drinking or filtering water while feeding, i.e., through environmental (indirect) transmission [13, 175]. Recently, a few authors have highlighted the importance of environmental transmission as a driver of AIV epidemics. Rohani et al. [165] demonstrated how neglecting environmental transmission could lead to underestimates for the explosiveness and duration of AIV epidemics. Breban et al. [164] developed a new host-pathogen model combining within-season transmission

dynamics, between-season migration and reproduction, and environmental variation, and showed that environmental transmission offers an explanation for the 2 to 4 year periodicity of AIV epidemics. Wang et al. [1] formulated a simple stochastic model to show that increasing environmental transmission can make the outbreak period shorter. Their model predicted an outbreak period of 2 to 8 years. Wang et al. [1] found this result consistent with the observed outbreak period obtained from wavelet analysis of empirical data [171]. Together, these papers and others point to environmental transmission as the key mechanism behind the approximate periodicity of AIV epidemics. They are based on the assumption that direct transmission is weak between wild birds. Recently, however, a simple SI model with only a direct transmission route, and without stochasticity, was found to provide the best fit to poultry outbreak data [42] suggesting that direct transmission may be stronger than originally thought. Motivated by these findings, we re-examine, mathematically, the contributions of the different transmission routes to the multi-year periodicity of avian flu epidemics.

The approximate multi-year periodicity of outbreaks is thought to be due to the random nature of contagion and recovery processes, together with demographic stochasticity (i.e., uncertainty in birth and death times), and the deterministic dynamics of the system [26]. It has been shown that demographic noise can sustain population oscillations that would otherwise damp to a stable equilibrium. These oscillations are commonly called noise sustained oscillations [31, 177, 178]. Other treatments of this phenomenon in various contexts call it coherence resonance [35], stochastic amplification [32–34], or stochastic resonance [179–181]. Based on known AIV biology, a plausible model [1] suggests that AIV dynamics may arise from noise sustained oscillations.

A system exhibiting noise sustained oscillations can be analyzed using a recently developed approximation method. Baxendale and Greenwood [50] showed that a stochastic process of two-dimensional noise sustained oscillations is, in distribution, approximately a rotation whose radius is modulated by a slowly varying bivariate standard Ornstein-Uhlenbeck (OU) process, a well-studied mean-reverting stochastic process [182].

In this thesis, we apply the approximation of Baxendale and Greenwood [50] to a three-dimensional stochastic host-pathogen model, and assess the contributions of the direct and environmental transmission rates to the recurrent epidemics it produces. First, we show that the avian flu epidemic process can be approximated by the sum of a scaled univariate OU process and the product of a rotation and a bivariate slowly varying standard OU processes. Using the approximate stochastic process, we show that the

outbreak period of the epidemics has a distribution centred at the intrinsic frequency of the associated deterministic part of the process, i.e., the deterministic analogue. We obtain the intrinsic frequency as a function of the two transmission rates and identify the relationship of each transmission rate with the dominant outbreak period. Furthermore, we determine how the outbreak intensity varies over a wide range of direct and environmental transmission rates.

We organize this chapter as follows. In Section 3.2, we discuss the stochastic avian flu model formulated in terms of stochastic differential equations using the result of Kurtz [10]. In the same section, we also suggest an appropriate range of values to use for the transmission rate parameters. We review previous analytic work. Section 3.3 contains our own analysis, which includes determining the approximate process, the theoretical power spectral density (PSD), and the formula for the intrinsic frequency. We present in Section 3.4 the interpretation of our analysis, that the disease recurrence observed in stochastic simulations is approximately governed by a rotation matrix multiplied by a standard Ornstein-Uhlenbeck (OU) process. We then describe the influence of each transmission route on the dominant period of outbreaks (based on the intrinsic frequency) as well as the intensity of outbreaks (based on the stationary standard deviation of the approximate process). Finally, in Section 3.5, we discuss the implications of our results for characterizing avian flu epidemics and providing insights into the dependence of the frequency and variation of recurrent avian influenza epidemics on each transmission route.

3.2 The stochastic avian influenza model

3.2.1 Model description

Wang et al. [1] formulated a stochastic model for avian influenza using the susceptible-infected-recovered (SIR) framework with an added environmental transmission rate. They found that their model was sufficient to explain the multi-year periodicity of flu outbreaks. In this host-pathogen model, there is a susceptible duck population of size S, an infected population of size I, a population of recovered individuals of size R, and an environmental virus concentration V. Note that S, I, and R are integers, and all populations are functions of time. We also assume that a new susceptible duck is born once a host dies so that the total duck population is constant, i.e. $S + I + R = N$. Thus, we can solve for R in terms of S and I. By considering a short time interval $[t, t + \Delta t]$ and denoting by $T(\boldsymbol{\sigma}'|\boldsymbol{\sigma})$ the

transition rate from state $\boldsymbol{\sigma} = (S, I, V)$ to $\boldsymbol{\sigma'} = \boldsymbol{\sigma} \pm \boldsymbol{\nu}$, where $\nu_i \in \{0, 1\}$, the different system events and their corresponding transition rates are:

1. Infection
$$T(S-1, I+1, V|S, I, V) = \beta S \frac{I}{N} + \rho S \frac{V}{N_V} \quad (3.1a)$$
2. Birth and Death
$$T(S+1, I, V|S, I, V) = \mu(N - S - I), \quad (3.1b)$$
$$T(S, I+1, V|S, I, V) = \mu I, \quad (3.1c)$$
$$T(S, I, V+1|S, I, V) = \tau I + \delta V, \quad (3.1d)$$
$$T(S, I, V-1|S, I, V) = \eta V. \quad (3.1e)$$
3. Recovery
$$T(S, I-1, V|S, I, V) = \gamma I. \quad (3.1f)$$

We schematically present these processes in Figure 3.1.

The first event (3.1a) describes the infection of a susceptible individual. Infection happens when a susceptible host is in close contact with an infected host or when it acquires the virus directly from the environment. The rate of transmission of the disease is given by the likelihood of contact between a susceptible individual and either infected individuals or virions in the environment, multiplied by the rate at which virions are acquired by susceptible individuals in each case. Note that the likelihood of contact depends on the fraction of infected individuals (I/N) and the concentration of virus in the environment normalised by a reference concentration (V/N_V), i.e., the likelihood of contact in a frequency-dependent process.

The second category of events (3.1b)-(3.1e) encompasses the birth and death processes of the host and the virus. For simplicity, it is assumed here that the per capita host birth and death rates have the same value μ. We assume that virus is introduced into the environment at a constant rate δ from alternative hosts. The virus concentration in the environment also grows when infected ducks shed virions; this shedding occurs at rate τ. The clearance rate of the virus in the environment is η.

Finally, the third category of events (3.1f) is the recovery of infected ducks at per capita rate γ.

The parameters β, μ, τ, δ, η and γ are stochastic rates.

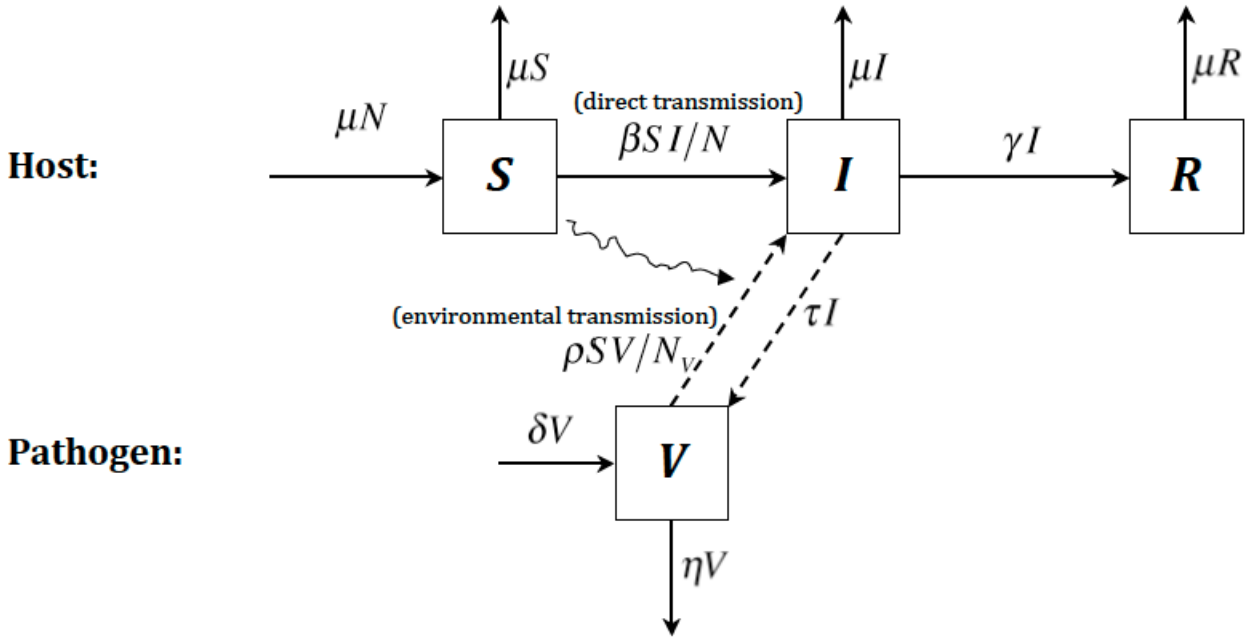

Figure 3.1: A schematic diagram of the host-pathogen model for avian influenza adapted from Wang et al. [1]. The host population has three compartments corresponding to susceptible, infected, and removed individuals. The solid arrows represent movement of individuals from one compartment to another as a result of birth, death, infection, and recovery processes. The dashed arrows represent the increase or decrease in the number of infected individuals due to the interaction (squiggly arrow) of the susceptible host with the avian influenza virus present in the environment.

The resulting stochastic avian flu host-pathogen model (see Appendix A.1) is approximated for large N by the following system of stochastic differential equations (SDEs):

$$\begin{aligned} ds &= (-\beta si - \rho sv + \mu(1-s))\,dt + \frac{1}{\sqrt{N}}\left(-G_1 dW_1 + G_2 dW_2 + G_3 dW_3\right), \\ di &= (\beta si + \rho sv - (\mu+\gamma)i)\,dt + \frac{1}{\sqrt{N}}\left(G_1 dW_1 - G_3 dW_3 - G_4 dW_4\right), \\ dv &= (k\tau i + \delta v - \eta v)\,dt + \frac{1}{\sqrt{N_V}}\left(G_5 dW_5 - G_6 dW_6\right), \end{aligned} \tag{3.2}$$

where,

$$\begin{aligned} G_1 &= \sqrt{\beta si + \rho sv}, \qquad G_2 = \sqrt{\mu(1-s-i)}, \qquad G_3 = \sqrt{\mu i}, \\ G_4 &= \sqrt{\gamma i}, \qquad G_5 = \sqrt{k\tau i + \delta v}, \qquad \text{and} \qquad G_6 = \sqrt{\eta v}. \end{aligned} \tag{3.3}$$

Here, $s = S/N, i = I/N, v = V/N_V$, and $k = N/N_V$. The SDE for the proportion of recovered ducks $r(t)$ is not necessary because we eliminate $r(t)$ using $r(t) = 1 - s(t) - i(t)$, which follows from $S + I + R = N$. In (3.2), the second term vanishes as $N, N_V \to \infty$ which leads us to the deterministic, or so-called mean-field, dynamics as found in Wang et al. [1]:

$$\begin{aligned} \dot{\phi_1} &= -\beta\phi_1\phi_2 - \rho\phi_1\psi + \mu(1-\phi_1), \\ \dot{\phi_2} &= \beta\phi_1\phi_2 + \rho\phi_1\psi - (\mu+\gamma)\phi_2, \\ \dot{\psi} &= \kappa\tau\phi_2 + \delta\psi - \eta\psi. \end{aligned} \tag{3.4}$$

The deterministic variables ϕ_1, ϕ_2, ψ represent fractions of the susceptible hosts, infected hosts, and virus in the environment, respectively, while $\kappa = \lim_{N,N_V\to\infty} \frac{N}{N_V}$. The disease is epidemic in model (3.4) if the number of infected ducks increases, i.e. $\dot{\phi_2} > 0$, which implies that

$$\frac{\beta\phi_1}{\mu+\gamma} + \frac{\rho\phi_1\psi}{(\mu+\gamma)\phi_2} > 1. \tag{3.5}$$

Note that $\dot{\phi_1} = 0$ and $\dot{\psi} = 0$ imply $\phi_2 = \dfrac{\mu(1-\phi_1)}{\mu+\gamma}$ and $\psi = \dfrac{\phi_2\kappa\tau}{\eta-\delta}$, respectively. We then write the inequality (3.5) in terms of ϕ_1 and obtain

$$\frac{\beta\phi_1}{\mu+\gamma} + \frac{\rho\kappa\tau\phi_1}{(\mu+\gamma)(\eta-\delta)} > 1. \tag{3.6}$$

At the outset of an epidemic, nearly all hosts are susceptible ($\phi_1 \approx 1$). By substituting $\phi_1 = 1$ into (3.6), we arrive at the condition for the disease to persist,

$$\mathcal{R}_0 \equiv \frac{\beta}{\mu+\gamma} + \frac{\kappa\rho\tau}{(\eta-\delta)(\mu+\gamma)} > 1, \tag{3.7}$$

where $\mathcal{R}_0$ is the basic reproduction number, the average number of secondary infections resulting from one infected individual in a susceptible population.

The deterministic system has a stable endemic equilibrium, which can be written in terms of $\mathcal{R}_0$,

$$(\phi_1^*, \phi_2^*, \psi^*) = \left(1/\mathcal{R}_0, \frac{\mu}{\mu+\gamma}(1-1/\mathcal{R}_0), \frac{\kappa\mu\tau}{(\eta-\delta)(\mu+\gamma)}(1-1/\mathcal{R}_0)\right). \tag{3.8}$$

When the basic reproductive number $\mathcal{R}_0 > 1$, the disease is epidemic. Results (3.4)-(3.8) are also found in Wang et al. [1].

We are interested in characterizing the fluctuations of the stochastic model around the steady-state solution. Hence, we linearize (3.2) around $(\phi_1^*, \phi_2^*, \psi^*)$ and obtain the linear diffusion equation (see Appendix A.2 for the detailed derivation),

$$d\boldsymbol{\xi} = \mathbf{A_0}\boldsymbol{\xi}\, dt + \mathbf{C_0}\, d\mathbf{W}, \qquad \boldsymbol{\xi}(t), \mathbf{W}(t) \in \mathbb{R}^3, \mathbf{A_0}, \mathbf{C_0} \in \mathbb{R}^{3\times 3}. \tag{3.9}$$

where

$$\mathbf{A_0} = \begin{bmatrix} -\beta\phi_2^* - \rho\psi^* - \mu & -\beta\phi_1^* & -\rho\phi_1^* \\ -\beta\phi_2^* & \beta\phi_1^* - \mu - \gamma & \rho\phi_1^* \\ 0 & \kappa\tau & \delta - \eta \end{bmatrix}, \tag{3.10}$$

and

$$\begin{aligned} \mathbf{C_0} &= \begin{bmatrix} C_{11} & C_{12} & 0 \\ C_{21} & C_{22} & 0 \\ 0 & 0 & C_{33} \end{bmatrix}^{1/2}, \\ C_{11} &= \beta\phi_1^*\phi_2^* + \rho\phi_1^*\psi^* + \mu(1-\phi_1^*), \\ C_{12} &= C_{21} = -\beta\phi_1^*\phi_2^* - \rho\phi_1^*\psi^* - \mu\phi_2^*, \\ C_{22} &= \beta\phi_1^*\phi_2^* + \rho\phi_1^*\psi^* + (\mu+\gamma)\phi_2^*, \\ C_{33} &= \kappa\tau\phi_2^* + \delta\psi^* + \eta\psi^*. \end{aligned} \tag{3.11}$$

Equations (3.9)-(3.11) are the Langevin equations derived by Wang et al. [1]. The drift coefficient matrix $\mathbf{A_0}$ is the Jacobian of the deterministic model (3.4) evaluated at the endemic equilibrium $(\phi_1^*, \phi_2^*, \psi^*)$. The diffusion matrix $\mathbf{C_0}$ is formed using the coefficients of the independent Wiener processes in

(3.2). This matrix is the square-root of the covariance matrix $\mathcal{B}$ found by Wang et al. [1]. This chapter focusses on the study of the linear system (3.9).

3.2.2 Parameter values

All simulations produced in this work use as default parameters the values in Table 3.1 largely taken from Wang et al. [1]. The values of parameters μ, η, β, and γ are based on empirical studies in the literature (see caption of Table 3.1). No data are available for ρ and δ and so they are varied within the range used by Wang et al. [1]. Note that the unit of the shedding rate τ is virion/mL/duck/year rather than virion/duck/day as erroneously reported in Wang et al. [1].

The values for the transmission parameters β and ρ can vary widely with seasonal climate changes and from one geographic area to another. We thus give a range of values for β and ρ and study the system's response to different levels and modes of transmission. As displayed in Table 3.1, we use a wider range of β values than was used by Wang et al. [1]. Observe that the infection term in (3.4) is given by $\beta\phi_2 = \beta I/N$ (rather than simply βI). In ecological terms, this means that β is the transmission rate for a frequency-dependent process rather than a density-dependent process. Roche and Lebarbenchon [175] find that β ranges from 0.00005 to 1500. Here, we plot our results for β values ranging from 0 to 300.

Avian influenza epidemic models exhibit noise sustained oscillations with a nonzero dominant frequency for a small range of β values, with some fixed value of ρ. Knowing only that β falls within a wide range of values, re-investigation of the relative contribution of each of the transmission modes is necessary. In particular, a larger β poses the possibility that direct transmission (β) alone, along with stochasticity, can drive avian flu epidemics with multi-annual periodicity.

Table 3.1: Descriptions of the parameters in the avian flu model and the values used in stochastic simulations. The range of values for β in bold-faced is the set of values that were used in [1].

Parameter	*Value/Range*	*Description*	*Unit*
N	10^3	Duck population size	duck
N_V	10^5	Virus concentration in the environment	virion/mL
μ	0.3	Duck birth and death rate	year^{-1}
δ	0.1	Virus replication rate	year^{-1}
τ	10^4	Virus shedding rate	virion mL^{-1}/duck/year
η	3	Virus clearance rate	year^{-1}
β	0.00005 to 1500 **(0-0.05)**	Direct transmission rate	$\text{duck}^{-1}\text{year}^{-1}$
ρ	$0-3$	Environmental transmission rate	year^{-1}
γ	5.5	Duck recovery rate	year^{-1}

Assessing the relative contribution of each of the transmission rates to disease recurrence requires a quantitative comparison of results. From (3.7), we see that if both

$$\beta < \mu + \gamma \quad \text{and} \quad \rho < \frac{(\eta - \delta)(\mu + \gamma)}{\kappa\tau}, \tag{3.12}$$

then $\mathcal{R}_0 < 1$. Using the values in Table 3.1, we find that when both $\beta < 5.8$ and $\rho < 0.16$ we have $\mathcal{R}_0 < 1$.

3.2.3 Preliminary analysis of the model

In this section we highlight key results from the analysis of the model of Wang et al. [1], and extend these results to include the role of $\mathcal{R}_0$ in the dynamics of avian flu. It is an established fact that the oscillations of a damped system can be sustained by stochasticity. Wang et al. [1] showed that the deterministic version of model (3.4) has a stable endemic steady-state (3.8) when $\mathcal{R}_0 > 1$. Here, we take the calculation one step further by determining the parameter ranges where (3.8) is a stable sink or a stable focus. We do this by plotting the eigenvalues of the Jacobian in (3.10) against $\mathcal{R}_0$ from (3.7). Figure 3.2 displays this plot.

In Figure 3.2, we see the eigenvalues of $\mathbf{A}_0$ plotted as functions of $\mathcal{R}_0$. We use the parameter values in Table 3.1 with $\beta = 0.05$. As ρ increases, so does $\mathcal{R}_0$. We observe that for $\mathcal{R}_0 < 1$, all of the eigenvalues are real and one has positive sign. As expected from Wang et al. [1], the endemic steady-state is unstable for this case and the system evolves to the disease-free equilibrium. A transition in the signs of the eigenvalues happens at $\mathcal{R}_0 = 1$. When $\mathcal{R}_0 > 1$, the system gives rise to a complex-conjugate pair of eigenvalues with negative real parts, and a negative real eigenvalue. Thus, the steady-state $(\phi_1^*, \phi_2^*, \psi^*)$ is a stable focus, i.e., the deterministic system exhibits damped population cycles. Note that a similar result is obtained if we fix ρ and let $\mathcal{R}_0$ vary with β.

Suppose that we represent the complex eigenvalues as $-\lambda \pm i\omega$ where λ and ω are magnitudes of the real and imaginary parts, respectively. For $\mathcal{R}_0 > 1$ in Figure 3.2, λ is clearly smaller than ω, because the upper solid curve is above the lower dashed curve with both curves drawn below the x-axis. Moreover, observe that ω increases faster than λ. Hence we deduce that the ratio λ/ω decreases as $\mathcal{R}_0$ increases.

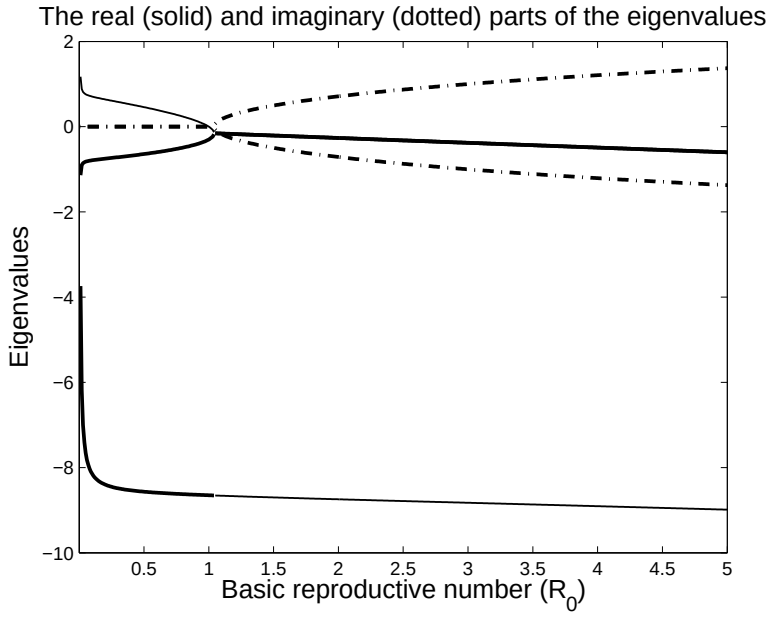

Figure 3.2: The real (solid curves) and imaginary (dash-dot curves) parts of the eigenvalues of $\mathbf{A}_0$ in (3.10) associated with the stability of the endemic steady-state (3.8) plotted against $\mathcal{R}_0$ in the case where $\beta = 0.05$. There are three real eigenvalues when $\mathcal{R}_0 < 1$, of which two are negative (thick solid lines). For $\mathcal{R}_0 > 1$, we have a complex-conjugate pair of eigenvalues with negative real parts (thick solid lines) and another negative eigenvalue (thin solid line). The imaginary parts of the complex eigenvalues are shown by the dotted lines. Other parameter values are shown in Table 3.1.

In Figure 3.3, we plot typical stochastic realizations of the avian flu model (3.2) for $\mathcal{R}_0 > 1$ using various combinations of parameters. These stochastic paths display oscillations sustained by noise.

We display the plots of stochastic realizations for the case when $\beta = 0.05$ but with different ρ values in Figures 3.3(a) and 3.3(b). Here we notice that higher amplitude and higher frequency of epidemics are observed in Figure 3.3(b) as compared to the fluctuation plotted in Figure 3.3(a) where ρ is twice as much. This observation is consistent with Figure 3.2.

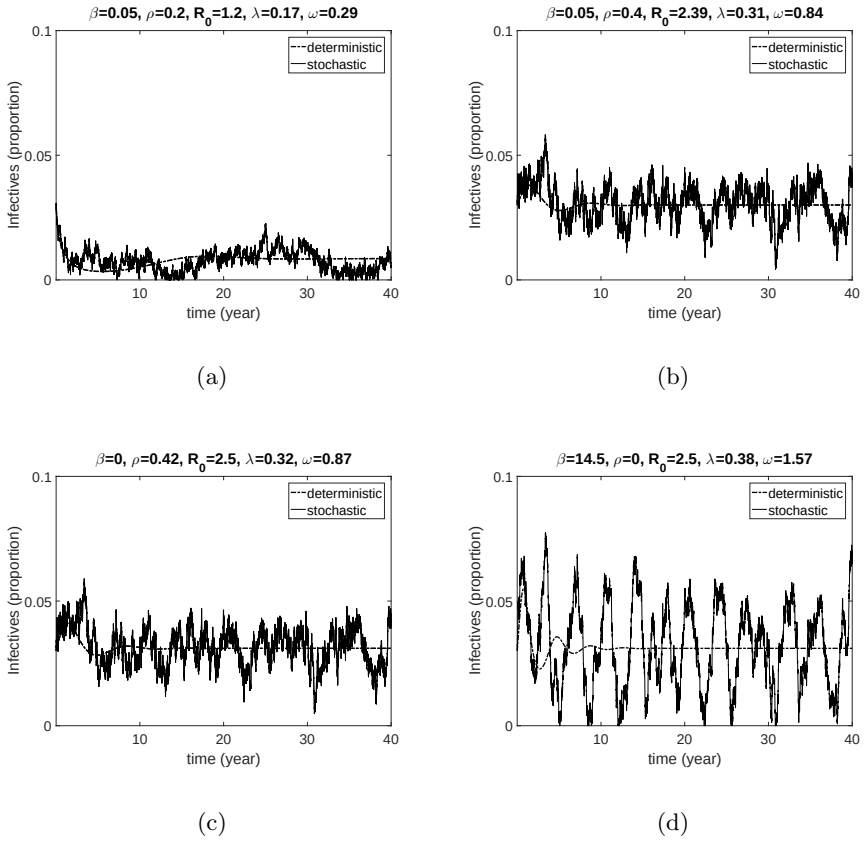

Figure 3.3: Simulation of the stochastic model (3.2) and its corresponding deterministic solution for $\beta = 0.05$ with (a) $\mathcal{R}_0 = 1.2$ and (b) $\mathcal{R}_0 = 2.5$, and for $\mathcal{R}_0 = 2.5$ with (c) $\beta = 0$ ($\rho = 0.4205$) and (d) $\rho = 0$ ($\beta = 14.5$).

In Figures 3.3(c) and 3.3(d), we plot stochastic paths for the case when either $\beta = 0$ or $\rho = 0$ but with roughly the same $\mathcal{R}_0$. In this comparison, $\mathcal{R}_0 \approx 2.5$, the upper bound of the confidence interval for the estimate of $\mathcal{R}_0$ for avian influenza in wild birds [183]. Comparing Figures 3.3(c) and 3.3(d), we observe that the periodicity and intensity of outbreaks in the two cases is different, even though the basic reproduction number is the same in the two cases. Current theory points toward the transmission mode as a determining factor for understanding the periodicity and intensity of avian flu outbreaks. Here, we develop a method that allows us to determine mathematically the effect of each transmission mode on the recurrence (periodicity and intensity)

of avian influenza.

3.3 Analytic methods

In this section we develop the analytic tools we need to understand the contribution of each transmission route to the dynamic behaviour of the model. In particular, our goal is to develop a mathematical description of the noise sustained oscillations that are observed in stochastic simulations, such as those shown in Figure 3.3.

3.3.1 Approximate solutions

We begin by defining an approximation for the process of oscillations produced by the stochastic avian flu model. Our starting point is the linear diffusion equation given by (3.9), which describes the process $\boldsymbol{\xi} = (\xi_S, \xi_I, \xi_V)$ near the endemic steady-state for large time. Under certain conditions, an approximate solution of (3.9) can be obtained using an extension of a result from Baxendale and Greenwood [50]. Specifically, if the eigenvalues of the drift coefficient matrix $\mathbf{A}_0$ (see (A.41) below) are of the form $-\zeta$, and $-\lambda \pm i\omega$ with λ/ω small, for $\zeta, \lambda, \omega > 0$, an approximate solution for (3.9) (see Appendix A.3 for details) is given by

$$\boldsymbol{\xi}^{app}(t) = y_1(t)\mathbf{Q}_{\bullet\mathbf{1}} + \frac{\tilde{\sigma}}{\sqrt{\lambda}}[\mathbf{Q}_{\bullet\mathbf{2}}, \mathbf{Q}_{\bullet\mathbf{3}}]\mathbf{R}_{-\omega t}\mathbf{S}_{\lambda t}, \tag{3.13}$$

where $\mathbf{Q}$ is the canonical form of the eigenvector matrix associated with the three eigenvalues. The vector $\mathbf{Q}_{\bullet\mathbf{j}}$ denotes the jth column of $\mathbf{Q}$. The stochastic process $y_1(t)$ is an Ornstein-Uhlenbeck (OU) process [182] with mean zero, decay rate ζ, and diffusion coefficient σ_1 obtained using the first row of the matrix $\mathbf{Q^{-1}C_0}$. The matrix $\mathbf{R}_{-\omega t}$ is a rotation matrix. It describes the circular motion of the process with frequency ω. The vector process $\mathbf{S}_{\lambda t}$ is a bi-variate OU process with independent components. The scalar $\tilde{\sigma}$ is determined by the last two rows of $\mathbf{Q^{-1}C_0}$ (the full expression is given by (A.22) in Appendix A.3). We express the large-time stationary solution of (3.2) as:

$$\begin{aligned} s(t) &= \phi_1^* + \frac{1}{\sqrt{N}}\xi_S(t) \approx \phi_1^* + \frac{1}{\sqrt{N}}\xi_S^{app}(t), \\ i(t) &= \phi_2^* + \frac{1}{\sqrt{N}}\xi_I(t) \approx \phi_2^* + \frac{1}{\sqrt{N}}\xi_I^{app}(t), \\ v(t) &= \psi^* + \frac{1}{\sqrt{N_V}}\xi_V(t) \approx \psi^* + \frac{1}{\sqrt{N_V}}\xi_V^{app}(t). \end{aligned} \tag{3.14}$$

The formulation (3.14) shows that the solution of (3.2) near the endemic steady-state behaves approximately like the product of a rotation and an OU process (3.13).

3.3.2 Power spectral density

We use the theoretical power spectral density (PSD) to determine the distribution of frequency components within the stochastic process produced by (3.9) with (3.10) and (3.11), and by their approximate form (3.13). A linear diffusion process is described as a general multivariate OU process, i.e.,

$$d\mathbf{x} = -\mathbf{A}\mathbf{x}(t)\ dt + \mathbf{B}\ d\mathbf{W}(t). \tag{3.15}$$

According to Gardiner [46], the PSD of an n-dimensional process is obtained from the main diagonal of the matrix given by:

$$\mathbf{S}(f) = \frac{1}{2\pi}(\mathbf{A} + if)^{-1}\mathbf{B}\mathbf{B}^T(\mathbf{A}^T - if)^{-1}. \tag{3.16}$$

From (3.16), it follows that the PSD of $\boldsymbol{\xi}(t)$ satisfying (3.9) is obtained from the main diagonal of the matrix

$$\mathbf{S}(f) = \frac{1}{2\pi}(-\mathbf{A}_0 + if)^{-1}\mathbf{C}_0\mathbf{C}_0^T(-\mathbf{A}_0^T - if)^{-1}. \tag{3.17}$$

On the other hand, the theoretical PSD of the approximate solution $\boldsymbol{\xi}^{app}(t)$ in (3.13) is determined using the coefficients of (see Appendix A.3 for derivation)

$$d\boldsymbol{\xi}^{app}(t) = \mathbf{A_0}\boldsymbol{\xi}^{app}\ dt + \mathbf{Q}\cdot\mathrm{diag}(\sigma_1, \tilde{\sigma}, \tilde{\sigma})\ d\mathbf{W}(t).$$

Thus, the PSD of $\boldsymbol{\xi}^{app}$ is obtained from

$$\mathbf{S}(f) = \frac{1}{2\pi}\cdot\mathrm{diag}(\sigma_1^2, \tilde{\sigma}^2, \tilde{\sigma}^2)\cdot(-\mathbf{A}_0 + if)^{-1}\mathbf{Q}\mathbf{Q}^T(-\mathbf{A}_0^T - if)^{-1}. \tag{3.18}$$

3.3.3 The intrinsic frequency and the decay rate of the deterministic dynamics

The approximation (3.13) depends explicitly on the intrinsic frequency ω and the decay rate λ of the damped oscillations predicted by the deterministic system (3.4). We can derive these quantities by obtaining the eigenvalues of the Jacobian matrix $\mathbf{A}_0$, which are the solutions of the characteristic polynomial given by

$$\nu^3 - a\nu^2 - b\nu - c = 0, \tag{3.19}$$

where:

$$\begin{aligned} a &= (\delta - \eta) - \mu\mathcal{R}_0 - \gamma - \mu + \beta/\mathcal{R}_0, \\ b &= -\mu(\eta - \delta + \gamma + \mu)\mathcal{R}_0 + \mu\beta/\mathcal{R}_0, \\ c &= -\mu(\eta - \delta)(\gamma + \mu)(\mathcal{R}_0 - 1). \end{aligned} \tag{3.20}$$

In Appendix A.6, we derive λ and ω as functions of β and ρ, using the roots of (3.19) and the avian flu parameters in Table 3.1. The results are shown in Figures 3.6 and 3.7(a) where we see λ/ω and ω are functions of β and ρ.

3.3.4 Numerical tools and functions

All numerical computations were done using MATLAB [184]. We computed the solution of the deterministic avian flu model (3.4) with the built-in function ode45(), an ordinary differential equation solver that is based on the Runge-Kutta (4,5) formula. Stochastic simulations of (3.2) and (3.9) were done using the Euler scheme (or the Euler-Maruyama scheme) [185], a first-order discretization method for stochastic differential equations. A time step of 0.01 was used for simulations of (3.2), (3.4), and (3.9).

3.4 Results

We present our results in two parts. First, we substitute the parameter values from Table 3.1 into the approximate solution (3.13) of (3.9) with (3.10) and (3.11). Second, we use the approximation to understand how the different transmission routes affect the dominant periodicity and the typical intensity of epidemics (see Section 3.4.2).

3.4.1 An approximate avian flu epidemic process

In this section, we use the approximation (3.13) to describe explicitly the noise sustained oscillations we saw in Figure 3.3. For consistency with previous work [1], we have chosen $\beta = 0.05$ and $\rho = 0.4$. This choice of parameters results in the endemic steady-state $\phi_1^* = 0.419$, $\phi_2^* = 0.03$, $\psi^* = 1.04$ with $\mathcal{R}_0 \approx 2.39$. The deterministic process defined by (3.4)

persists. The diffusion equation (3.9) with (3.10) and (3.11) becomes

$$\begin{aligned} d\boldsymbol{\xi} &= \mathbf{A}_0\boldsymbol{\xi}\ dt + \mathbf{C}_0\ d\mathbf{W}, \qquad \text{where} \\ \mathbf{A}_0 &= \begin{bmatrix} -0.716 & -0.021 & -0.168 \\ 0.410 & -5.78 & 0.168 \\ 0 & 100 & -2.9 \end{bmatrix}, \qquad \text{and} \\ \mathbf{C}_0 &= \begin{bmatrix} 0.568 & -0.161 & 0 \\ -0.161 & 0.568 & 0 \\ 0 & 0 & 2.494 \end{bmatrix} \end{aligned} \tag{3.21}$$

The eigenvalues of the Jacobian $\mathbf{A}_0$ in (3.21) are $-\zeta = -8.78$ and $-\lambda \pm i\omega = -0.309 \pm 0.838i$. The ratio $\lambda/\omega = \frac{0.309}{0.838} \approx 0.369$ is sufficiently small that we can approximate the process $\boldsymbol{\xi}(t)$ by (3.13), as evidenced by the comparison of PSDs in Figure 3.4.

Using the eigenvalues above, we arrive at the canonical matrix of eigenvectors, i.e., the columns are eigenvectors of $\mathbf{A}_0$, given by

$$\mathbf{Q} = \begin{bmatrix} 0.021 & -0.078 & 0.16 \\ -0.059 & 0.026 & 0.008 \\ 0.998 & 0.984 & 0 \end{bmatrix}. \tag{3.22}$$

The matrix $\mathbf{C}_0$ in the diffusion term of (3.21) gives us

$$\boldsymbol{\Sigma} = \mathbf{Q}^{-1}\mathbf{C}_0 = \begin{bmatrix} 2.13 & -6.43 & 0.834 \\ -2.16 & 6.52 & 1.69 \\ 2.23 & 3 & 0.715 \end{bmatrix}. \tag{3.23}$$

We compute σ_1 (see Appendix A.3) by taking the norm of the first row of the matrix $\boldsymbol{\Sigma}$ in (3.23),

$$\sigma_1 = ||(2.13, -6.43, 0.834)|| \approx 6.82.$$

We form the matrix $\tilde{\mathbf{C}} = (\tilde{\boldsymbol{\Sigma}}\tilde{\boldsymbol{\Sigma}}^\intercal)^{1/2}$ where,

$$\tilde{\boldsymbol{\Sigma}} = \begin{bmatrix} -2.16 & 6.52 & 1.69 \\ 2.23 & 3 & 0.715 \end{bmatrix}, \tag{3.24}$$

to obtain $\tilde{\sigma}^2 = Tr(\tilde{\mathbf{C}}\tilde{\mathbf{C}}^\intercal)/2$ and so $\tilde{\sigma} \approx 5.68$.

Using (3.13), the solution to (3.21) near the endemic steady-state is approximately

$$\begin{bmatrix} \xi_S^{app}(t) \\ \xi_I^{app}(t) \\ \xi_V^{app}(t) \end{bmatrix} = y_1(t) \begin{bmatrix} 0.021 \\ -0.059 \\ 0.998 \end{bmatrix} + 10.2 \begin{bmatrix} -0.078 & 0.16 \\ 0.026 & 0.008 \\ 0.983 & 0 \end{bmatrix} \mathbf{R}_{-0.838t} \mathbf{S}_{0.309t}, \tag{3.25}$$

where

$$dy_1 = -8.78 y_1 \, dt + 6.82 \, dW_1. \tag{3.26}$$

One way to see if the process (3.25) is a reasonable approximate solution for (3.21) is to compute the theoretical PSDs of the exact solution $\boldsymbol{\xi}(t)$ of (3.21) and the approximation $\boldsymbol{\xi}^{app}(t)$ in (3.25) using formulae (3.17) and (3.18), respectively. In Figure 3.4, the PSDs of fluctuations $\boldsymbol{\xi}(t)$ and $\boldsymbol{\xi}^{app}(t)$ agree fairly well. The dominant frequency is close to the intrinsic frequency $\omega = 0.8377$.

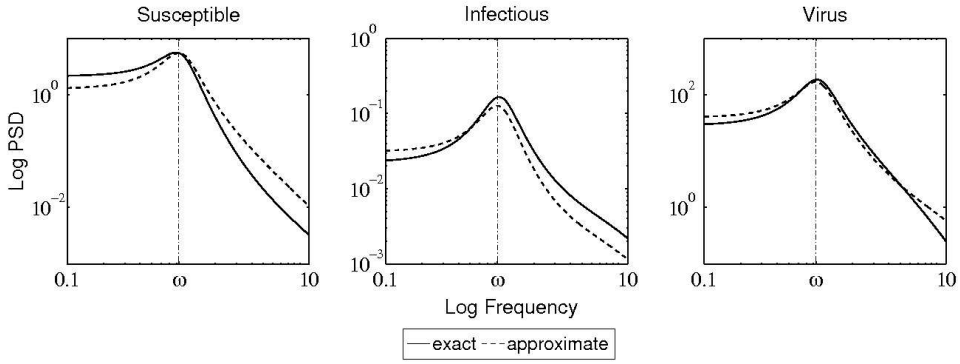

Figure 3.4: Comparisons between the theoretical PSD of the exact process $\boldsymbol{\xi}(t)$ (solid line) satisfying (3.21) and the approximate process $\boldsymbol{\xi}^{app}(t)$(dashed line) given by (3.25), for the fluctuations of the susceptible, infectious, and the virus populations. Default parameter values are in Table 3.1 with $\beta = 0.05$ and $\rho = 0.4$.

The process $\boldsymbol{\xi}^{app}(t)$ depends on the OU process $y_1(t)$ whose dynamics are described by (3.26), an OU process with asymptotic mean zero, decay rate 8.78, and diffusion coefficient 6.82. From the first term of (3.25), we find that the contribution of the process $y_1(t)$ to host fluctuation processes, $\xi_S(t)$ and $\xi_I(t)$, is very small as compared to that of the virus fluctuation process $\xi_V(t)$. We use the stationary standard deviation to measure the

typical amplitude of the population fluctuations. Note that the stationary variance of the process $y_1(t)$ is $46.51/(2 \times 8.78) \approx 2.65$, i.e. stationary standard deviation $\sqrt{2.65} \approx 1.63$. The stationary standard deviation, i.e. typical amplitude, of the stochastic path for the process $\boldsymbol{\xi}^{app}(t)$ (see (3.29) or (A.30) in Appendix A.3), is given by

$$SSD_i \approx \sqrt{2.65 q_{i1}^2 + 10.2^2 r_i^2}. \tag{3.27}$$

The computed typical amplitudes of the susceptible, infectious, and virus population fluctuations are $1.81, 0.29$, and 10.18, respectively. In Figure 3.5, the stochastic realizations for the different population fluctuations given by (3.21) and (3.13) are plotted along with their stationary standard deviations indicated by horizontal lines to indicate that the stochastic oscillations generally lie within one stationary standard deviation.

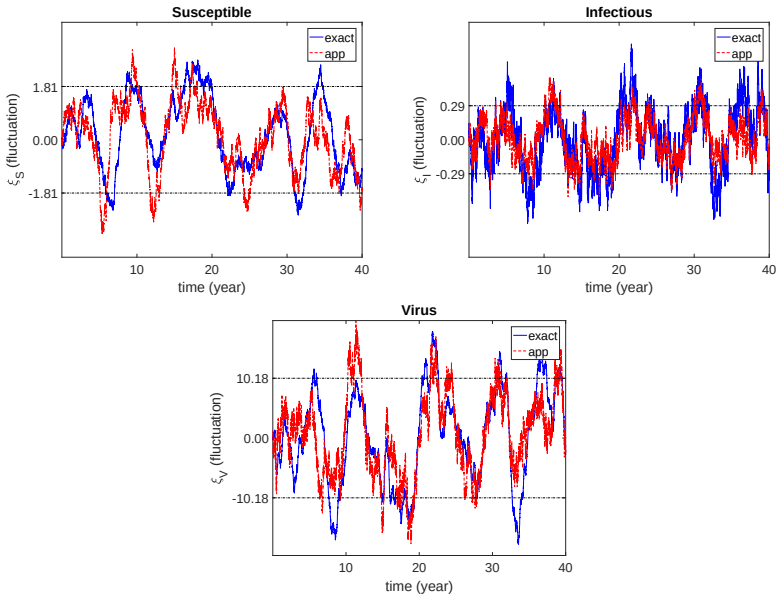

Figure 3.5: A stochastic realization of the population fluctuations by simulating (3.21) (solid line) and (3.25) (dashed line) and their corresponding stationary standard deviations, i.e. typical amplitudes (in horizontal lines) computed using (3.28).

Writing (3.25) in polar form (see Appendix A.3), we obtain

$$\begin{aligned}
\xi_S(t) &\approx 0.021 y_1(t) + 1.82|\mathbf{S}_{0.309t}| \cos(\varphi_{0.309t} - 0.838t - 2.02),\\
\xi_I(t) &\approx -0.059 y_1(t) + 0.275|\mathbf{S}_{0.309t}| \cos(\varphi_{0.309t} - 0.838t - 0.313),\\
\xi_V(t) &\approx 0.998 y_1(t) + 10|\mathbf{S}_{0.309t}| \cos(\varphi_{0.309t} - 0.838t).
\end{aligned} \tag{3.28}$$

We know from the approximate form (3.28) that the phase differences between the population fluctuation processes $\xi_i(t)$ are constants. For instance, the susceptible duck population fluctuation is out of phase with other populations in the system. With respect to the virus population, the susceptible duck population exhibits noise-sustained oscillations with a phase advance, with respect to the virus population, of approximately $2.02/\omega = 2.02/0.838 \approx 2.4$ years. The infectious duck population, on the other hand, oscillates with a phase advance of $0.313/0.838 \approx 0.37$ years from the virus population.

3.4.2 The relative contribution of the different transmission routes

One of the key factors leading to outbreaks is the rate of transmission. As outlined previously, there are two transmission routes for avian flu: direct transmission of virus from one duck to another, and indirect transmission of viruses via the environment. We use the approximation $\boldsymbol{\xi}^{app}(t)$ to shed light on the relative importance of direct and indirect transmission to outbreak occurrence.

As a first step, we identify the constraints for β and ρ under which one expects to observe recurrent epidemics and where the approximation is valid. We use the parameter ranges from Table 3.1 and display in the top panels of Figure 3.6 a plot of λ/ω as a function of β and ρ.

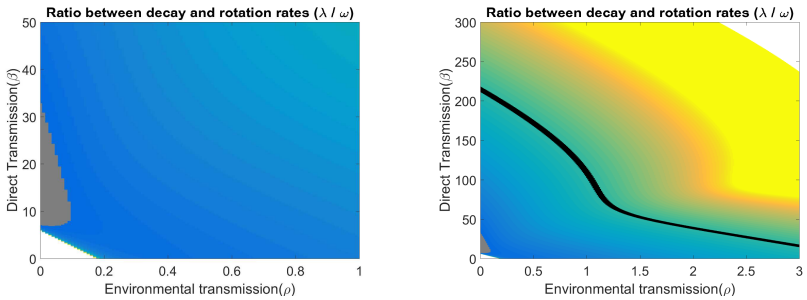

(a)

(b)

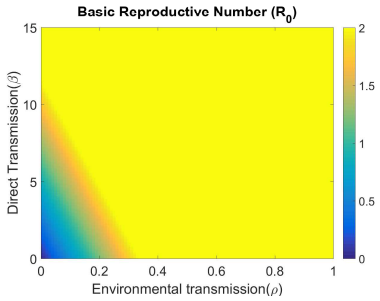

(c)

Figure 3.6: (a,b) Plot of the ratio λ/ω as a function of β and ρ. The triangular white region in the lower left is where no recurrence is observed. Panel (a) considers $0 \leq \beta \leq 50$ and $0 \leq \rho \leq 1$ while Panel (b) considers $0 \leq \beta \leq 300$ and $0 \leq \rho \leq 3$. The grey region in both panels is where $\lambda/\omega \leq 0.35$. In Panel (b), the black curve corresponds to $\lambda/\omega = 1$. (c) Plot of the basic reproduction number $\mathcal{R}_0$ as a function of β and ρ. The darker (blue online) shade indicates that no epidemic can be observed in the model for this parameter region. Parameter values and ranges from the literature are in Table 3.1.

In Figure 3.6(a), we see a triangular region surrounding $\beta = \rho = 0$ where the approximation is no longer relevant because no recurrent epidemics can be observed there. In the triangular parameter region, $\mathcal{R}_0 \leq 1$ as seen in Figure 3.6(c) and there are no recurrent epidemics. Within a large portion of the remaining parameter region defined by $0 \leq \beta \leq 15$ and $0 \leq \rho \leq 1$ (see

Figure 3.6(a)), λ/ω is sufficiently small that the approximation is valid.

We further extend the range of transmission parameters to $0 \leq \beta \leq 300$ and $0 \leq \rho \leq 3$ as displayed in Figure 3.6(b) to show the behaviour of λ/ω for larger values of β and ρ. We observe that when β and ρ are both very large, as depicted by the white region in the upper portion of Figure 3.6(b), $\lambda/\omega > 1$ and so the approximation is not necessarily valid. In Figure 3.6(b), a black curve is drawn, which corresponds to $\lambda/\omega = 1$. The approximation is valid for β and ρ values in the region well below this curve. For instance, it is guaranteed that the approximation can be used to precisely describe the system in our parameter space when $0 < \lambda/\omega \leq 0.35$ (grey region). Since there is a sufficient portion of the region defined by $0 \leq \beta \leq 300$ and $0 \leq \rho \leq 3$ where the approximation is applicable, the following analysis focusses on the region well below the black curve to study how the different routes of transmission influence the periodicity and intensity of recurrent epidemics reflected by the model.

Dominant outbreak period

The period of any oscillating function is the inverse of the frequency. We analyze the dominant outbreak period of the simulated epidemic from (3.9) by considering the intrinsic frequency of the deterministic system. For a parameter range where the approximation (3.13) is close to the exact process satisfying (3.9) (see Figure 3.4), the dominant frequencies predicted by the two are very close. In addition, this frequency is close to that from the deterministic system when λ is small [186]. Hence we use ω given by formula (A.44) (see Appendix A.6).

Using formula (A.44) in Appendix A.6, we compute the intrinsic frequency $\omega = \omega(\rho, \beta)$ over $0 \leq \rho \leq 3$ and $0 \leq \beta \leq 300$ for the parameters in Table 3.1 to obtain Figure 3.7(a).

We are interested in the parameter domain when $\mathcal{R}_0 > 1$, that is, where the disease has recurring epidemics (see Figure 3.6(c)). In Figure 3.7(a), we find a region where the intrinsic frequency is relatively high, namely for low environmental transmission ($\rho \leq 0.5$) and high direct transmission ($\beta \geq 100$). When the β and ρ values are both very low or very high, the intrinsic frequency is near zero, and so all populations fluctuate around their endemic equilibrium very slowly.

The steady-state infectious proportion is approximately 0.05 and is accompanied by a very low steady-state proportion of susceptibles (see Figure 3.7(b)). Thus in this parameter region, the host population is mainly composed of individuals that have recovered from the disease.

We also find that, for (β, ρ) values where the approximation is valid, the dominant outbreak period is 2 to 8 years, as seen by comparing the grey region of Figure 3.6(b) with Figure 3.7(a).

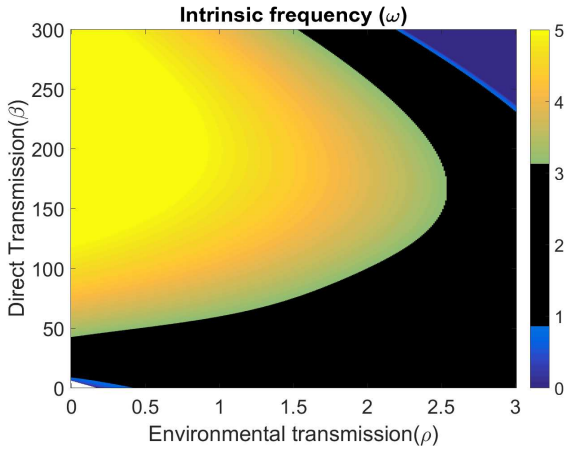

(a)

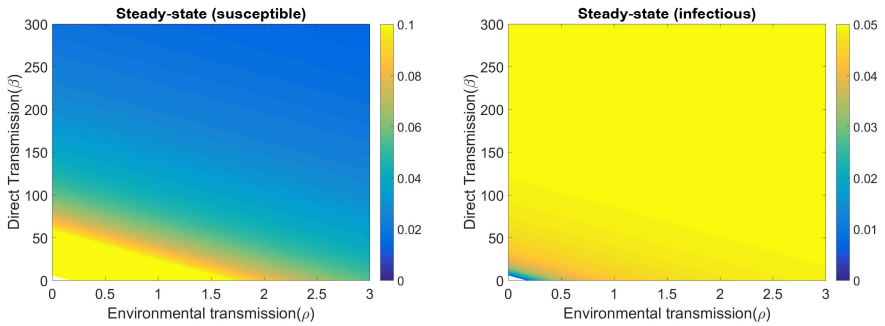

(b)

Figure 3.7: Plots of (a) the intrinsic frequency ω and (b) the steady-state proportions of the susceptible and infectious populations as functions of the direct transmission rate β (left) and the environmental transmission rate ρ (right). The dark region in (a) is where the 2 to 8 year recurrence period is observed. Parameter values are in Table 3.1.

For the default parameter values with $\beta = 224$ and ρ from 0 to 0.05, the largest 5.6 radians per year, corresponding to an avian flu outbreak period of $2\pi/5.6 \approx 1.12$ years. For the default parameter values with $\beta = 224$, the highest intrinsic frequency reached is 5.6 radians per year corresponding to $0 < \rho < 0.05$. This maximum intrinsic frequency corresponds to an avian flu outbreak period of $2\pi/5.6 \approx 1.12$ years (Figure 3.7(a)).

We determine the outbreak periodicity for various values of either β or ρ alone by computing the theoretical PSD of the linear system (3.9) with (3.10) and (3.11) (Figure 3.8). When there is no direct transmission, the dominant frequency of the simulated outbreaks increases with the environmental transmission rate (Figure 3.8(a)). Similarly, the dominant frequency increases with the direct transmission rate in the absence of environmental transmission (Figure 3.8(b)).

In parallel with the increasing dominant frequency, the width of the PSD also increases with increasing environmental transmission rate. This means that, at low transmission rates, the outbreak pattern is more regular, and becomes more irregular as transmission rate increases. Consequently, when transmission rates are high, the timing of outbreaks is more difficult to predict.

Note here that we have chosen values of ρ (when $\beta = 0$) and β (when $\rho = 0$) that give roughly the same basic reproduction number $\mathcal{R}_0$, allowing for comparison between the theoretical PSDs. Consider the PSDs associated with $(\rho, \beta) = (0.22, 0)$ and $(\rho, \beta) = (0, 7.5)$ in Figure 3.8(b) and 3.8(a), respectively. Both parameter values correspond to $\mathcal{R}_0 \approx 1.3$, a value used by [1] to define a boundary between disease persistence and stochastic extinction for their model. If we compare the PSDs between Figures 3.8(a) and 3.8(b), we find that, with the values in Table 3.1, the model predicts larger-valued PSDs in the case when environmental transmission is absent than when direct transmission is absent.

The corresponding dominant outbreak period is shown in Figure 3.8(c) and 3.8(d). Both dominant periods of the approximate and exact process are shown. The results are indistinguishable. We also observe in Figure 3.8(c) that, for $\beta = 0$, an increase in ρ from 0.22 to 1.1 results in a decline of approximately 12 years in the outbreak period. However, for $\rho = 0$, an increase in β from 7.5 to 37.5 only results in a decrease of approximately 7 years in the outbreak period (see Figure 3.8(d)). In other words, when the disease is epidemic but $\mathcal{R}_0$ is close to 1, increasing the environmental transmission can cause a greater drop in the outbreak period than increasing direct transmission. However, for larger transmission rates we find that the dominant outbreak period declines slowly as transmission rate increases and

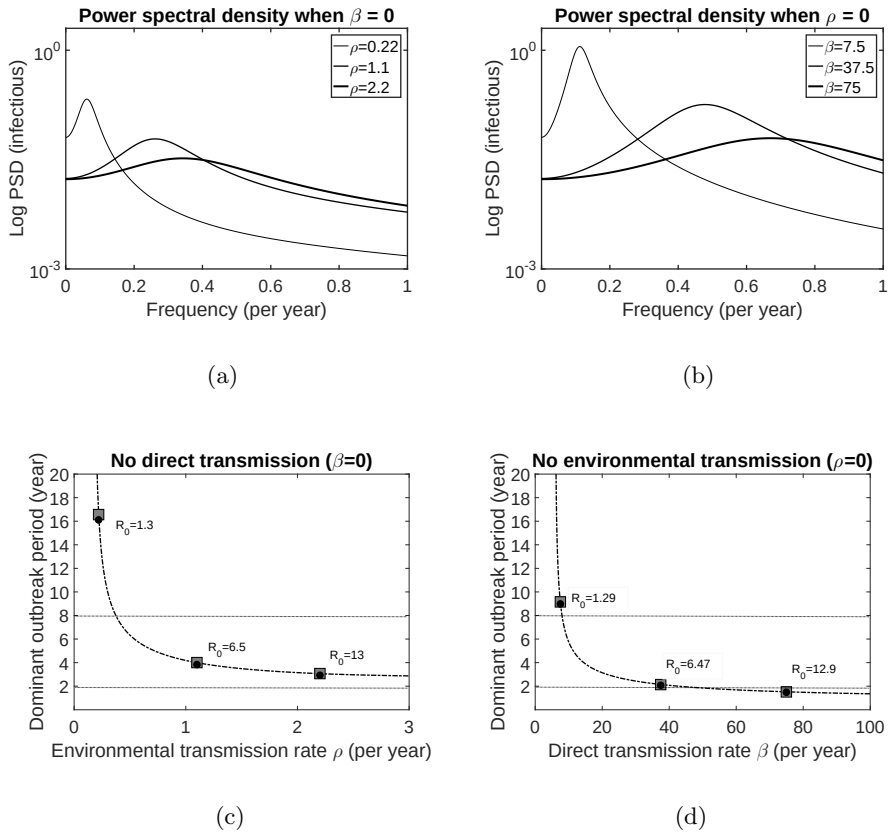

Figure 3.8: *Top panels:* Theoretical PSDs of the infectious population fluctuations $\xi_I(t)$ for (a) $\rho = 0.22, 1.1, 2.2$ when $\beta = 0$ and (b) $\beta = 7.5, 37.5, 75$ when $\rho = 0$. The linewidth of the PSD curves increases with the transmission parameter values. *Bottom panels:* Approximate dominant outbreak period, $2\pi/\omega$ with formula (A.42), as a function of (c) ρ when $\beta = 0$ and (d) β when $\rho = 0$. The square markers in (c) and (d) are located at $\rho = 0.22, 1.1, 2.2$ and $\beta = 7.5, 37.5, 7.5$, respectively. The black dots represent the exact dominant outbreak period obtained using the theoretical PSDs in the top panels. The black dots and square markers are indistinguishable from each other. The horizontal lines in (c) and (d) indicate the 2 to 8 year periods observed in actual prevalence data (See [1]). The corresponding R_0 values are also shown. Default values for all other parameters are given in Table 3.1.

so the effects of changes in the individual transmission rates may be difficult to distinguish.

Typical intensity of outbreaks

For each $i = S, I, V$, the stationary standard deviation of $\xi_i^{app}(t)$ is

$$SSD_i = \sqrt{\frac{q_{i1}^2 \sigma_1^2}{2\zeta} + r_i^2 \frac{\tilde{\sigma}^2}{\lambda}} \tag{3.29}$$

for $r_i^2 = q_{i2}^2 + q_{i3}^2$ where q_{ij} are entries of the matrix $\mathbf{Q}$, e.g. (3.22), to determine the typical intensity of outbreaks. Here we show how the typical outbreak intensity is influenced by each type of transmission. In Figure 3.9, we display the plots of SSD_i's of each process $\xi_i^{app}(t)$ as functions of β and ρ.

In Figure 3.9, we have focused on the (ρ, β) region that corresponds to $\mathcal{R}_0 > 1$ and λ/ω small, i.e. where the approximation method is valid. Typical amplitudes in simulated epidemics when $0 \leq \rho \leq 1$ and $0 \leq \beta \leq 100$ are depicted in Figure 3.9.

In Figure 3.9(b), we see that in general, fluctuation amplitudes are higher for larger values of β, the direct transmission rate. On the other hand, in Figure 3.9(a), the fluctuation amplitudes for the susceptibles are lower for larger β, and there is high sensitivity to β. Figure 3.9(c) shows an optimal region in β for the fluctuation amplitude of virus especially for low ρ.

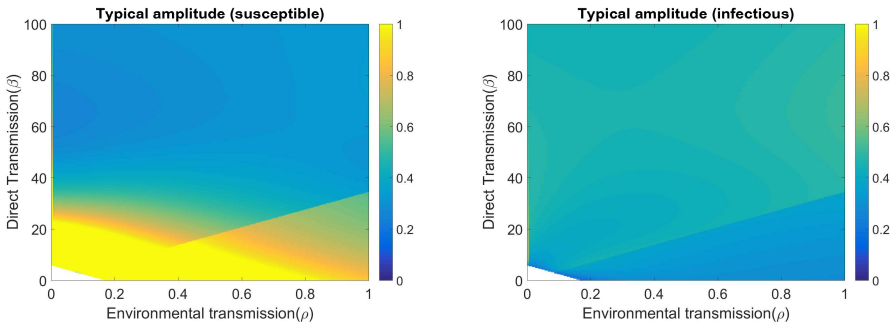

(a) (b)

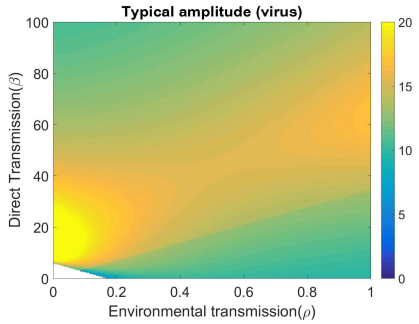

(c)

Figure 3.9: Typical amplitude (intensity) of the fluctuations in the proportion of (a) susceptible, (b) infectious, and (c) virus populations, measured by their stationary standard deviations (3.29) as a function of the environmental transmission rate ρ and β. All other parameters are at the default values in Table 3.1.

3.5 Discussion

We have written the Wang et al. [1] stochastic model for avian influenza including direct and environmental transmission routes as stochastic differential equations using the method of Kurtz [10], following Greenwood and Gordillo [47]. Under large host and virus populations, the stochastic model approaches the deterministic system wherein, for $\mathcal{R}_0 > 1$, the endemic steady state is a stable focus. Our discussion of the avian flu model

in Section 3.2 suggests that the disease can persist ($\mathcal{R}_0 > 1$) if either one of the two transmission routes is sufficiently strong. We have also shown via stochastic simulations that the model gives rise to noise sustained oscillation in the presence of either transmission route.

Our analysis allows us to conclude that the temporal pattern of epidemic recurrence is the sum of two processes: (1) a scaled OU process with long-term mean zero, and (2) the product of a rotation and a slowly varying standard OU process in two dimensions. This structure holds for any disease where the decay rate in the amplitude of successive epidemics is sufficiently slower than the frequency of recurrent epidemics. That is, as the deterministic process decays, there will be several noticeable epidemics before the system decays to near the steady state.

After linearisation, we study the stochastic path in three-dimensional space. The sample path behaves as an OU process that travels along the axis pointing in the direction of an eigenvector associated with the negative real eigenvalue, and cycles on the subspace spanned by the eigenvectors associated with the complex eigenvalues (See Appendix A.4).

We have shown that there is good agreement between the theoretical PSDs of the exact and approximate processes for each population type considered in the system. Although we observe small differences in the PSDs of the approximate and exact processes, we find that the two PSDs have closely matching dominant frequencies. The dominant frequency of the simulated epidemics is close to the intrinsic frequency ω. We know from e.g. Greenwood et al. [186] that the difference between the dominant and intrinsic frequencies is $\mathcal{O}(\lambda)$, where λ, which is small here, represents the decay rate of the deterministic solution. Based on the polar form of the approximate process (3.28), each population cycles at a frequency corresponding to the intrinsic frequency ω perturbed by a stochastic phase process $\varphi_{\lambda t}$.

We also notice that the PSDs of the exact process appear flat for low frequency and have a downward slope for high frequency, which are features of the PSD of a stationary OU process [46]. This observation is in agreement with the approximate process we derived (3.25), which is a sum of an OU process (3.26), and the product of a rotation and a bi-variate standard OU process.

Previous studies [1, 13, 165] of the recurrence of avian flu epidemics have focussed on identifying mechanisms that explain the multi-annual periodicity of the disease. Wang et al. [1] claimed that environmental transmissibility is an important ingredient in explaining the 2 to 8 year period of avian flu. Using theoretical PSDs, they showed that for a fixed direct transmission rate, the outbreak period decreases as the environmental transmission rate

is increased. Their results are based on the assumption that direct transmission is weak. However, according to Roche and Lebarbenchon [175], the direct transmission rate β can have a wide range of values. Our results show that the 2-8 year outbreak period can also be obtained chiefly as a result of direct transmission, and even in the absence of environmental transmission. Thus we conclude that both transmission rates are important factors in understanding the multi-year periodicity of disease outbreaks.

Our approach also allows us to obtain approximate values for the typical amplitude of the population fluctuations, because the stationary behaviour of the OU process is known. For the given avian flu parameter values, we find that the virus population fluctuations peak after the infectious population fluctuations peak. Typically, the phase lag is on the order of $0.3127/\omega = 0.31/0.8377 \approx 0.37$ of a year, i.e. approximately 4 months. This lag is reasonable as we have evidence that virus can be excreted by an infected bird for many days after infection [97].

High amplitude epidemics arise when the direct transmission rate is high. In this case, the stochastic perturbation phase process changes slowly and so the dominant frequency of epidemics is comparatively regular.

Our analysis emphasizes that the interaction of stochasticity and transmission routes indeed plays an important role in determining outbreak periodicity and intensity. We suggest here that the recurrent pattern of avian flu outbreaks in itself is a result of noise amplification wherein its periodicity and amplitudes are influenced by either or both of the modes of transmission. The approach we introduced here could be used to perform a systematic study of other recurrent diseases.

Chapter 4

Sustained Oscillations in Stochastic Models With Periodic Parametric Forcing

4.1 Motivation

Modellers have long been interested in identifying the mechanisms behind cyclic population fluctuations in natural systems such as those observed in infectious diseases [3, 187, 188]. In one theory, the fluctuations are attributed to the stochastic nature of the system. For example, in population biology, the number of individuals over time could fluctuate simply due to the presence of demographic stochasticity (i.e. uncertainty in the birth and death times) together with stochasticity in infection and recovery rates. In the absence of any stochasticity, we have damped oscillations over a large parameter range [32]. Sometimes the cyclic dynamics are modelled as a deterministic system with time-periodic parameter, i.e. parametric forcing, such as seasonal forcing driving recurrent epidemics [28, 39]. A rather more general model of irregular cyclic dynamics has been introduced and simulated quite recently. The model incorporates both randomness and periodic forcing to describe the fluctuating patterns observed in systems with large populations [11, 33, 44] and expressed in terms of Itô stochastic differential equations (SDEs). These SDEs can be constructed starting from an ODE model derived from compartmental analysis and adding Gaussian white noise with covariance matrix that depends on the terms of the ODEs. Periodic parametric forcing is introduced in the model by assigning at least one of the parameters to be a periodic function of time. Here I coin the phrase *stochastic periodically parametrically forced (stochastic PPF) models* to mean stochastic models with time-periodic parameters. Such models are SDE systems with time-dependent periodic drift and/or diffusion coef-

ficients.

Stochastic PPF models is appear in studies of disease dynamics [33, 37, 164] that are mainly concerned with characterizing the sustained oscillations exhibited in stochastic simulations of the system. In stochastic PPF models, the stochastic fluctuations around a limit cycle are identified by "linearising" the stochastic PPF model around the solution of its deterministic analogue. Though the nature of stochastic fluctuations around a limit point is well understood [26, 35, 50], limited knowledge is available about stochastic fluctuations around a limit cycle.

Typically, solutions of linear SDE models are studied using numerical approaches [51]. However, it is sometimes possible for approximate solutions to be written in closed form. In the work of Baxendale and Greenwood [50], for example, an approximate solution was obtained for n-dimensional ($n \geq 2$) linear SDE systems whose drift and diffusion coefficient matrices are constant matrices, and where the eigenvalues of the drift coefficient matrix include a complex-conjugate pair, $-\lambda \pm i\omega$, with $\lambda, \omega > 0$, and other negative real eigenvalues. They showed that as long as $\lambda \ll \omega$, such a SDE system has an approximate solution in closed form that describes the nature of noise-sustained oscillations as a constant times a circular motion multiplied by a bivariate standard Ornstein-Uhlenbeck (OU) process [182] time-scaled by λ. They compared the power spectral densities (PSD) of the numerical and approximate solutions of the SDE system and found agreement. The closed form approximation allows the identification of the source of the dominant frequency of the fluctuations and the parameters that control amplification. Our aim here is to obtain such a closed form approximate solution for stochastic PPF models linearized around a limit cycle.

From numerical evidence found in the literature [11, 44], we know that the stochastic fluctuations around the limit cycle, produced by stochastic PPF models, have three governing frequencies: the frequency the around the limit cycle in response to the stochastic perturbation, the sum and difference of the response and limit cycle frequencies. The response frequency is the dominant one among the three and is identified as the imaginary part of the complex-conjugate pair of Floquet exponents [189]. Though it has been suggested that these frequencies resulted from stochastic amplifications, it has not been understood how they arise from the solutions of the model.

We begin with a general formulation of discrete state-space two-dimensional stochastic PPF models and their macroscopic limit, using the method of Kurtz [10], an approach for developing SDE models which parallels the Van Kampen [9] system-size expansion. Assuming that a limit cycle solution exists in the macroscopic limit, we show that the stochastic fluctuations can

be written as a linear diffusion equation with time-dependent drift and diffusion coefficients. We use the approach of Baxendale and Greenwood [50] to obtain an approximate solution of the linear stochastic model. First, we re-formulate the problem using a series of transformations similar to those of Baxendale and Greenwood [50] but for time-varying coefficients. In one of these transformations, we apply Floquet theory [52].

We find that when the Floquet exponents are a complex-conjugate pair with negative real part and the perturbation rotates more quickly than it decays, the stochastic PPF model can approximated by a standard OU process multiplied by periodic matrices carrying the response frequency predicted by Floquet theory and the limit cycle frequency. Moreover, the process is amplified by the ratio of a time-averaged standard deviation from the time-varying co-variance matrix and the square-root of the magnitude of the real part of the complex-valued Floquet exponent.

We illustrate our approximation result using a linear harmonic oscillator model with one-dimensional noise. We compare the power spectral densities (PSDs) of the exact and approximate solutions computed numerically, for various forcing amplitudes and noise levels. By considering a simple case of the model and using a fundamental matrix solution that contains the well-studied Mathieu functions [190], we provide further insight into the approximate solution. For instance, in Section 4.4, we compute stochastic differential equations for the amplitude and phase processes. In Section 4.5, we apply to a stochastic epidemic model with seasonal forcing, in the context of a host-pathogen model for avian influenza with time-dependent environmental transmission.

This chapter is organized as follows. In Section 2, we present the model and its assumptions, and derive an expression for the linearisation around its limit cycle. This fluctuation process is a stochastic PPF model. We derive in Section 3 a useful approximation to the stochastic PPF model of Section 2. This explicit form of the solution of the system that allows us to tease apart the effects of stochasticity and periodic forcing. In Section 4, we illustrate our approximation technique with a parametrically forced linear oscillator model with noise. In Section 5 is an example of the applicability of the approximation to an avian flu model with demographic stochasticity and seasonal forcing. Finally, further analysis and discussion of theoretical results and the significance of the approximation are in Section 6 with emphasis on how the approach can shed light on fluctuations observed in epidemic models.

4.2 A periodically parametrically forced (PPF) Markov model

4.2.1 Description

We consider a continuous-time $\mathbb{Z}^2$-valued Markov process $\mathbf{X}(t) = (X_1(t), X_2(t))^T$ with transition rates, or jump rates, $f^{(\mathbf{r})}(\mathbf{X}(t), t)$ where $\mathbf{r} \in \mathbb{R}^2$ ranges over a set of possible jumps between pairs of integers. These rates explicitly depend on time t. Following Kurtz [10], we write the process $\mathbf{X}(t)$ as

$$\mathbf{X}(t) = \mathbf{X}(0) + \sum_{\mathbf{r}} \mathbf{r}\mathcal{N}^{(\mathbf{r})}(t), \tag{4.1}$$

where $\mathcal{N}^{(\mathbf{r})}(t)$ is the number of jumps of type $\mathbf{r}$ jumps within the time interval $[0, t]$. Here $\mathcal{N}^{(\mathbf{r})}(t)$ is a counting process with rate $f^{(\mathbf{r})}(\mathbf{X}(t), t)$ and $\mathcal{N}^{(\mathbf{r})}(t) - \int_0^t f^{(\mathbf{r})}(\mathbf{X}(s), s)\ ds$ is a martingale and this implies that

$$\mathcal{N}^{(\mathbf{r})}(t) = \Psi^{(\mathbf{r})}\left(\int_0^t f^{(\mathbf{r})}(\mathbf{X}(s), s)\ ds\right), \tag{4.2}$$

where $\Psi^{(\mathbf{r})}(u)$ are independent, unit Poisson processes with $u = \int_0^t f^{(\mathbf{r})}(\mathbf{X}(s), s)\ ds = E[\mathcal{N}^{(\mathbf{r})}(t)]$ (Section 10.4 of Kurtz [53]).

Suppose that $X_1(t) + X_2(t) = N$ where N is constant for all $t \geq 0$. Combining (4.2) to (4.1), we write the scaled process $\mathbf{X}^N(t) \equiv \frac{\mathbf{X}(t)}{N}$ as

$$\mathbf{X}^N(t) = \mathbf{X}^N(0) + \sum_{\mathbf{r}} \frac{\mathbf{r}}{N}\Psi^{(\mathbf{r})}\left(\int_0^t N f^{(\mathbf{r})}(\mathbf{X}^N(s), s)\ ds\right). \tag{4.3}$$

The integrand in (4.3) represents stochastic rates in density-dependent processes. In this thesis, the separate dependence on the time variable in the jump rate will be a periodic parametric forcing.

Using essentially the proof of Kurtz [10], we see that the diffusion approximation of (4.3) can be written similarly as

$$\tilde{\mathbf{X}}^N(t) = \tilde{\mathbf{X}}^N(0) + \sum_{\mathbf{r}} \frac{\mathbf{r}}{N}B^{(\mathbf{r})}\left(\int_0^t N f^{(\mathbf{r})}(\tilde{\mathbf{X}}^N(s), s)\ ds\right), \tag{4.4}$$

where $B^{(\mathbf{r})}(t) = W^{(\mathbf{r})}(t) + t$ and $W^{(\mathbf{r})}(t)$ are independent, standard Brownian motion (Wiener process). Hence, (4.4) can be written as the Itô equation

$$\tilde{\mathbf{X}}^N(t) = \tilde{\mathbf{X}}^N(0) + \int_0^t \mathbf{F}(\tilde{\mathbf{X}}^N(s), s)\, ds + \sum_{\mathbf{r}} \frac{\mathbf{r}}{\sqrt{N}} \left(\int_0^t \sqrt{f^{(\mathbf{r})}(\tilde{\mathbf{X}}^N(s), s)}\, dW^{(\mathbf{r})}(s) \right), \tag{4.5}$$

where $\mathbf{F}(\cdot) = \sum_{\mathbf{r}} \mathbf{r} f^{(\mathbf{r})}(\cdot)$.

The process (4.5), in more compact form, is

$$d\tilde{\mathbf{X}}^N(t) = \mathbf{F}(\tilde{\mathbf{X}}^N(t), t)\, dt + \frac{1}{\sqrt{N}} \mathbf{C}(\tilde{\mathbf{X}}^N(t), t)\, d\mathbf{W}(t). \tag{4.6}$$

Here $\mathbf{C}(\tilde{\mathbf{X}}^N(t), t)$ is a 2×2 matrix that is obtained by taking the square-root of the covariance matrix function defined by $[V_{ij}] = \sum_{\mathbf{r}} \mathbf{r}_i \mathbf{r}_j f^{(\mathbf{r})}(\tilde{\mathbf{X}}^N(t), t)$. The vector $\mathbf{F} \in \mathbb{R}^2$ represents the deterministic dynamics of the macroscopic limit for (4.6) and $\mathbf{W}(t)$ is a two-dimensional Brownian motion.

As $N \to \infty$, the process $\tilde{\mathbf{X}}^N(t)$ approaches a macroscopic limit $\boldsymbol{\phi}(t)$ satisfying the two-dimensional ODE

$$\dot{\boldsymbol{\phi}} = \mathbf{F}(\boldsymbol{\phi}(t), t) \equiv \mathbf{F}(\boldsymbol{\phi}(t); \theta(t)). \tag{4.7}$$

In (4.7), the notation $\theta(t)$ appears in the re-written form of $\mathbf{F}(\boldsymbol{\phi}(t), t)$ to indicate that the vector-field $\mathbf{F}$ varies with t explicitly because a parameter that periodically varies with time is introduced. Hence, we refer to (4.7) as periodically parametrically forced (PPF) model.

Using the same argument as Kurtz [10], by the Law of Large Numbers for $\Psi^{(\mathbf{r})}$ under the assumption that $\mathbf{F}(\cdot)$ is Lipschitz and as a consequence of the central limit theorem, it follows that:

$$\mathbf{X}^N(t) = \boldsymbol{\phi}(t) + \mathcal{O}\left(\frac{1}{\sqrt{N}}\right). \tag{4.8}$$

Since $\mathbf{X}^N(t) \approx \tilde{\mathbf{X}}^N(t)$, we have

$$\tilde{\mathbf{X}}^N(t) \approx \boldsymbol{\phi}(t) + \mathcal{O}\left(\frac{1}{\sqrt{N}}\right) \equiv \boldsymbol{\phi}(t) + \frac{1}{\sqrt{N}} \boldsymbol{\xi}(t). \tag{4.9}$$

The process $\boldsymbol{\xi}(t)$ defined in (4.9) represents the random fluctuations around the macroscopic limit $\boldsymbol{\phi}(t)$. Analysis of this process when $\boldsymbol{\phi}(t)$ has a stable fixed point is the common theme in studies on sustained oscillations around this fixed point observed in stochastic simulations of various population models [32, 33, 189]. In this chapter, we study the behaviour of $\boldsymbol{\xi}(t)$ when $\boldsymbol{\phi}(t)$ has a stable limit cycle.

4.2.2 Stochastic fluctuations around the limit cycle solution

Existing work suggests that models of the form (4.7) may have a stable limit cycle [33, 191]. In this section, we derive a stochastic differential equation (SDE) for the process that describes the stochastic fluctuations around a stable limit cycle where it exists. Let us assume that the system (4.7) has a stable limit cycle solution $\mathbf{L}(t)$ with period T_{LC}.

For large t, keeping in mind that N is also large and using (4.9), we can replace $\boldsymbol{\phi}(t)$ by $\mathbf{L}(t)$ and obtain:

$$\tilde{\mathbf{X}}^N(t) \approx \mathbf{L}(t) + \frac{1}{\sqrt{N}}\boldsymbol{\xi}(t). \tag{4.10}$$

We substitute (4.10) into $\mathbf{F}$ and $\mathbf{C}$ in (4.6) and linearise them around the limit cycle $\mathbf{L}(t)$ to obtain

$$\begin{aligned} \mathbf{F}(\tilde{\mathbf{X}}^N(t), t) &\approx \mathbf{F}\left(\mathbf{L}(t) + \frac{1}{\sqrt{N}}\boldsymbol{\xi}(t), t\right) \\ &\approx \mathbf{F}(\mathbf{L}(t), t) + \frac{1}{\sqrt{N}}\mathbf{DF}(\mathbf{L}(t), t)\ \boldsymbol{\xi}(t), \\ \text{and} \quad \mathbf{C}(\tilde{\mathbf{X}}^N(t), t) &\approx \mathbf{C}(\mathbf{L}(t), t), \end{aligned} \tag{4.11}$$

where

$$\mathbf{DF}(\mathbf{L}(t), t) = \left[\begin{matrix} \frac{\partial \mathbf{F}_1}{\partial \boldsymbol{\phi}_1} & \frac{\partial \mathbf{F}_1}{\partial \boldsymbol{\phi}_2} \\ \frac{\partial \mathbf{F}_2}{\partial \boldsymbol{\phi}_1} & \frac{\partial \mathbf{F}_2}{\partial \boldsymbol{\phi}_2} \end{matrix}\right]\Bigg|_{\boldsymbol{\phi}(t)=\mathbf{L}(t)} \equiv \mathbf{A}(t), \tag{4.12}$$

i.e. the Jacobian of $\mathbf{F}$ with respect to the first variable evaluated at $\mathbf{L}(t)$. The matrix (4.12) carries the forcing frequency embedded in the time-periodic forcing parameter $\theta(t)$ and the frequency of the limit cycle $\mathbf{L}(t)$.

We integrate (4.6) and substitute (4.10) and (4.11) into $\tilde{\mathbf{X}}^N(t)$, $\mathbf{F}$ and $\mathbf{C}$, respectively to obtain

$$\begin{aligned} \mathbf{L}(t) + \frac{1}{\sqrt{N}}\boldsymbol{\xi}(t) \approx \mathbf{L}(0) + \frac{1}{\sqrt{N}}\boldsymbol{\xi}(0) &+ \int_0^t \mathbf{F}(\mathbf{L}(s), s)\ ds \\ &+ \frac{1}{\sqrt{N}}\int_0^t \mathbf{DF}(\mathbf{L}(s), s)\ \boldsymbol{\xi}(s)\ ds \\ &+ \frac{1}{\sqrt{N}}\int_0^t \mathbf{C}(\mathbf{L}(s), s)\ d\mathbf{W}(s). \end{aligned} \tag{4.13}$$

Since $\mathbf{L}(t)$ satisfies (4.7),

$$\mathbf{L}(t) - \mathbf{L}(0) = \int_0^t \mathbf{F}(\mathbf{L}(s), s)\ ds, \tag{4.14}$$

and. writing $\mathbf{C}(L(s), s) = \mathbf{C}(s)$, (4.13) simplifies to,

$$\boldsymbol{\xi}(t) = \boldsymbol{\xi}(0) + \int_0^t \mathbf{A}(s)\ \boldsymbol{\xi}(s)\ ds + \int_0^t \mathbf{C}(s)\ d\mathbf{W}(s). \tag{4.15}$$

In differential form,

$$d\boldsymbol{\xi}(t) = \mathbf{A}(t)\boldsymbol{\xi}(t)\ dt + \mathbf{C}(t)\ d\mathbf{W}(t). \tag{4.16}$$

We now refer to (4.16) as the "linearisation" of the stochastic PPF model (4.6). It is an equation of motion for the fluctuations $\boldsymbol{\xi}(t)$, about the deterministic trajectory $\mathbf{L}(t)$. In physics language, such an equation is known as a linear Langevin equation, which can be obtained by means of a Van Kampen [9] system-size expansion as in Black and McKane [191].

Consider (4.16) in the absence of noise, i.e. when $\mathbf{C}(t) = 0$. The remaining term describes the behaviour of the system when perturbed away from the limit cycle $\mathbf{L}(t)$. We call this behaviour the response of the system to a deterministic perturbation. We expect this response to exhibit damped oscillations with a frequency that is not necessarily the same as the frequency of the limit cycle. We call this new frequency the response frequency.

Simulations of systems of the form (4.16) with $\mathbf{A}(t)$ given by (4.12) applied to disease and population dynamics produce sustained oscillations [11, 33, 44, 189]. The nature of the oscillations described by $\boldsymbol{\xi}(t)$ has been studied using the power spectral density (PSD), i.e. the distribution of frequencies in their stochastic simulations. The PSD of $\boldsymbol{\xi}(t)$ in specific examples [189, 191] consistently shows a dominant peak at the imaginary part of complex Floquet exponents associated to the limit cycle and two smaller peaks at frequencies equal to the sum and difference of the imaginary part of these Floquet exponents and the limit cycle frequency.

The nature of the fluctuation in (4.16) has been analyzed using Floquet theory [52], which is useful when establishing the stability of a limit cycle. For example, Boland et al. [189] showed that stochastic noise gives rise to large-amplitude, coherent sustained oscillations for systems with stable limit cycles having complex Floquet multipliers. On the other hand, Black [11] developed an analytic tool based on Floquet quantities to predict the periodicity in oscillations produced by a stochastic SIR model with seasonal forcing. However, it remains to show how the interaction of the stochastic

noise and parametric forcing produce large-amplitude oscillations that are sustained over time. Moreover, the differences between the characteristics of the fluctuations arising from a stochastic PPF model and an unforced stochastic model remains unclear. In the next section, we derive an approximate form of $\boldsymbol{\xi}(t)$ which makes apparent the source of the PSD frequencies found by simulation in Boland et al. [189], Black and McKane [191].

4.3 The approximation

The solution $\boldsymbol{\xi}(t)$ of the SDE (4.16) fluctuates at a rate that is influenced by parametric forcing and by the limit cycle embedded in $\mathbf{A}(t)$, and also varies according to Brownian noise with diffusion matrix $\mathbf{C}(t)$ that, again, depends on the forcing parameter $\theta(t)$.

Clearly, it is not possible to separate the roles of stochasticity and of parametric forcing by simply examining the numerical simulations of (4.16). Here we develop an approximation that allows us to separate the roles of stochasticity and forcing in a stochastic PPF model whose deterministic analogue has a limit cycle solution.

4.3.1 Transformations

Our starting point is the system of SDEs defined by (4.16) where $\boldsymbol{\phi}(t)$ in (4.7) has a limit cycle. We apply a series of transformations. First, we re-write (4.16), for brevity, as:

$$d\boldsymbol{\xi}_t = \mathbf{A}_t\boldsymbol{\xi}_t\ dt + \mathbf{C}_t\ d\mathbf{W}_t, \tag{4.17}$$

The subscript means that each variable is a function of t. Let T be the period of $\mathbf{A}(t)$.

We can see from (4.17) that when $\mathbf{C}_t$ is the zero matrix, we obtain a linear ODE system with T-periodic coefficient matrix $\mathbf{A}(t)$. Let us consider the system

$$\dot{\mathbf{x}} = \mathbf{A}(t)\mathbf{x}, \quad \mathbf{x}(t) \in \mathbb{R}^2. \tag{4.18}$$

One can think of (4.18) as resulting from linearising (4.7) about the limit cycle solution $\mathbf{L}(t)$. In other words, $\mathbf{x}(t)$ is a perturbation around $\mathbf{L}(t)$ whose dynamics is governed by (4.18). Now suppose that $\mathbf{x}^1(t)$ and $\mathbf{x}^2(t)$ are linearly independent vector solutions of (4.18), then the matrix $\boldsymbol{\Phi}(t) = [\mathbf{x}^1\ \mathbf{x}^2]$ is called a fundamental matrix solution of

$$\dot{\mathbf{\Phi}} = \mathbf{A}(t)\mathbf{\Phi}. \tag{4.19}$$

According to Floquet theory [52], if $\mathbf{\Phi}(t)$ is a fundamental matrix solution for (4.18) so is $\mathbf{\Phi}(t+T)$ and there exists a constant matrix $\mathbf{B}$ that satisfies the relation $\mathbf{\Phi}(t+T) = \mathbf{\Phi}(t)\mathbf{B}$. The eigenvalues of $\mathbf{B}$, which we denote here as ρ_j for $j = 1, 2$, are called the Floquet multipliers. The Floquet exponents are $\mu_j = \ln \rho_j / T$. If their real parts are both negative, then the limit cycle $\mathbf{L}(t)$ is stable. Since $\mathbf{B} = \mathbf{\Phi}(t)^{-1}\mathbf{\Phi}(t+T)$ is constant in t, a simple way of expressing this matrix is by putting $t = 0$ so that $\mathbf{B} = \mathbf{\Phi}(0)^{-1}\mathbf{\Phi}(T)$. One can choose the principal fundamental matrix solution, i.e. $\mathbf{\Phi}(0) = \mathbf{I}$, so that the Floquet multipliers are the eigenvalues of $\mathbf{B} = \mathbf{\Phi}(T)$.

Given ρ_j and μ_j, according to Floquet theory, there exists a T-periodic function $\mathbf{p}(t) \in \mathbb{R}^2$ such that $\mathbf{x}(t) = \mathrm{diag}[e^{\mu_1 t}, e^{\mu_2 t}] \cdot \mathbf{p}(t)$. Thus, the principal fundamental matrix $\mathbf{\Phi}_0(t)$ for (4.18) has the form

$$\mathbf{\Phi}_0(t) = \mathbf{P}_0(t)\mathbf{Y}_0(t), \tag{4.20}$$

where the nonsingular 2×2 matrix $\mathbf{P}_0(t)$ satisfies $\mathbf{P}_0(t+T) = \mathbf{P}_0(t), \forall t$ and $\mathbf{Y}_0(t) = \mathrm{diag}[e^{\mu_1 t}\ e^{\mu_2 t}]$. Moreover, one sees that $\mathbf{Y}_0(t)$ satisfies the matrix differential equation with constant coefficients of the form

$$\dot{\mathbf{Y}}_0 = \mathbf{D}_0\mathbf{Y}_0,$$

with $\mathbf{D}_0 = \mathrm{diag}[\mu_1, \mu_2]$.

Since the limit cycle $\mathbf{L}(t)$ is stable, then the solution of (4.18) has damped oscillations, which implies that we have complex-valued Floquet exponents with $\mathbb{R}\mathrm{e}\{\mu_j\} < 0$. As a result, the solutions $\mathbf{\Phi}_0(t)$ are complex-valued. We used these complex-valued $\mathbf{\Phi}_0(t)$ to construct linearly independent, real-valued solutions for (4.19).

As in Grimshaw [52], if we suppose that μ and $\bar{\mu}$ are complex- conjugate pair, then $\mu = -\lambda + i\omega$ (for $\lambda, \omega > 0$) where $|\rho| = e^{-\lambda T}$ and $\arg \rho = \omega T$, and $\mathbf{p}(t) = \mathbf{q}(t) + i\mathbf{r}(t)$, where $\mathbf{q}(t), \mathbf{r}(t) \in \mathbb{R}^2$ are T-periodic, then the real and imaginary parts of $e^{\mu t}\mathbf{p}(t)$,

$$\begin{aligned} \mathbb{R}\mathrm{e}\{e^{\mu t}\mathbf{p}(t)\} &= e^{-\lambda t}\mathbf{q}(t)\cos\omega t - e^{-\lambda t}\mathbf{r}(t)\sin\omega t, \\ \mathbb{I}\mathrm{m}\{e^{\mu t}\mathbf{p}(t))\} &= e^{-\lambda t}\mathbf{q}(t)\sin\omega t + e^{-\lambda t}\mathbf{r}(t)\cos\omega t, \end{aligned} \tag{4.21}$$

form the real-valued fundamental matrix solution for (4.19). Hence, we can rewrite $\mathbf{\Phi}_0(t)$ as a real-valued solution

$$\begin{aligned}\mathbf{\Phi}_0(t) &= [\mathbb{R}\mathrm{e}\{e^{\mu t}\mathbf{p}(t)\}, \mathbb{I}\mathrm{m}\{e^{\mu t}\mathbf{p}(t)\}], \\ &= \underbrace{[\mathbf{q}(t)\ \mathbf{r}(t)]}_{\mathbf{Q}(t)}\ \underbrace{e^{-\lambda t}\begin{bmatrix}\cos\omega t & \sin\omega t \\ -\sin\omega t & \cos\omega t\end{bmatrix}}_{\mathbf{Y}(t)}. \end{aligned} \tag{4.22}$$

We see from (4.22) that the matrix $\mathbf{P}_0(t)$ in (4.20) can be written as the invertible periodic matrix $\mathbf{Q}(t) = [\mathbf{q}(t)\ \mathbf{r}(t)]$ and

$$\mathbf{Y}(t) \equiv e^{-\lambda t}\mathbf{R}_{-\omega t}, \tag{4.23}$$

where $\mathbf{R}_\theta$ is the rotation matrix. Note that $\mathbf{Q}(t)$ has period T. On the other hand, $\mathbf{Y}(t)$ comes from the ODE (4.18) whose period is $2\pi/\omega$ not necessarily equal to T. Additionally, $\mathbf{Y}(t)$ satisfies the equation

$$\dot{\mathbf{Y}} = \mathbf{\Lambda}\mathbf{Y} \qquad \text{where} \qquad \mathbf{\Lambda} = \begin{bmatrix}-\lambda & \omega \\ -\omega & -\lambda\end{bmatrix}.$$

With this information about $\mathbf{\Phi}_0$, the fundamental matrix solution of the deterministic equation (4.19), we go back to the stochastic equation (4.17). Let us write $\boldsymbol{\xi}(t) = \mathbf{Q}(t)\mathbf{y}(t)$ in (4.17). Since $\mathbf{y}(t)$ is a stochastic process, we describe its dynamics using Itô calculus. By Itô's formula, we have

$$d\mathbf{y} = \dot{\mathbf{Q}}^{-1}\mathbf{Q}\mathbf{y}\ dt + \mathbf{Q}^{-1}\mathbf{A}\mathbf{Q}\mathbf{y}\ dt + \mathbf{Q}^{-1}\mathbf{C}\ d\mathbf{W}. \tag{4.24}$$

We wish to simplify the SDE (4.24) so that it is of the form

$$d\mathbf{y} = \mathbf{\Lambda}\mathbf{y}\ \mathbf{dt} + \mathbf{Q}^{-1}\mathbf{C}\ \mathbf{dW}. \tag{4.25}$$

Denote by $[\mathbf{Q}(t)]_{ij}$ and $[\mathbf{Q}^{-1}(t)]_{jk}$ (for $i, j, k = 1, 2$) the components of $\mathbf{Q}(t)$ and $\mathbf{Q}^{-1}(t)$. For every t,

$$\sum_{j=1}^{2}[\mathbf{Q}]_{ij}[\mathbf{Q}^{-1}]_{jk} = \delta_{ik}, \tag{4.26}$$

where δ_{ik} is the Kronecker delta. The time derivative of (4.26) gives us

$$\sum_{j=1}^{2}\left[[\mathbf{Q}]_{ij}\left(\frac{d}{dt}[\mathbf{Q}^{-1}]_{jk}\right) + \left(\frac{d}{dt}[\mathbf{Q}]_{ij}\right)[\mathbf{Q}^{-1}]_{jk}\right] = 0, \tag{4.27}$$

which implies that

$$\sum_{j=1}^{2}[\mathbf{Q}]_{ij}\left(\frac{d}{dt}[\mathbf{Q}^{-1}]_{jk}\right) = -\sum_{j=1}^{2}\left(\frac{d}{dt}[\mathbf{Q}]_{ij}\right)[\mathbf{Q}^{-1}]_{jk}. \tag{4.28}$$

A shorthand form of (4.28) is:

$$[\mathbf{Q}\cdot\dot{\mathbf{Q}}^{-1}]_{ik} = -[\dot{\mathbf{Q}}\cdot\mathbf{Q}^{-1}]_{ik}. \tag{4.29}$$

From (4.29), we conclude that $\mathbf{Q}\cdot\dot{\mathbf{Q}}^{-1} = -\dot{\mathbf{Q}}\cdot\mathbf{Q}^{-1}$ and so,

$$\dot{\mathbf{Q}}^{-1} = -\mathbf{Q}^{-1}\dot{\mathbf{Q}}\mathbf{Q}^{-1}. \tag{4.30}$$

Substituting (4.30) into (4.24), we have

$$d\mathbf{y} = \mathbf{Q}^{-1}(\mathbf{AQ} - \dot{\mathbf{Q}})\mathbf{y}\ dt + \mathbf{Q}^{-1}\mathbf{C}\ d\mathbf{W}. \tag{4.31}$$

In (4.22), we see that

$$\mathbf{Q}(t) = \mathbf{\Phi}_0(t)\mathbf{Y}^{-1}(t) = \mathbf{\Phi}_0(t)e^{\lambda t}\mathbf{R}_{\omega t}. \tag{4.32}$$

It follows that

$$\dot{\mathbf{Q}} = \dot{\mathbf{\Phi}}_0 e^{\lambda t}\mathbf{R}_{\omega t} + \lambda\mathbf{\Phi}_0 e^{\lambda t}\mathbf{R}_{\omega t} + e^{\lambda t}\mathbf{\Phi}_0\dot{\mathbf{R}}_{\omega t}. \tag{4.33}$$

Define the notation $\tilde{\mathbf{R}}_{\omega t}$ by

$$\dot{\mathbf{R}}_{\omega t} = \omega\begin{bmatrix}-\sin\omega t & -\cos\omega t\\ \cos\omega t & -\sin\omega t\end{bmatrix} \equiv \omega\tilde{\mathbf{R}}_{\omega t}. \tag{4.34}$$

From (4.33), (4.34), (4.22), (4.19), (4.23), and simplifying, we obtain

$$\dot{\mathbf{Q}} = (\mathbf{A} + \lambda\mathbf{I})\mathbf{Q} + \omega e^{\lambda t}\mathbf{\Phi}_0\tilde{\mathbf{R}}. \tag{4.35}$$

Knowing from (4.32) that

$$\mathbf{\Phi}_0(t) = e^{-\lambda t}\mathbf{Q}(t)\mathbf{R}_{-\omega t} \tag{4.36}$$

and writing $\omega\mathbf{R}_{\omega t}\tilde{\mathbf{R}} = \begin{bmatrix}0 & -\omega\\ \omega & 0\end{bmatrix}$, (4.35) now reads

$$\dot{\mathbf{Q}} = \mathbf{AQ} - \mathbf{Q\Lambda}. \tag{4.37}$$

Therefore, using (4.37), the SDE system (4.31) simplifies to (4.25) to which the proof of Baxendale and Greenwood [50] applies with some minor changes.

Following Baxendale and Greenwood [50], we apply three changes of variables to (4.25). First, we write $\mathbf{y}(t) = \mathbf{R}_{-\omega t}\mathbf{z}(t)$ to simplify the drift

term. Again, by Itô's formula, the two-dimensional SDE for $\mathbf{z}(t)$ is found to be:

$$d\mathbf{z} = -\lambda \mathbf{z}\ dt + \mathbf{R}_{\omega t}\mathbf{Q}^{-1}\mathbf{C}\ d\mathbf{W}. \tag{4.38}$$

This means that

$$\mathbf{z}(t) = \mathbf{z}(0) - \lambda \int_0^t \mathbf{z}(s)\ ds + \int_0^t \mathbf{R}_{\omega s}\mathbf{Q}^{-1}(s)\mathbf{C}(s)\ d\mathbf{W}(s). \tag{4.39}$$

Rescaling time by replacing t by t/λ, (4.39) then reads:

$$\mathbf{z}(t/\lambda) = \mathbf{z}(0) - \lambda \int_0^{t/\lambda} \mathbf{z}(s)\ ds + \int_0^{t/\lambda} \mathbf{R}_{\omega s}\mathbf{Q}^{-1}(s)\mathbf{C}(s)\ d\mathbf{W}(s). \tag{4.40}$$

We apply the substitution $s = u/\lambda \implies ds = du/\lambda$ to (4.40) and obtain

$$\mathbf{z}(t/\lambda) - \mathbf{z}(0) = -\int_0^t \mathbf{z}(u/\lambda)\ du + \int_0^t \mathbf{R}_{\omega u/\lambda}\mathbf{Q}^{-1}(u/\lambda)\mathbf{C}(u/\lambda)\ d\mathbf{W}(u/\lambda). \tag{4.41}$$

Let $\tilde{\mathbf{C}}_t = \mathbf{Q}^{-1}(t)\mathbf{C}(t)$. Define

$$\sigma^2(t) = \frac{1}{2}\,\mathrm{Tr}\left(\tilde{\mathbf{C}}_t\tilde{\mathbf{C}}_t^*\right) \tag{4.42}$$

and

$$\bar{\sigma}^2 = \frac{1}{T}\int_0^T \sigma^2(t)\ dt. \tag{4.43}$$

By defining $\mathbf{U}(t) = \sqrt{\lambda}\mathbf{z}(t/\lambda)/\bar{\sigma}$, Equation (4.41) becomes

$$\mathbf{U}(t) - \mathbf{U}(0) = -\int_0^t \mathbf{U}(u)\ du + \int_0^t \frac{\sqrt{\lambda}}{\bar{\sigma}}\mathbf{R}_{\omega u/\lambda}\mathbf{Q}^{-1}(u/\lambda)\mathbf{C}(u/\lambda)\ d\mathbf{W}(u/\lambda). \tag{4.44}$$

Using the scaling property of Brownian motion, i.e. $\tilde{\mathbf{W}}(t) = \sqrt{\lambda}\mathbf{W}(t/\lambda)$, and the notation $\mathbf{D}(t/\lambda) = \frac{1}{\bar{\sigma}}\mathbf{Q}^{-1}(t/\lambda)\mathbf{C}(t/\lambda)$, (4.44) takes the differential form

$$d\mathbf{U}(t) = -\mathbf{U}(t)\ dt + \mathbf{R}_{\omega t/\lambda}\mathbf{D}(u/\lambda)\ d\tilde{\mathbf{W}}(t). \tag{4.45}$$

We note that (4.45) takes a similar form as with the SDE found in Eq. (15) in Baxendale and Greenwood [50], which was compared to the bivariate standard Ornstein-Uhlenbeck process.

Using the Martingale Problem method, Baxendale and Greenwood [50] proved that, on any fixed bounded time interval $[0, \tau]$, the distribution of $\tilde{\mathbf{U}}(t)$ satisfying the equation

$$d\tilde{\mathbf{U}}(t) = -\tilde{\mathbf{U}}(t)\ dt + \mathbf{R}_{\omega t/\lambda}\mathbf{D}\ d\tilde{\mathbf{W}}(t), \qquad \text{where } \mathrm{Tr}\left(\mathbf{D}\mathbf{D}^*\right) = 2 \tag{4.46}$$

converges to the distribution of the bivariate standard Ornstein-Uhlenbeck process $\mathbf{S}(t)$ generated by the SDE

$$d\mathbf{S}(t) = -\mathbf{S}(t)\ dt + d\mathbf{W}(t) \tag{4.47}$$

as $\lambda/\omega \to 0$. In their context, $\mathbf{D}$ is a constant matrix.

We check that in our context where $\mathbf{D}$ is a function of t, $\lim_{\lambda\to 0} \mathrm{Tr}(\mathbf{D}\mathbf{D}^*) = 2$ holds for (4.45). Observe that

$$\mathrm{Tr}(\mathbf{D}_{t/\lambda}\mathbf{D}^*_{t/\lambda}) = \frac{1}{\bar{\sigma}^2}\,\mathrm{Tr}\left(\tilde{\mathbf{C}}_{t/\lambda}\tilde{\mathbf{C}}^*_{t/\lambda}\right) = \frac{2\sigma^2(t/\lambda)}{\bar{\sigma}^2}. \tag{4.48}$$

Since $\sigma^2(t/\lambda)$ is periodic, its frequency increases as $\lambda \to 0$. This implies that in the limit, $\sigma^2(t/\lambda)$ can be approximated by its time-average over the interval $[0, T]$, i.e. $\bar{\sigma}^2$. Hence, the $\mathrm{Tr}(\mathbf{D}_{t/\lambda}\mathbf{D}^*_{t/\lambda}) \to 2$ as $\lambda \to 0$, and the theorem of Baxendale and Greenwood [50] applies to (4.45). We conclude that the process $\mathbf{U}(t)$ converges weakly to the process $\mathbf{S}(t)$.

4.3.2 Result

The approximate process

We conclude that the solution $\boldsymbol{\xi}(t)$ of (4.17) when $\lambda \ll \omega$ can be approximated as follows:

$$\begin{aligned}\boldsymbol{\xi}(t) = \mathbf{Q}(t)\mathbf{y}(t) = \mathbf{Q}(t)\mathbf{R}_{-\omega t}\mathbf{z}(t) &= \frac{\bar{\sigma}}{\sqrt{\lambda}}\mathbf{Q}(t)\mathbf{R}_{-\omega t}\mathbf{U}_{\lambda t} \\ &\approx \frac{\bar{\sigma}}{\sqrt{\lambda}}\mathbf{Q}(t)\mathbf{R}_{-\omega t}\mathbf{S}_{\lambda t} \equiv \boldsymbol{\xi}^{app}(t).\end{aligned} \tag{4.49}$$

We see from (4.49) that the stochastic fluctuations $\boldsymbol{\xi}(t)$ around the limit cycle oscillate at frequencies which are combinations of the frequency of the drift coefficient $\mathbf{A}(t)$ and the frequency ω, which arise already from the deterministic system (4.18). Note that the frequency ω is the imaginary part of the Floquet exponents associated with the deterministic portion of (4.17). The typical amplitude of the fluctuation $\boldsymbol{\xi}(t)$ depends on the factor $\bar{\sigma}/\sqrt{\lambda}$, where $\bar{\sigma}$ is square-root of the average variance $\sigma^2(t)$ over the time interval $[0, T]$ and λ is the magnitude of the real part of the complex Floquet exponents.

The phase and amplitude processes

We write $\mathbf{R}_{-\omega t}\mathbf{S}_{\lambda t}$ in polar form to see the role of the two-dimensional standard Ornstein-Uhlenbeck process $\mathbf{S}_{\lambda t}$ appearing in (4.49) and obtain

$$\boldsymbol{\xi}^{app}(t) = \frac{\bar{\sigma}}{\sqrt{\lambda}}\mathbf{Q}(t)Z_{\lambda t}\begin{bmatrix}\cos(\omega t - \varphi_{\lambda t})\\ \sin(\omega t - \varphi_{\lambda t})\end{bmatrix}, \tag{4.50}$$

where $Z_{\lambda t} = |\mathbf{S}_{\lambda t}|$ and $\varphi_{\lambda t} = \arg[\mathbf{S}_1(\lambda t) + i\mathbf{S}_2(\lambda t)]$. In (4.50), we have a well-defined phase process $\varphi(t)$ and a radial process $Z(t)$ which are known to satisfy the following stochastic diffential equations [46]:

$$\begin{aligned} dZ(t) &= \left[\frac{1}{2Z(t)} - Z(t)\right]\, dt + dW_Z(t),\\ d\varphi(t) &= \frac{1}{Z(t)}dW_\varphi(t), \end{aligned} \tag{4.51}$$

where $W_Z(t)$ and $W_\varphi(t)$ are independent Wiener processes: $W_Z(t)$ is a standard Brownian motion and $W_\varphi(t)$ is a Brownian motion run on a unit circle. Note here that in the context of (4.50), $Z(t)$ and $\varphi(t)$ in (4.51) should be run at a rate λ. Hence, the amplitude of $\boldsymbol{\xi}^{app}(t)$ does not depend only on the scalar factor and the magnitude of the T-periodic matrix $\mathbf{Q}_0(t)$ but is also modulated by the two-dimensional slowly varying standard Ornstein-Uhlenbeck process $\mathbf{S}(\lambda t)$. Furthermore, the process $W_\varphi(t)$ is responsible for the random phase slips (instantaneous change in the phase of an oscillator) affecting the deterministic phase of the cycles produced by $\mathbf{Q}(t)\mathbf{R}_{-\omega t}$. From (4.51), we observe that when the radial process $Z(t)$ is large for a random time interval, the phase process moves at a slow rate and so implies that the phase process of $\boldsymbol{\xi}(t)$ predominantly follows $\mathbf{Q}(t)\mathbf{R}_{-\omega t}$ in an approximate sense. In this case, the radial process behaves much like an Ornstein-Uhlenbeck process. On the other hand, the increments of $\varphi(t)$ become prominent when $Z(t)$ is small.

The form of $\mathbf{Q}(t)$ and its consequence

At this point, we only know that $\mathbf{Q}(t) \in \mathbb{R}^{2\times 2}$ is T-periodic, i.e. $\mathbf{Q}(t)$ has the same period as $\mathbf{A}(t)$. When $\mathbf{Q}(t)$ have function entries that belong to a class of smooth functions whose Fourier series coefficients decay rapidly with increasing frequency index [192], then we can write

$$\mathbf{Q}(t) \sim \mathbf{Q}_0 + \mathbf{Q}_1 \cos \nu t + \mathbf{Q}_2 \sin \nu t, \tag{4.52}$$

where $\mathbf{Q}_0, \mathbf{Q}_1$, and $\mathbf{Q}_2$ are constant matrices of Fourier coefficients with $[\mathbf{Q}_0]_{ij} > [\mathbf{Q}_1]_{ij} > [\mathbf{Q}_2]_{ij}$ for $i, j = 1, 2$ and $\nu = 2\pi/T$. Thus,

$$\mathbf{Q}(t)\mathbf{R}_{-\omega t} \sim \mathbf{Q}_0\mathbf{R}_{-\omega t} + \mathbf{Q}_1\mathbf{R}_{-\omega t}\cos\nu t + \mathbf{Q}_2\mathbf{R}_{-\omega t}\sin\nu t. \tag{4.53}$$

Using product-to-sum trigonometric identities, we have

$$\mathbf{R}_{-\omega t}\cos\nu t = \frac{1}{2}\begin{bmatrix}\cos\psi_t^+ + \cos\psi_t^- & \sin\psi_t^+ - \sin\psi_t^- \\ \sin\psi_t^- - \sin\psi_t^+ & \cos\psi_t^+ + \cos\psi_t^-\end{bmatrix} \tag{4.54}$$

and

$$\mathbf{R}_{-\omega t}\sin\nu t = \frac{1}{2}\begin{bmatrix}\sin\psi_t^+ + \sin\psi_t^- & \cos\psi_t^- - \cos\psi_t^+ \\ \cos\psi_t^+ - \cos\psi_t^- & \sin\psi_t^+ + \sin\psi_t^-\end{bmatrix}, \tag{4.55}$$

where $\psi_t^\pm = (\nu \pm \omega)t$. Therefore, the entry of $\mathbf{Q}(t)\mathbf{R}_{-\omega t}$ is a sum of sine and cosine functions with frequencies ω and $\nu \pm \omega$.

Given the form of $\mathbf{Q}(t)$ in (4.52), we let

$$\mathbf{Q}_k = \begin{bmatrix}Q_k^{(1,1)} & Q_k^{(1,2)} \\ Q_k^{(2,1)} & Q_k^{(2,2)}\end{bmatrix}, \qquad k = 0, 1, 2 \tag{4.56}$$

and rewrite (4.50) as

$$\boldsymbol{\xi}^{app}(t) = \frac{\bar{\sigma}}{\sqrt{\lambda}} Z_{\lambda t}\begin{bmatrix} r_0^{(1)}\cos\Psi_{01} + \frac{1}{2}r_1^{(1)}\left(\cos\Psi_{11}^+ + \cos\Psi_{11}^-\right) + \frac{1}{2}r_2^{(1)}\left(\sin\Psi_{21}^+ + \sin\Psi_{21}^-\right) \\ r_0^{(2)}\cos\Psi_{02} + \frac{1}{2}r_1^{(2)}\left(\cos\Psi_{12}^+ + \cos\Psi_{12}^-\right) + \frac{1}{2}r_2^{(2)}\left(\sin\Psi_{22}^+ + \sin\Psi_{22}^-\right)\end{bmatrix}, \tag{4.57}$$

where

$$r_k^{(j)} = \sqrt{\left(Q_k^{(j,1)}\right)^2 + \left(Q_k^{(j,2)}\right)^2}, \tag{4.58}$$

$$\theta_k^{(j)} = \arctan\left(\frac{Q_k^{(j,2)}}{Q_k^{(j,1)}}\right), \tag{4.59}$$

$$\Psi_{0j} = \omega t - \varphi_{\lambda t} - \theta_0^j, \tag{4.60}$$

and

$$\Psi_{ij}^\pm = \nu t \pm \omega t \mp \varphi_{\lambda t} \mp \theta_i^{(j)}. \tag{4.61}$$

In (4.57), with (4.58)-(4.61), we find that the approximate process $\boldsymbol{\xi}^{app}(t)$ representing the stochastic perturbation around the limit cycle is a linear combination of sinusoidal functions whose central frequencies are ω and $\nu \pm$

ω, which are determined from the deterministic matrix function $\mathbf{Q}(t)\mathbf{R}_{-\omega t}$. Based on (4.60) and (4.61), each central frequency is perturbed by the slowly varying stochastic phase process $\varphi_{\lambda t}$ and has $\theta_k^{(j)}$, given by (4.59), as phase shifts. Moreover, the amplitude of $\boldsymbol{\xi}^{app}(t)$ in (4.57) is modulated by the slowly varying amplitude process $Z_{\lambda t}$ (as in (4.50)) and depends on the constants $r_k^{(j)}$, which is given by (4.58). These constants are associated to sinusoidal waves that determine the rotational dynamics of the process $\boldsymbol{\xi}(t)$. From (4.58), we find that $r_k^{(j)}$ is obtained from a sequence of decaying Fourier coefficients and so we expect that the process $\boldsymbol{\xi}(t)$ predominantly rotates at a central frequency ω, in an approximate sense.

In the following section, we will illustrate that $\boldsymbol{\xi}(t) \approx \boldsymbol{\xi}^{app}(t)$ in an example by verifying that their numerical power spectral densities (averaged over many realizations) are in good agreement.

4.4 Example: Driven harmonic oscillator with 1D noise

Consider the stochastic PPF model:

$$d\boldsymbol{\xi}(t) = \mathbf{A}(t)\boldsymbol{\xi}(t)\ dt + \mathbf{C}(t)\ d\mathbf{W}(t), \quad \text{where} \tag{4.62}$$

$$\mathbf{A}(t) = \begin{bmatrix} 0 & 1 \\ -k_0 & -b_0(1 + b\cos 2\pi a t) \end{bmatrix} \text{ and } \mathbf{C}(t) = \begin{bmatrix} 0 & 0 \\ 0 & \sigma_0(1 + b\cos 2\pi a t) \end{bmatrix}. \tag{4.63}$$

Model (4.62) is linear in $\boldsymbol{\xi}(t) = [\xi_1, \xi_2]^T$ and if we let $x = \xi_1$, we can write it as

$$\ddot{x} + k_0\dot{x} + b_0(1 + b\cos 2\pi a t)x = \sigma_0(1 + b\cos 2\pi a t)\dot{W}. \tag{4.64}$$

Equation (4.64) describes a harmonic oscillator which is driven by periodic variation of one of its parameters at frequency a and is further affected by a white noise whose variance depends on time and other parameters in the model. This white noise acts as an external force applied to the oscillator. In the model, the parameters affecting the frequency of the oscillator are the forcing frequency (a) and amplitude (b).

In the absence of parametric forcing and noise, i.e. $b = 0, \sigma_0 = 0$, (4.64) is the well-known damped harmonic oscillator model. For the harmonic oscillator system, the coefficient k_0 represents the damping rate and $\omega_0 =$

$\sqrt{b_0}$ is the oscillator's angular frequency when it is not damped. A nonzero k_0 implies that the harmonic oscillator is damped i.e., the oscillator's amplitude gradually goes to zero. In this case, the frequency of the oscillator does not only depend on ω_0 but also to the damping ratio $\zeta = k_0/2\sqrt{b_0}$. In particular, the frequency of a damped harmonic oscillator is given by $\omega_1 = \omega_0\sqrt{1-\zeta^2}$. When k_0 is zero, we recover the simple harmonic oscillator whose frequency is ω_0.

4.4.1 Power spectral density (PSD)

One aim of this work is to determine that the approximation is a good description for the stochastic oscillations produced by (4.62) as represented by the PSD for various values of the forcing amplitude b and noise level σ_0. Two main parameter regimes are considered here, namely when the deterministic system is damped ($k_0 \neq 0$) or undamped ($k_0 = 0$). We choose these regimes because both can give rise to noisy but sustained oscillations.

We obtained 100 realizations of stochastic simulations and computed the average power spectral density (PSD) numerically. We compare the PSD outputs for different regimes and various levels of b and σ_0 (See Figure 4.1). We choose the forcing frequency to be $a = 1$. We compare these with the PSD of the stochastic simulations (on average), based on the approximation (4.49). In Figure 4.1, there is a good agreement in the PSDs of the approximate and exact solutions with respect to capturing the governing frequencies of the process. The approximate process tends to give higher PSD values than the exact process.

In the damped regime, the deterministic system displays decaying oscillations approaching to zero solution while in the undamped regime, the system oscillates regularly at a frequency ω_0 without damping. In both regimes, the process $\boldsymbol{\xi}(t)$ have large PSD peaks at the system's intrinsic frequency ω_0 indicating that the process' dominant frequency is amplified by stochastic and parametric forcing. The undamped regime however gives rise to higher PSD values than the PSD values in the damped regime. Other observed PSD structure is the broadening of PSD peaks which results from the stochastic phase perturbations explained by the form of our approximation (4.49). The flattening of the PSDs in the right end indicates that the process is comparable to the Ornstein-Uhlenbeck process.

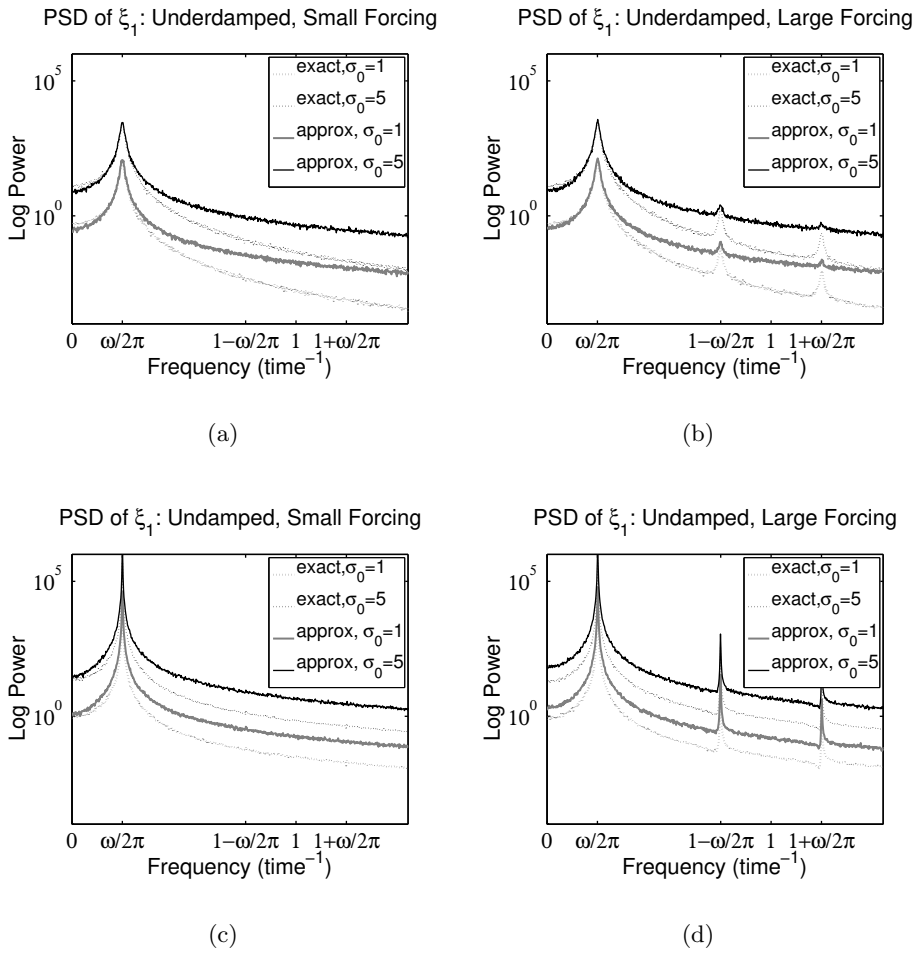

Figure 4.1: Numerical PSDs of the approximate (solid curves) and exact (dashed curves) solutions of (4.62), given (a,b) damped and (c,d) undamped regimes as defined in Section 4.4.1, obtained using forcing amplitudes (a,b) $b = 0.01$ and (c,d) $b = 0.5$ for noise levels $\sigma_0 = 1$ (gray curves) and $\sigma_0 = 5$ (black curves). Other parameters are held fixed, namely $a = 1, b_0 = 2, k_0 = 0.1$ for underdamped case, and $k_0 = 0$ for the undamped case.

4.4.2 Amplitude and phase as stochastic processes

We now apply the approximation to mathematically describe the amplitude and phase of the stochastic fluctuations produced by (4.62),(4.63) in terms of the model parameters. We use the fundamental matrix solution $\mathbf{\Phi}_0(t)$ of the system

$$\dot{\mathbf{x}}(t) = \begin{bmatrix} 0 & 1 \\ -k_0 & -b_0(1 + b\cos 2\pi a t) \end{bmatrix} \mathbf{x}(t) \tag{4.65}$$

and write the approximation as

$$\boldsymbol{\xi}^{app}(t) = \frac{\bar{\sigma}}{\sqrt{\lambda}} e^{\lambda t} \mathbf{\Phi}_0(t) \mathbf{S}_{\lambda t}. \tag{4.66}$$

Here (4.66) is obtained by re-writing $\boldsymbol{\xi}^{app}(t)$ in (4.49) using (4.36). Recall that $\mathbf{\Phi}_0(t)$ is the principal fundamental matrix solution that satisfies (4.19).

We compute the fundamental matrix solution of (4.65) using *DSolve* command in Mathematica [193] and obtain

$$\mathbf{\Phi}(t) = e^{-\frac{1}{2}k_0 t} \begin{bmatrix} \mathscr{C}(\alpha, q, x) & \mathscr{S}(\alpha, q, x) \\ -\frac{k_0}{2}\mathscr{C}(\alpha, q, x) + a\pi\mathscr{C}'(\alpha, q, x) & -\frac{k_0}{2}\mathscr{S}(\alpha, q, x) + a\pi\mathscr{S}'(\alpha, q, x) \end{bmatrix}, \tag{4.67}$$

where $\alpha = \dfrac{4b_0 - k_0^2}{4a^2\pi^2}$, $q = \dfrac{bb_0}{2a^2\pi^2}$, and $x = a\pi t$. The functions $\mathscr{C}$ and $\mathscr{S}$ are known as Mathieu cosine and sine, respectively, which are unique solutions to the Mathieu equation [194, 195] given by

$$\frac{d^2y}{dx^2} + [a - 2q\cos(2x)]y = 0.$$

The functions $\mathscr{C}'$ and $\mathscr{S}'$ are derivatives with respect to x.

For simplicity, we consider the case when the forcing amplitude is small, i.e. $b \approx 0$, so that q is small. In theory, when q is small, we have $\mathscr{C}(\alpha, q, x) \approx \cos(\sqrt{\alpha}x)$ and $\mathscr{S}(\alpha, q, x) \approx \sin(\sqrt{\alpha}x)/\sqrt{\alpha}$ [190]. Hence, assuming that the forcing amplitude b is small with all other parameters fixed, it follows that $q \ll 1$,

$$\mathscr{C}(\alpha, q, x) \approx \cos\left(\frac{1}{2}t\sqrt{4b_0 - k_0^2}\right), \text{ and}$$
$$\mathscr{S}(\alpha, q, x) \approx \frac{2a\pi}{\sqrt{4b_0 - k_0^2}} \sin\left(\frac{1}{2}t\sqrt{4b_0 - k_0^2}\right).$$

Define $\theta = \frac{1}{2}\sqrt{4b_0 - k_0^2}$, then $\mathscr{C}' = -\theta\sin(\theta t)/a\pi$ and $\mathscr{S}' = \cos(\theta t)$. Therefore, for small forcing amplitude, the fundamental matrix solution of (4.65) reads

$$\boldsymbol{\Phi}(t) = e^{-\frac{1}{2}k_0 t}\begin{bmatrix} \cos(\theta t) & \frac{a\pi}{\theta}\sin(\theta t) \\ -\frac{k_0}{2}\cos(\theta t) - \theta\sin(\theta t) & -\frac{a\pi k_0}{2\theta}\sin(\theta t) + a\pi\cos(\theta t) \end{bmatrix}. \tag{4.68}$$

We hence construct the principal fundamental matrix solution of (4.65) using $\boldsymbol{\Phi}_0(t) = \boldsymbol{\Phi}(t)\boldsymbol{\Phi}^{-1}(0)$ and obtain

$$\boldsymbol{\Phi}_0(t) = e^{-\frac{1}{2}k_0 t}\begin{bmatrix} \cos(\theta t) + \frac{k_0}{2\theta}\sin(\theta t) & \frac{1}{\theta}\sin(\theta t) \\ \left(-\theta - \frac{k_0^2}{4\theta}\right)\sin(\theta t) & -\frac{k_0}{2\theta}\sin(\theta t) + \cos(\theta t) \end{bmatrix}. \tag{4.69}$$

The real and imaginary part of the complex Floquet exponents $-\lambda \pm i\omega$, computed by taking the eigenvalues of $\boldsymbol{\Phi}_0(T)$, are $\lambda = -\cos\theta T$ and $\omega = |\sin\theta T|$, respectively. To guarantee that $\lambda > 0$ and $\lambda \ll \omega$, we must have that $\pi/2T < \theta < 3\pi/4T$ or $5\pi/4T < \theta \leq 3\pi/2T$.

Therefore, for appropriate θ and by (4.66), the approximate solution for (4.62) when $b \ll 1$ is given by

$$\begin{aligned} \boldsymbol{\xi}(t) &\approx \boldsymbol{\xi}^{app}(t) \\ &= \frac{\bar{\sigma}}{\sqrt{\lambda}}e^{(\lambda - k0/2)t} \quad \times \\ &\qquad \begin{bmatrix} \cos(\theta t) + \frac{k_0}{2\theta}\sin(\theta t) & \frac{1}{\theta}\sin(\theta t) \\ \left(-\theta - \frac{k_0^2}{4\theta}\right)\sin(\theta t) & -\frac{k_0}{2\theta}\sin(\theta t) + \cos(\theta t) \end{bmatrix}\begin{bmatrix} S_1(\lambda t) \\ S_2(\lambda t) \end{bmatrix}. \end{aligned} \tag{4.70}$$

In (4.70), we have $\boldsymbol{\xi}^{app}(t)$ expressed as an explicit SDE system which has a unique solution. We write (4.70) in terms of phase-shifted sine and cosine to characterise the amplitude and phase of the approximate process. Let $S_1(\lambda t) = \hat{Z}_{\lambda t}\cos\hat{\varphi}_{\lambda t}$ and $S_2(\lambda t) = \theta\hat{Z}_{\lambda t}\sin\hat{\varphi}_{\lambda t}$ where $\hat{Z}(\lambda t) = |S_1(\lambda t) + i\frac{1}{\theta}S_2(\lambda t)|$ and $\hat{\varphi}(\lambda t) = \arg\{S_1(\lambda t) + i\frac{1}{\theta}S_2(\lambda t)\}$. By expanding (4.70) and using formulas for products of sine and cosine functions, we have

$$\begin{aligned} \boldsymbol{\xi}^{app}(t) = \frac{\bar{\sigma}}{\sqrt{\lambda}}e^{\left(\lambda - \frac{k_0}{2}\right)t}\hat{Z}_{\lambda t} \quad \times \\ \begin{bmatrix} \cos\Theta_t^- + \frac{k_0}{4\theta}\sin\Theta_t^+ + \frac{k_0}{4\theta}\sin\Theta_t^- \\ -\frac{k_0}{4}\cos\Theta_t^- + \frac{k_0}{4}\cos\Theta_t^+ - \frac{k_0^2}{8\theta}\sin\Theta_t^+ + (\theta - \frac{k_0^2}{8\theta})\sin\Theta^- \end{bmatrix}, \end{aligned} \tag{4.71}$$

where $\Theta_t^{\pm} = \theta t \pm \hat{\varphi}_{\lambda t}$.

The amplitude of $\boldsymbol{\xi}^{app}(t)$ varies stochastically in a slow manner due to the radial process $\hat{Z}_{\lambda t}$. On the other hand, the stochastic process rotates at a dominant angular frequency θ and has a phase that varies according to the stochastic perturbation given by $\hat{\varphi}_{\lambda t}$.

We can take a further step in our analysis by obtaining the stochastic dynamics of the radial process $\hat{Z}(t)$ and phase process $\hat{\varphi}(t)$. To do this, we consider

$$\log\left(S_1(t) + i\frac{1}{\theta}S_2(t)\right) = \log\hat{Z}(t) + i\hat{\varphi}(t). \tag{4.72}$$

We then apply the Itô formula to obtain

$$d\left(\log\hat{Z} + i\hat{\varphi}\right) = \frac{d(S_1 + iS_2/\theta)}{S_1 + iS_2/\theta} - \frac{1}{2}\frac{[d(S_1 + iS_2/\theta)]^2}{(S_1 + iS_2/\theta)^2}. \tag{4.73}$$

By expanding the dS_i terms in (4.73) using (4.47) and noting that $dW_1(t)dW_2(t) = 0$, $dW_i^2(t) = dt$, and $dW_i(t)dt \to 0$ faster than $dW_i^2(t)$ as $dt \to 0$, we find that (4.73) simplifies to

$$d\left(\log\hat{Z} + i\hat{\varphi}\right) = -\frac{(S_1 + iS_2/\theta)}{S_1 + iS_2/\theta}dt + \frac{dW_1 + idW_2/\theta}{S_1 + iS_2/\theta} - \frac{(1 - 1/\theta)}{2(S_1 + iS_2/\theta)^2}\ dt. \tag{4.74}$$

We write $S_1 + iS_2/\theta = \hat{Z}e^{i\hat{\varphi}}$ and group together appropriate terms in (4.74) so that we arrive at

$$\begin{aligned} d\left(\log\hat{Z} + i\hat{\varphi}\right) = &\left(-1 - \left(\frac{\theta - 1}{2\theta}\right)\frac{\cos\hat{\varphi} + i\sin\hat{\varphi}}{\hat{Z}^2}\right)\ dt \\ &+ \frac{(dW_1 + idW_2/\theta)(\cos\hat{\varphi} + i\sin\hat{\varphi})}{\hat{Z}}. \end{aligned} \tag{4.75}$$

We now take the real part of (4.75) and apply the Itô formula to $\hat{Z(t)} = e^{\log\hat{Z}(t)}$ and obtain the SDE for $\hat{Z}(t)$, which is

$$\begin{aligned} d\hat{Z}(t) = &\left(\frac{1 - \theta}{2\theta\hat{Z}(t)}\cos\hat{\varphi}(t) - \hat{Z}(t)\right)\ dt + dW_{\hat{Z}}(t) \\ &+ \left(\frac{1}{2\hat{Z}(t)}\cos^2\hat{\varphi}(t) + \frac{1}{2\hat{Z}(t)\theta^2}\sin^2\hat{\varphi}(t)\right)\ dt. \end{aligned} \tag{4.76}$$

The imaginary part of (4.75) gives the SDE for the phase process $\hat{\varphi}(t)$, which is

$$d\hat{\varphi}(t) = \frac{1 - \theta}{2\theta\hat{Z}^2(t)}\sin\hat{\varphi}\ dt + \frac{1}{\hat{Z}(t)}\ dW_{\hat{\varphi}}(t). \tag{4.77}$$

The scalar Wiener processes $dW_{\hat{Z}}$ and $dW_{\hat{\varphi}}$ are independent of each other. As a check, we can set $\theta = 1$ and find that the radial process $\hat{Z}(t)$ in (4.76) and phase process $\hat{\varphi}(t)$ in (4.77) satisfy (4.51). In this example, we can see from (4.76) and (4.77) that the angular frequency θ, which depends on the damping rate k_0 and the parameter b_0, plays an important role in describing the stochastic dynamics of $\hat{Z}(t)$ and $\hat{\varphi}(t)$. For instance when $\theta \ll 1$, we observe that in a random time interval, the phase $\hat{\varphi}(t)$ tends to be more influenced by its drift term whenever $\hat{Z}(t)$ is small. This behaviour is not observed in the phase process described in (4.51).

4.5 Application: an avian flu model

Stochastic epidemic models have been used to capture the qualitative pattern of recurrent epidemics. Some of these stochastic models incorporate both demographic stochasticity and periodic parametric forcing [33, 37, 189]. These stochastic PPF model account for the seasonal but stochastic nature of the epidemics. In this section, we describe a stochastic model for avian flu that takes into account seasonal environmental transmission and show how our analytic tool can be applied.

4.5.1 Stochastic avian flu model with seasonal forcing

A simple stochastic avian flu model was recently developed by Wang et al. [1] and further by Mata et al. [196]. There are three stochastic processes representing the susceptible and infected host populations, and the virus concentration in the environment. In the model, the disease is assumed to be transmitted via direct contact by infected host to a susceptible individual (direct transmission) and/or via ingestion of virus particles from a contaminated aquatic habitat by a susceptible host (environmental transmission). The model reveals that the dominant outbreak period of the disease varies with environmental transmission. Motivated by this result and given that there is biological evidence supporting seasonal variation in environmental transmission, e.g. virus persistence in cold water [93, 169], we explore here the dynamics of the stochastic avian flu model in the presence of seasonal forcing. The system of SDEs for the unforced stochastic avian flu model was originally derived using a Van Kampen [9] system-size expansion [1] and has been developed alternatively using Kurtz [10] method [196]. We obtain a seasonally forced stochastic model for avian influenza by replacing the constant environmental transmission rate parameter ρ, in the unforced

system, with a time-periodic sinusoidal function (i.e. $\rho(t) = \rho_0(1+b\cos 2\pi t)$) given by

$$\begin{aligned} ds &= (-\beta si - \rho(t)sv + \mu(1-s))\,dt + \frac{1}{\sqrt{N}}\left(-G_1\ dW_1 + G_2\ dW_2 + G_3\ dW_3\right), \\ di &= (\beta si + \rho(t)sv - (\mu+\gamma)i)\,dt + \frac{1}{\sqrt{N}}\left(G_1\ dW_1 - G_3\ dW_3 - G_4\ dW_4\right), \\ dv &= (k\tau i + \delta v - \eta v)\,dt + \frac{1}{\sqrt{N_V}}\left(G_5\ dW_5 - G_6\ dW_6\right), \end{aligned} \tag{4.78}$$

where

$$\begin{aligned} &G_1 = \sqrt{\beta si + \rho(t)sv},\ G_2 = \sqrt{\mu(1-s-i)},\ G_3 = \sqrt{\mu i},\ G_4 = \sqrt{\gamma i}, \\ &G_5 = \sqrt{k\tau i + \delta v}, \quad \text{and} \quad G_6 = \sqrt{\eta v}. \end{aligned} \tag{4.79}$$

The stochastic processes $s(t), i(t)$, and $v(t)$ represent proportions of susceptible, infected, and virus populations, respectively. Infection occurs by direct transmission with a constant rate β and by environmental transmission with a time-periodic rate $\rho(t)$. The environmental transmission rate varies around a reference rate ρ_0 in a sinusoidal manner whose intensity is represented by a forcing amplitude b. Note that the variation is expressed in terms of a cosine function with one-year period. Viruses are more persistent and so are likely to be transmitted during the winter season, i.e. the beginning and end of the year. For simplicity, a host is assumed to be born and to die at the same constant rate μ. Infected individuals recover at the rate γ. The virus population in the environment increases with the shedding rate τ of infected ducks and produced from an alternate population of infected birds at a rate δ. The population of the virus decreases with the clearance rate η. The host population is also assumed to be constant with size N while the viral reference concentration is represented by a constant parameter N_V. In the model (4.78), the scaling parameter $k = N/N_V$ resulted from the derivation of the SDE, and the Wiener process $W_i(t)$ whose standard deviation is G_j. The Wiener processes are independent of each other. Note that G_1 is time-periodic since it depends on $\rho(t)$. Using equivalences among Brownian motions [48], (4.78) can be written as

$$d\mathbf{x}(t) = \mathbf{F}(\mathbf{x}(t), t)\ dt + \mathbf{DC}(\mathbf{x}(t)), t)\ d\mathbf{W}(t), \tag{4.80}$$

where $\mathbf{x}(t) = (s(t), i(t), v(t))$, $\mathbf{D} = \text{diag}\left(\frac{1}{\sqrt{N}}, \frac{1}{\sqrt{N}}, \frac{1}{\sqrt{N_V}}\right)$, $\mathbf{W}(t) \in \mathbb{R}^3$ represent independent Wiener processes,

$$\mathbf{F}(\mathbf{x}, t) = \begin{bmatrix} -\beta si - \rho(t)sv + \mu(1-s) \\ \beta si + \rho(t)sv - (\mu+\gamma)i \\ k\tau i + \delta v - \eta v \end{bmatrix}$$

and

$$\mathbf{C}(\mathbf{x}, t) = \begin{bmatrix} C_{11} & C_{12} & 0 \\ C_{21} & C_{22} & 0 \\ 0 & 0 & C_{33} \end{bmatrix}^{1/2}, \tag{4.81}$$

for $C_{11} = \beta si + \rho(t)sv + \mu(1-s)$, $\quad C_{12} = C_{21} = -\beta si - \rho(t)sv - \mu i$, $C_{22} = \beta si + \rho sv + (\mu+\gamma)i$, and $C_{33} = k\tau i + \delta v + \eta v$.

4.5.2 Deterministic dynamics

As $N, N_V \to \infty$, (4.78) gives rise to the macroscopic limit

$$\begin{aligned} \dot{\phi_1} &= -\beta\phi_1\phi_2 - \rho(t)\phi_1\psi + \mu(1-\phi_1), \\ \dot{\phi_2} &= \beta\phi_1\phi_2 + \rho(t)\phi_1\psi - (\mu+\gamma)\phi_2, \\ \dot{\psi} &= \kappa\tau\phi_2 + \delta\psi - \eta\psi. \end{aligned} \tag{4.82}$$

The avian flu SIR-V deterministic system (4.82) exhibits dynamics that is similar to an SIR model with time-dependent forcing studied by Black and McKane [191]. In the absence of forcing, i.e. $b = 0$, the avian flu system, using appropriate avian flu parameter values (Table 4.1), exhibits damped oscillations. On the other hand, when forcing is present (e.g. $b = 1$), a stable limit cycle is observed (See Figure 4.2).

The existence of the stable limit cycle generated by (4.82), induced by seasonal forcing, implies that the deterministic system (4.82) displays regular oscillations for large t. In fact, the amplitude of these oscillations increases as the intensity of forcing is increased (Figure 4.3). The frequency of the limit cycle is, in this example, equal to the forcing frequency $a = 1$.

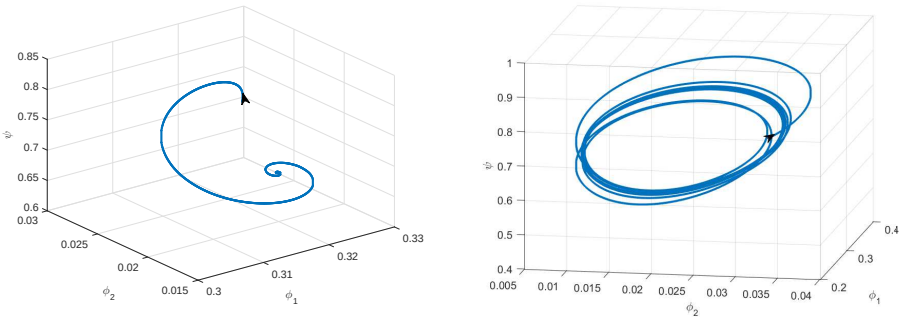

(a) (b)

Figure 4.2: Deterministic dynamics when (a) $b = 0$ and (b) $b = 1$. The initial condition is indicated by a black arrow. The initial conditions used are: $(\phi_1, \phi_2, \psi) = (0.3295, 0.0298, 0.6935)$.

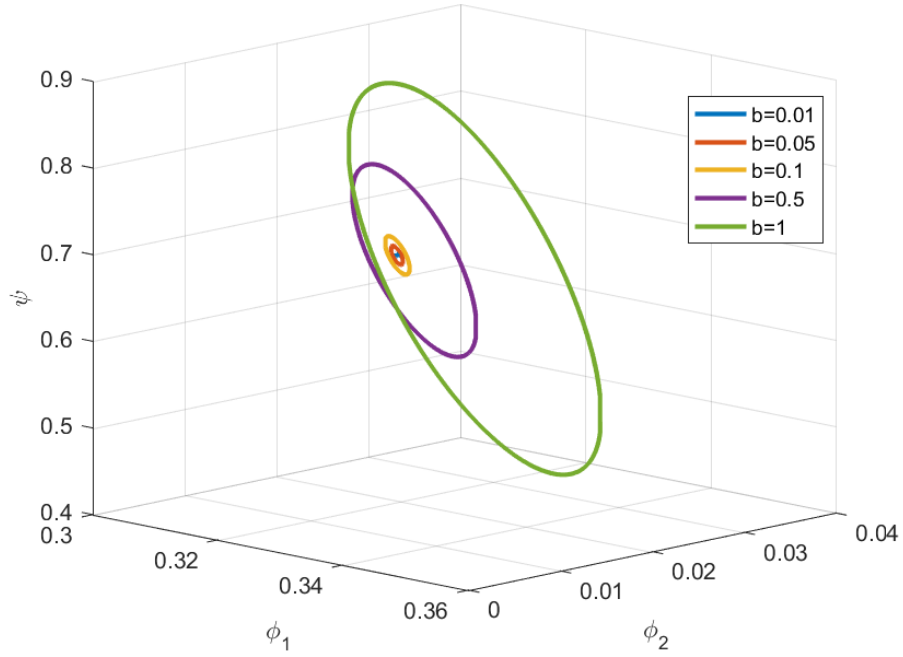

Figure 4.3: Limit cycle generated from the solution of (4.82) for different values of the forcing amplitude b.

Table 4.1: Descriptions of the parameters in the avian flu model and the values used in stochastic simulations of (4.78).

Parameter	*Value/Range*	*Description*	*Unit*
N	10^3	Duck population size	duck
N_V	10^5	Virus concentration in the environment	virion/mL
μ	0.3	Duck birth and death rate	year^{-1}
δ	0.1	Virus replication rate	year^{-1}
τ	10^4	Virus shedding rate	virion mL^{-1}/duck/year
η	3	Virus clearance rate	year^{-1}
β	15	Direct transmission rate	$\text{duck}^{-1}\text{year}^{-1}$
ρ_0	0.5	Environmental transmission rate	year^{-1}
γ	10	Duck recovery rate	year^{-1}
a	1	Forcing frequency	year^{-1}
b	1	Forcing amplitude	

4.5.3 Stochastic fluctuation around the limit cycle and its approximation

We are interested in the stochastic fluctuation around the limit cycle solution associated with the deterministic analogue of (4.78). Suppose that $(\bar{\phi_1}, \bar{\phi_2}, \bar{\psi})$ denotes the limit cycle solution of (4.78). The stochastic fluctuations around $(\bar{\phi_1}, \bar{\phi_2}, \bar{\psi})$ can be described as in Section 4.2 by the system of SDEs given by

$$d\boldsymbol{\xi}(t) = \mathbf{A}(t)\boldsymbol{\xi}(t)\ dt + \mathbf{C}(t)\ d\mathbf{W}(t), \tag{4.83}$$

where

$$\mathbf{A}(t) = \begin{bmatrix} -\beta\bar{\phi_2} - \rho(t)\bar{\psi} - \mu & -\beta\bar{\phi_1} & -\rho(t)\bar{\phi_1} \\ -\beta\bar{\phi_2} & \beta\bar{\phi_1} - \mu - \gamma & \rho(t)\bar{\phi_1} \\ 0 & \kappa\tau & \delta - \eta \end{bmatrix}, \tag{4.84}$$

and

$$\begin{aligned} \mathbf{C}(t) &= \begin{bmatrix} V_{11} & V_{12} & 0 \\ V_{21} & V_{22} & 0 \\ 0 & 0 & V_{33} \end{bmatrix}^{1/2}, \qquad \text{where} \\ V_{11} &= \beta\bar{\phi_1}\bar{\phi_2} + \rho(t)\bar{\phi_1}\bar{\psi} + \mu(1 - \bar{\phi_1}), \\ V_{12} &= V_{21} = -\beta\bar{\phi_1}\bar{\phi_2} - \rho(t)\bar{\phi_1}\bar{\psi} - \mu\bar{\phi_2}, \\ V_{22} &= \beta\bar{\phi_1}\bar{\phi_2} + \rho(t)\bar{\phi_1}\bar{\psi} + (\mu + \gamma)\bar{\phi_2}, \qquad \text{and} \\ V_{33} &= \kappa\tau\bar{\phi_2} + \delta\bar{\psi} + \eta\bar{\psi}. \end{aligned} \tag{4.85}$$

Here $\boldsymbol{\xi}$ and $\mathbf{W}$ take values in $\mathbb{R}^3$, and $\mathbf{A}, \mathbf{C}$ take values in $\mathbb{R}^{3\times 3}$. Equations (4.83)-(4.85) are obtained by linearising (4.80) around $\mathbf{x}_{LC}(t) = (\bar{\phi_1}, \bar{\phi_2}, \bar{\psi})$ using the substitution

$$\mathbf{x}(t) = \mathbf{x}_{LC}(t) + \mathbf{D}\boldsymbol{\xi}(t),$$

where $\mathbf{D} = diag\left(N^{-1/2}, N^{-1/2}, N_V^{-1/2}\right)$. Using avian flu parameter values displayed in Table 4.1, we find that the drift and diffusion matrices are periodic with period $T = 1$. We illustrate this point by plotting the values of $\mathbf{A}_{11}(t)$ and $\mathbf{C}_{11}(t)$ in Figure 4.4.

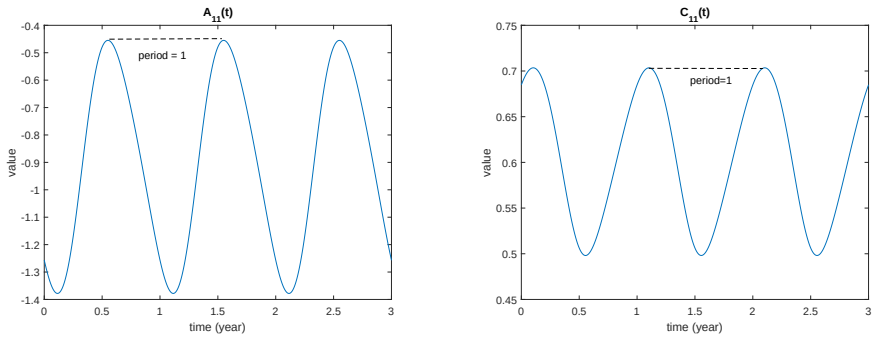

(a) (b)

Figure 4.4: Computed values of (a) $\mathbf{A}_{11}(t)$ and (b) $\mathbf{C}_{11}(t)$ in (4.83)-(4.85). The parameter values used are in Table 4.1. Each function has a periodic behaviour with period equal to 1, the period of the limit cycle and the forcing frequency.

Since $\mathbf{A}(t)$ in (4.83) is periodic for avian flu parameter values, we use Floquet theory to determine the quantities needed to confirm that (4.83) can be approximated using (4.49).

The Floquet matrix associated to the deterministic analogue of (4.83) is

$$\mathbf{B} = \begin{bmatrix} -0.0787 & -1.3454 & -0.0884 \\ 0.1208 & 0.0619 & 0.0043 \\ 2.6447 & 3.8381 & 0.2582 \end{bmatrix}. \tag{4.86}$$

We compute the ratio of the natural logarithm of the eigenvalues of the Floquet matrix $\mathbf{B}$ and the period of $\mathbf{A}(t)$ to obtain the Floquet exponents which are $-0.4967 \pm 1.3714i$ and -8.1455. These quantities imply that a deterministic perturbation in three-dimensional space damps toward a limit cycle on a plane. The subspace where the limit cycle lies is spanned by the eigenvectors of the Floquet matrix $\mathbf{B}$ corresponding to the complex eigenvalues.

Now, we observe that the ratio of the decay rate and cycle frequency is $0.4969/1.3715 = 0.3622$, which is significantly less than 1. Hence, one can use (4.49) to make an approximate description of the stochastic process $\boldsymbol{\xi}$(t) satisfying (4.83).

Though we have limited tools to obtain an explicit form of the matrix $\mathbf{Q}(t)$ in terms of avian flu parameters, it is still possible to describe the

approximate dynamics of the stochastic fluctuations $\boldsymbol{\xi}$(t) for the stochastic avian flu model with seasonal forcing. In Mata et al. [196], we know that without seasonal forcing, the stochastic fluctuation is drawn toward a plane spanned by the eigenvectors associated by the complex eigenvalues of the constant drift coefficient matrix. The fluctuations chiefly lie on this plane and its dynamics follow a cyclic path modulated by a bi-variate standard OU process. We expect the stochastic fluctuations in the seasonally forced case, i.e. (4.83), to behave in a similar manner with slight modifications. First, note that since the fluctuations are stochastic perturbations around the limit cycle, the subspace where the fluctuations will be attracted to is equivalent to a plane where the limit cycle lies. Second, the governing frequencies of the stochastic fluctuations are determined by the periodicity of $\mathbf{Q}(t)$ and the angular frequency identified using Floquet exponent (e.g. 1.3715). Finally, the amplitude of the fluctuations around the limit cycle depends on the amplitude of the entries of $\mathbf{Q}(t)$, the decay rate of the deterministic perturbation (e.g. 0.4969), and a time-averaged standard deviation. Thus, based on approximation (4.49) and the previous analysis, the stochastic population fluctuations in our avian flu system (4.78) satisfying (4.83) must be a sum of a scaled one-dimensional OU process, and a product of deterministic and a stochastic (i.e. slowly-varying bi-variate OU) processes. The deterministic processes involve the interactions of (i) periodic transformation ($\mathbf{Q}(t)$), (ii) rotation ($\mathbf{R}_{-\omega t}$), and ratio of time-averaged standard deviation ($\bar{\sigma}$) and square-root of the decay rate ($\sqrt{\lambda}$) of the deterministic perturbation.

4.6 Discussion

Stochastic models with periodic parametric forcing are seen to produce a limit cycle with noise in stochastic simulations [11, 26, 33]. We have shown that the stochastic fluctuation around the limit cycle can be approximated by a product of a scalar $\bar{\sigma}/\sqrt{\lambda}$, a periodic matrix $\mathbf{Q}(t)$, a rotation matrix $\mathbf{R}_{-\omega t}$, and a slowly varying bivariate standard Ornstein-Uhlenbeck (OU) process $\mathbf{S}_{\lambda t}$. The parameters λ, ω, and the matrix $\mathbf{Q}(t)$ arose from Floquet theory applied to the solution of the deterministic analogue of the linear SDEs with time-periodic coefficients. In particular, λ and ω are magnitudes of the real and imaginary part of the Floquet exponents while $\mathbf{Q}(t)$ depends on the forcing frequency a, which determines the periodicity of the deterministic solution. In numerical PSDs generated by a model examples, i.e., the driven harmonic oscillator model with one-dimensional noise and the

avian flu model (not shown), we see that the approximate process describes the exact process well in terms of the peak frequencies observed. The PSD outputs show that stochasticity and parametric forcing result in a process whose dominant frequency is close to the intrinsic Floquet frequency of the deterministic analogue.

Linear SDE models as in (4.17) arise from systems that incorporate parametric forcing and stochastic noise. Though in our example we only assume one forcing parameter that is time-periodic, the approximation result we derived here also applies to the case where there is more than one time-periodic forcing parameter. The resulting approximate process in such a case would have a complicated structure for the periodic matrix $\mathbf{Q}(t)$.

Our work differs from that of Baxendale and Greenwood [50] in that we consider a diffusion process described by a linear SDE system with *time-periodic* drift and diffusion coefficients. The mathematical structure of our approximate process (4.49) is very similar to the approximate process in Baxendale and Greenwood [50] but with a different interpretation of its factors. In this study, the approximate process is a perturbation process, due to stochastic noise and parametric forcing, around a stable limit cycle. In Baxendale and Greenwood [50], however, the approximate process is a perturbation process around a stable limit point. As a result, our approximate process contains frequencies that depend on the limit cycle frequency, aside from the intrinsic frequency of the deterministic analogue. Note that for both types of approximate process, the description of sustained oscillations contains a slowly varying bivariate standard OU process.

In our examples, we found that the interaction of stochasticity and parametric forcing can make hidden frequencies visible. When the intensity of forcing is high and the stochastic noise level is sufficient, the process described by (4.17) will have three main frequencies: (1) an intrinsic frequency $\omega/2\pi$, (2) the sum of the intrinsic frequency and the limit cycle frequency (e.g. $1 + \omega/2\pi$), and (3) the difference of the limit cycle frequency and the intrinsic frequency (e.g. $1 - \omega/2\pi$). According to the approximate form (4.49), we see that these frequencies all come from the product of $\mathbf{Q}(t)\mathbf{R}_{-\omega t}$, which is related to the fundamental matrix solution associated with the deterministic analogue of the stochastic PPF model.

Given the approximate description of the sustained oscillations produced by the simple stochastic PPF model, such as the driven harmonic oscillator with noise and the stochastic avian flu model with seasonal forcing, we arrive at the following conclusions. First, the prominent frequencies of the sustained oscillations in the linear stochastic PPF model can be derived from its deterministic analogue. For example, if we want to identify the dominant

frequency of the stochastic perturbations in a stochastic PPF model, we must determine the response frequency of the parametrically forced linear system (i.e. without noise).

Second, our description of the stochastically amplified frequencies enhances our understanding of processes generated by stochastic models with parametric forcing. Take, for example, the PSD of the oscillations observed from the seasonally forced stochastic SIR model of Black and McKane [191]. Note that in Black and McKane [191], it was shown by using a Van Kampen [9] system-size expansion that a process in the seasonally forced stochastic epidemic model can be expressed as the sum of the deterministic periodic solution and the stochastic fluctuation scaled by the reciprocal of the square-root of the population size. The evolution of the stochastic fluctuation is derived by linearising the model around the limit cycle solution. This results in a linear stochastic PPF model of the form (4.17). Black and McKane [191] observed that the sharp but narrow peak in their PSD corresponds to the limit cycle frequency while the broader (stochastic) peaks in the PSD are due to the stochastic amplification of the transients.

With the analysis presented here, we can now see that all of the frequencies predicted by the aforementioned stochastic peaks in the PSD arise from the deterministic aspect of the model represented by (4.18). The fundamental matrix solution of the deterministic system (4.18) has the form (4.22), which contains frequencies ω from $\mathbf{R}_{-\omega t}$ and, $2\pi/T \equiv \nu$ from $\mathbf{Q}(t)$. The smoothness condition we have for $\mathbf{Q}(t)$, as discussed in Section 4.3.2, allows us to decompose $\mathbf{Q}(t)$ into a constant matrix and some constant matrices multiplied by sinusoidal functions with frequency ν. Hence, using product-to-sum trigonometric identities, the product $\mathbf{Q}(t)\mathbf{R}_{-\omega t}$ have frequencies ω and $\nu \pm \omega$. From these general principles, we therefore expect that the product in (4.53) leads to the emergence of the central frequencies ω and $\nu \pm \omega$ observed in the PSD of $\boldsymbol{\xi}(t)$ where the largest power corresponds to frequency ω. The form of the approximate process in (4.57) also allows us to conclude that the broad peaks observed in the PSD of $\boldsymbol{\xi}(t)$ are due to the slowly varying stochastic phase perturbation process around the central frequencies, which are predicted by the deterministic aspect of the system (4.17).

Third, for a linear stochastic PPF model, the noise intensity level contributes only to the overall amplification of the system. Thus, for sufficient population size, the stochastic fluctuation may become dominant over the limit cycle. The closed form approximation may be a good tool to mathematically analyze the stochastic PPF disease model to predict the periodicity of outbreaks in the presence of stochasticity and seasonal forcing. For

stochastic epidemic modelling, the approximation can be used to compare the importance of parameters (or drivers) that contribute to fluctuation amplification or emergence of frequencies. The question on whether seasonality matters in the presence of demographic stochasticity may be further explored mathematically now that an approximate form of the fluctuation process for stochastic PPF models has been derived. The theory of Mathieu equations may enter into any further progress in the analysis of the nonlinear interactions occurring in the stochastic fluctuation.

Finally, it may be that the approximation method is limited by the unknown aspects of the fundamental matrix solution (4.22). This limitation provides motivation for modellers to develop mathematical tools to compute the fundamental matrix solutions of particular differential equation models for complex systems.

Chapter 5

Conclusions and Future Work

The main theme of this thesis is the mathematical analysis of recurrent epidemics, in general, and in avian flu in particular. From our overview of the existing literature on the epidemiology, ecology, and epidemic recurrence of avian influenza in Chapter 2, we see that the recurrent behaviour of the disease is a complex process and further investigation using models and mathematical analysis is needed. SDE models [197] are a promising tool in this study, but existing analysis has been restricted to computer simulations.

The pattern of epidemic recurrence can be described by the period between epidemics, the amplitude or intensity of epidemics, length of inter-epidemic (endemic) time interval, and the amount of variability. This thesis is focused on understanding recurrent pattern of epidemics with respect to the period and amplitude of epidemics.

Epidemic recurrence can be studied by formulating the system as a continuous-time Markov jump processes, and then by modelling the dynamics via a master equation. Unfortunately, the only way to obtain exact solutions to the master equation is by stochastic simulation. Another approach to model the stochastic dynamics is by approximating the Markov jump process by a system of SDEs either via system-size expansion [9], a well-known method in the physical literature, or equivalently via the method of Kurtz[198]. The stochastic path of the SDEs is then investigated by computing the theoretical power spectra which can be used to study how fluctuations vary with the parameter of interest. The major drawback with this approach is that it cannot fully explain the mechanisms behind observed fluctuations. Analysing how the dominant period and typical amplitudes of fluctuating epidemics vary with the parameters is computationally cumbersome.

In this thesis, we emphasise the importance of analytic tools to better understand epidemic models exhibiting recurrent behaviour as they shed light on the underlying mechanisms that were not realised before. This chapter is devoted to conclusions drawn from previous results. We broadly

summarise them in the following sections. We also discuss potential research directions for future considerations.

5.1 Factors influencing epidemic recurrence

Generally speaking, the factors influencing epidemic recurrence of avian influenza can be determined from the epidemiology and ecology of the disease. The differences in immune responses of host individuals, host interactions and movement, variations in virus strains, and variability of environmental factors all contribute to the recurrence pattern. As an example, we would expect the recurrence period to be shorter in a population with high rate of exposure to the novel avian influenza viruses, or in a population with low exposure of virus in the environment but higher movement, i.e. high contact rate [61]. The growing body of knowledge regarding the epidemiology and ecology of avian flu offers an opportunity for the formulation of new hypotheses to explain epidemic recurrence. One must be cautious in formulating the hypothesis as existing literatures pose problem in basic terminologies. For example, "outbreaks" and "epidemics" may have the same meaning since several authors seemed to be using these terms interchangeably. Apart from word usage, epidemic recurrence is a complex dynamical phenomenon that mathematical approaches are ideally suited to untangle [11].

Our theoretical approach allows us to study, within a stochastic framework, factors that are thought to influence epidemic recurrence. As our starting point, we considered the stochastic model developed by Wang et al. [1]. We chose this model because it is simple yet complex enough to mimic the overall dynamics of avian flu recurrence data, e.g. the dominant outbreak period. Using an approach different from that in Wang et al. [1], we re-derive the stochastic avian flu model and so deduce that the element of stochasticity comes from centred Poisson increments. These increments represent the uncertainty in our knowledge of various aspects of the disease. This inherent uncertainty makes a stochastic model appropriate for describing the avian flu system.

The presence of demographic stochasticity makes it difficult to identify exactly how individual factors influence epidemic recurrence. In modelling terms, this task involves determining the parameters in the model that can give rise to recurrent epidemics and finding meaningful parameter ranges that are consistent with biological data. In Chapter 3, we overcame this challenge by extending the method of Baxendale and Greenwood [50] to the

three-dimensional case. We then applied the new result to the stochastic model, and found that avian flu epidemic recurrence can be represented as a sum of two processes: (1) a scaled one-dimensional OU process and (2) a scaled rotation multiplied by a slowly-varying bi-variate standard OU process. We conclude from this formulation that the stochastic elements of avian flu recurrence act as perturbations of the phase and amplitude of the transient deterministic dynamics. The stochastic perturbations of OU processes follow a distribution that has been studied in the literature [46]. By identifying the stochasticity of avian flu as arising from an OU process, we are able to understand the role of stochasticity in modulating the pattern of epidemic recurrence for avian flu.

One factor that is identified to have a key role in driving avian flu epidemic recurrence, by previous modellers, is environmental transmission. However, our study shows that having a sufficient amount of transmission, from either direct or environmental sources, is an important ingredient for recurrence. Our analytic approach has shed light on this fact and found that when one transmission rate is weak, the other has a critical role in altering the features of epidemic recurrence, e.g. the typical amplitude and dominant period. We conclude that in a stochastic setting, either direct or indirect transmission is an important factor that influences epidemic recurrence and understanding their contributions may be necessary for the development of appropriate policies for controlling the disease.

5.2 The stochastic fluctuations around a deterministic skeleton

We defined stochastic fluctuations as the "fuzziness" around the deterministic dynamics. This description suggests that stochastic noise in this study has a passive role.

In this thesis, we considered two models of avian flu epidemic recurrence: (1) the stochastic host-pathogen model (the SIR-V model) developed by Wang et al. [1] and (2) an extension of the SIR-V model incorporating a seasonally forced environmental transmission rate. The main motivation for considering the latter model is the fact that environmental transmission has an important role in explaining multi-year periodicity in avian flu epidemics [1, 13, 165] and is well-known to show a seasonal pattern. We note here that though the second model is more complex than the first one, we can still mathematically contrast the stochastic fluctuations that they generate.

Our novel approach which is discussed in Chapter 4, shows that the pro-

cess describing stochastic fluctuations around a periodic solution induced by (seasonal) forcing can be approximated by another periodic process modulated by a standard Ornstein-Uhlenbeck process. We conclude that, for both types of stochastic fluctuations (with or without seasonal forcing), stochasticity perturbs the deterministic dynamics in a similar way. Stochastic fluctuations around an endemic equilibrium are noise-sustained oscillations whose dominant frequency is close to the intrinsic frequency of the deterministic version. On the other hand, fluctuations around a forced limit cycle are also noise-sustained oscillations but their dominant frequency is close to the intrinsic frequency of the deterministic perturbation of the limit cycle, not necessarily the intrinsic frequency of the deterministic version of the model. This point implies that the key to characterising these stochastic fluctuations is the understanding of the deterministic perturbation around the limit cycle, which gives rise to the product $\mathbf{Q}(t)\mathbf{R}_{-\omega t}$ in (4.49).

Rozhnova and Nunes [44] showed how the population size affects the full stochastic dynamics of a forced stochastic epidemic system. Since we have an approximate process that describes the stochastic fluctuation around the limit cycle, we can use the approximate process to investigate how the resonance produced by the interaction of a deterministic periodic solution and the stochastic fluctuation vary with population size. This way, we can answer the question: To what extent does population size affect the full stochastic dynamics? The answer to this question relies on the magnitude of the stochastic fluctuations which is approximately determined by the scalar factor $\bar{\sigma}/\sqrt{\lambda}$ in (4.49).

5.3 Avian flu in a stochastic and seasonally forced environment

A typical approach for analysing avian flu epidemic recurrence is by incorporating demographic stochasticity. In this formulation, we do not have to make any assumptions about the form or strength of the noise the system is subjected because the variance is defined in the formulation of the stochastic model. In this thesis, we have explored the possibility of modelling avian flu epidemic recurrence by combining stochastic and seasonal effects.

The way we include seasonal effects is by representing the environmental (virus-host) transmission rate as a time-periodic function. In this setting, the dynamics of avian flu epidemics exhibit a limit cycle (i.e. forced limit cycle) as the intensity of forcing increases. The frequency of the epidemics, however, does not change with the forcing intensity but depends on the

periodicity of the environmental transmission rate. Moreover, it has been shown previously that for a low direct transmission rate, the period of avian flu epidemics can be influenced by the environmental transmission rate that measures how frequently the virus is transmitted to the host from the environment (See Chapter 3).

Our theoretical approach describes avian flu epidemic recurrence, produced from a seasonally forced and stochastic environment, as oscillations that can be expressed as a sum of the forced limit cycle and stochastic fluctuations scaled by the square-root of the total population size. The stochastic fluctuations have a dominant frequency that largely depends on the intrinsic frequency of the deterministic perturbation of the limit cycle although other frequencies, e.g. the forcing frequency and the limit cycle frequency, are also involved in driving the fluctuations. Now in the case where the dominant frequency of the stochastic fluctuations is larger than the frequency of the deterministic dynamics, we mathematically identified possible mechanisms whereby stochastic effects could dominate over seasonal effects, based on the form of the approximate process we formulated in Chapter 4:

1. When the population size is sufficiently small. For a density-dependent process, it is know that its stochastic dynamics can be regarded as the sum of the macroscopic dynamics and the stochastic fluctuations divided by the square-root of the population size N. Therefore, if N is sufficiently small, the stochastic fluctuations term would be greater than the macroscopic term hence, will have substantial effects to the full dynamics.

2. The time-average of noise variance is sufficiently large. This point is due to the fact that the amplitude of the approximate process for stochastic fluctuations tends to increase as the time-average of the noise variance increases.

3. The decay rate of the deterministic perturbation around the periodic solution is small enough. This point is related to the form of the approximate process, which is inversely proportional to the square-root of the decay rate. The decay rate is determined by the real part of the Floquet exponent associated to the deterministic perturbation of the limit cycle.

For future work, it would be interesting to identify the components that make up the time-average noise variance and the decay rate of the deterministic perturbation. Furthermore, a detailed numerical or mathematical

study on the conclusions drawn above would be useful for validation and explore the active role of stochastic noise in the full dynamics. Our analysis could pave a way to develop new tools in quantifying the differences between effects of stochasticity and parametric forcing for other SDE models from different disciplines.

5.4 Open questions

The results and analysis presented in this thesis lead us to ask a variety of open questions left for the reader to explore. We end this thesis by presenting the following open questions:

1. Are there other biological factors that contribute to periodicity and amplitude of recurrence pattern in the avian flu system?

2. It is known that, in a stochastic setting, either direct or environmental transmission has a major influence in the dynamics of avian flu epidemics. How does this result change in the presence of other mechanism such as seasonality?

3. Given that the nature of stochastic fluctuations describing epidemic recurrence can be determined via an approximate solution, how can these results be used to understand other diseases displaying epidemic recurrence? How can we quantify the distinction between two diseases, e.g. measles and whooping cough, displaying epidemic recurrence according to the nature of their stochastic oscillations?

4. How will the results and analysis change if environmental stochasticity is involved?

5. How can we use the analytic methods here to approximately determine other features of recurrence pattern, e.g. the length of inter-epidemic time interval, amount of variability?

6. How does our mathematical results be used for fitting avian flu data displaying recurrent pattern?

This thesis has provided new tools for studying stochastic disease dynamics, or any dynamics with noise-sustained oscillations or noisy limit cycles. One can use these tools as starting point to answer the open questions above. For instance, the first three questions above can be answered by investigating the effects of other parameters and applying the methods to other

diseases, i.e. as done in Chapter 3 of this thesis. On the other hand, the general derivation of the stochastic system with parametric forcing shown in Chapter 4 may be a useful framework for model involving environmental stochasticity as mentioned in question 4. The approach for answering the last two questions are unclear at this point but we think that a careful analysis of the phase and amplitude processes of the OU process, as well as its associated curve fitting techniques, is necessary to address them.

Bibliography

[1] R H Wang, Z Jin, Q X Liu, J van de Koppel, and D Alonso. A simple stochastic model with environmental transmission explains multi-year periodicity in outbreaks of avian flu. *PloS one*, 7(2):e28873, January 2012. ISSN 1932-6203. doi: 10.1371/journal.pone.0028873. URL `http://www.pubmedcentral.nih.gov/articlerender.fcgi?artid=3281819&tool=pmcentrez&rendertype=abstracthttp://dx.plos.org/10.1371/journal.pone.0028873.g003`. → pages viii, ix, xi, 2, 3, 5, 6, 18, 22, 23, 25, 26, 27, 28, 29, 30, 35, 43, 44, 46, 47, 70, 82, 83, 113, 114, 121, 122, 123

[2] Lars Folke Olsen, Gregory L Truty, and William Morris Schaffer. Oscillations and chaos in epidemics: a nonlinear dynamic study of six childhood diseases in copenhagen, denmark. *Theoretical population biology*, 33(3):344–370, 1988. → pages ix, 2, 3

[3] S Altizer, A Dobson, P Hosseini, P Hudson, M Pascual, and P Rohani. Seasonality and the dynamics of infectious diseases, 2006. ISSN 1461023X. → pages ix, 3, 5, 19, 49

[4] Mercedes Pascual, Menno J Bouma, and Andrew P Dobson. Cholera and climate: revisiting the quantitative evidence. *Microbes and Infection*, 4(2):237–245, 2002. → pages ix, 3

[5] T Coulson, P Rohani, and M Pascual. Skeletons, noise and population growth: The end of an old debate? *Trends in Ecology and Evolution*, 19(7):359–364, 2004. ISSN 01695347. doi: 10.1016/j.tree.2004.05.008. → pages ix, 5, 6, 8

[6] A J Black and A J McKane. Stochasticity in staged models of epidemics: quantifying the dynamics of whooping cough. *Journal of the Royal Society, Interface / the Royal Society*, 7(49): 1219–27, August 2010. ISSN 1742-5662. doi: 10.1098/rsif.2009.0514. URL `http://www.pubmedcentral.nih.gov/articlerender.`

fcgi?artid=2894870&tool=pmcentrez&rendertype=abstract. → pages 1

[7] Matthew O Jackson and Leeat Yariv. Diffusion on social networks. *Economie publique/Public economics*, (16), 2006. → pages 1

[8] Noam Berger, Christian Borgs, Jennifer T Chayes, and Amin Saberi. On the spread of viruses on the internet. In *Proceedings of the sixteenth annual ACM-SIAM symposium on Discrete algorithms*, pages 301–310. Society for Industrial and Applied Mathematics, 2005. → pages 1

[9] N G Van Kampen. *Stochastic processes in physics and chemistry*, volume 11. North- Holland personal library, Amsterdam, 2nd edition, 1992. ISBN 0444893490. doi: 10.2307/2984076. URL http://books.google.com/books?hl=en&lr=&id=3e7XbMoJzmoC&pgis=1. → pages 1, 9, 50, 55, 70, 79, 81, 113

[10] T G Kurtz. Strong approximation theorems for density dependent Markov chains, 1978. ISSN 03044149. → pages 1, 9, 23, 46, 50, 52, 53, 70, 113

[11] A J Black. *The stochastic dynamics of epidemic models*. PhD thesis, 2010. → pages 2, 5, 49, 50, 55, 77, 82

[12] Wayne P London and James A Yorke. Recurrent outbreaks of measles, chickenpox and mumps i. seasonal variation in contact rates. *American journal of epidemiology*, 98(6):453–468, 1973. → pages 2, 5

[13] R Breban and J M Drake. The role of environmental transmission in recurrent avian influenza epidemics. *PLoS Computational Biology*, 5(4):e1000346, April 2009. ISSN 1553-7358. doi: 10.1371/journal.pcbi.1000346. URL http://www.pubmedcentral.nih.gov/articlerender.fcgi?artid=2660440&tool=pmcentrez&rendertype=abstracthttp://dx.plos.org/10.1371/journal.pcbi.1000346.g007. → pages 2, 21, 47, 83

[14] Chris T Bauch and David JD Earn. Transients and attractors in epidemics. *Proceedings of the Royal Society of London B: Biological Sciences*, 270(1524):1573–1578, 2003. → pages 2

[15] Petre Stoica and Randolph L Moses. *Spectral analysis of signals*, volume 452. Pearson Prentice Hall Upper Saddle River, NJ, 2005. → pages 2, 10

[16] May Anne Mata, Meghan Dutot, Leah Edelstein-Keshet, and William R Holmes. A model for intracellular actin waves explored by nonlinear local perturbation analysis. *Journal of theoretical biology*, 334:149–161, 2013. → pages 4

[17] Susanne Ditlevsen and Priscilla Greenwood. The morris–lecar neuron model embeds a leaky integrate-and-fire model. *Journal of mathematical biology*, 67(2):239–259, 2013. → pages

[18] James Dickson Murray. *Mathematical biology [electronic resource].: An introduction*. Springer, 2002. → pages

[19] James D Murray. *Mathematical Biology. II Spatial Models and Biomedical Applications {Interdisciplinary Applied Mathematics V. 18}*. Springer-Verlag New York Incorporated, 2001. → pages 4

[20] William O Kermack and Anderson G McKendrick. Contributions to the mathematical theory of epidemicsi. *Bulletin of mathematical biology*, 53(1):33–55, 1991. → pages 4

[21] Roy M Anderson, Robert M May, and B Anderson. *Infectious diseases of humans: dynamics and control*, volume 28. Wiley Online Library, 1992. → pages 5

[22] Dieter Schenzle. An age-structured model of pre-and post-vaccination measles transmission. *Mathematical Medicine and Biology*, 1(2):169–191, 1984. → pages 5, 6

[23] Herbert W Hethcote. An age-structured model for pertussis transmission. *Mathematical biosciences*, 145(2):89–136, 1997. → pages

[24] Herbert W Hethcote and P Van Den Driessche. Two sis epidemiologic models with delays. *Journal of mathematical biology*, 40(1):3–26, 2000. → pages

[25] Herbert W Hethcote and P Van den Driessche. Some epidemiological models with nonlinear incidence. *Journal of Mathematical Biology*, 29 (3):271–287, 1991. → pages 5

[26] R M Nisbet and W Gurney. *Modelling fluctuating populations*. John Wiley and Sons Limited, 1982. → pages 5, 22, 50, 77

[27] Nicholas C Grassly and Christophe Fraser. Seasonal infectious disease epidemiology. *Proceedings of the Royal Society of London B: Biological Sciences*, 273(1600):2541–2550, 2006. → pages 5

[28] MJ Keeling, Pejman Rohani, and BT Grenfell. Seasonally forced disease dynamics explored as switching between attractors. *Physica D: Nonlinear Phenomena*, 148(3-4):317–335, 2001. URL `http://www.sciencedirect.com/science/article/pii/S0167278900001871`. → pages 5, 6, 49

[29] Pejman Rohani, Matthew J Keeling, and Bryan T Grenfell. The interplay between determinism and stochasticity in childhood diseases. *The American Naturalist*, 159(5):469–481, 2002. → pages 5, 6, 7

[30] MS Bartlett. Deterministic and stochastic models for recurrent epidemics. In *Proceedings of the third Berkeley symposium on mathematical statistics and probability*, volume 4, page 109, 1956. → pages 5

[31] J P Aparicio and H G Solari. Sustained oscillations in stochastic systems. *Mathematical biosciences*, 169(1):15–25, 2001. URL `http://www.sciencedirect.com/science/article/pii/S002555640000050X`. → pages 5, 22

[32] A J McKane and T J Newman. Predator-prey cycles from resonant amplification of demographic stochasticity. *Physical review letters*, 94(21):4, January 2005. doi: 10.1103/PhysRevLett.94.218102. URL `http://arxiv.org/abs/q-bio/0501023http://prl.aps.org/abstract/PRL/v94/i21/e218102`. → pages 5, 22, 49, 53

[33] D Alonso, A J McKane, and M Pascual. Stochastic amplification in epidemics. *Journal of the Royal Society Interface*, 4(14): 575–582, June 2007. ISSN 1742-5689. doi: 10.1098/rsif.2006.0192. URL `http://www.pubmedcentral.nih.gov/articlerender.fcgi?artid=2373404&tool=pmcentrez&rendertype=abstracthttp://171.66.127.193/content/4/14/575.short`. → pages 6, 49, 50, 53, 54, 55, 70, 77

[34] A J McKane, J D Nagy, T J Newman, and M O Stefanini. Amplified biochemical oscillations in cellular systems. *Journal of Statistical Physics*, 128(1-2):165–191, 2007. ISSN 00224715. doi: 10.1007/s10955-006-9221-9. → pages 5, 22

[35] R Kuske, L F Gordillo, and P Greenwood. Sustained oscillations via coherence resonance in SIR. *Journal of Theoretical Biology*, 245(3):459–469, April 2007. ISSN 0022-5193. doi: 10.1016/j.jtbi.2006.10.029. URL `http://www.ncbi.nlm.nih.gov/pubmed/17173935http://www.sciencedirect.com/science/article/pii/S0022519306004930`. → pages 6, 22, 50

[36] Jon Greenman, Masashi Kamo, and Mike Boots. External forcing of ecological and epidemiological systems: a resonance approach. *Physica D: Nonlinear Phenomena*, 190(1):136–151, 2004. → pages 6

[37] A J Black and A J McKane. Stochastic formulation of ecological models and their applications. *Trends in ecology & evolution*, 27(6):337–345, June 2012. ISSN 0169-5347. doi: 10.1016/j.tree.2012.01.014. URL `http://www.ncbi.nlm.nih.gov/pubmed/22406194http://www.sciencedirect.com/science/article/pii/S016953471200033X`. → pages 6, 7, 50, 70

[38] Ira B Schwartz. Multiple stable recurrent outbreaks and predictability in seasonally forced nonlinear epidemic models. *Journal of mathematical biology*, 21(3):347–361, 1985. → pages 6

[39] J L Aron and I B Schwartz. Seasonality and period-doubling bifurcations in an epidemic model. *Journal of theoretical biology*, 110:665–679, 1984. ISSN 00225193. doi: 10.1016/S0022-5193(84)80150-2. → pages 7, 49

[40] Yu A Kuznetsov and C Piccardi. Bifurcation analysis of periodic seir and sir epidemic models. *Journal of mathematical biology*, 32(2):109–121, 1994. → pages

[41] David JD Earn, Pejman Rohani, Benjamin M Bolker, and Bryan T Grenfell. A simple model for complex dynamical transitions in epidemics. *Science*, 287(5453):667–670, 2000. → pages 7

[42] N Tuncer and M Martcheva. Modeling seasonality in avian influenza h5n1. pages 1–27, 2013. ISSN 02183390. doi: 10.1142/S0218339013400044. → pages 7, 19, 22

[43] Food and Agriculture Organization of the United Nations. Animal production and health division. http://www.fao.org/avianflu/en/overview.htm, 2013. → pages 7

[44] G. Rozhnova and a. Nunes. Stochastic effects in a seasonally forced epidemic model. *Physical Review E*, 82(4):041906, oct 2010. ISSN 1539-3755. doi: 10.1103/PhysRevE.82.041906. URL http://link.aps.org/doi/10.1103/PhysRevE.82.041906. → pages 7, 49, 50, 55, 84

[45] Steven H Strogatz. *Nonlinear dynamics and chaos: with applications to physics, biology, chemistry, and engineering*. Westview press, 2014. → pages 9

[46] C Gardiner. Handbook of stochastic methods for physics, chemistry and the natural sciences, 1986. → pages 9, 10, 34, 47, 62, 83

[47] P E Greenwood and L F Gordillo. Stochastic epidemic modeling. *Mathematical and Statistical Estimation Approaches in Epidemiology*, pages 1–23, 2009. URL http://link.springer.com/chapter/10.1007/978-90-481-2313-1_2. → pages 9, 46, 111

[48] E J Allen, L J Allen, A Arciniega, and P E Greenwood. Construction of Equivalent Stochastic Differential Equation Models. *Stoch. Anal. Appl.*, 26:274–297, 2008. → pages 71, 113, 116

[49] Linda JS Allen. *An introduction to stochastic processes with applications to biology*. CRC Press, 2010. → pages 9

[50] P H Baxendale and P E Greenwood. Sustained oscillations for density dependent Markov processes. *Journal of Mathematical Biology*, 63(3):433–457, September 2011. ISSN 1432-1416. doi: 10.1007/s00285-010-0376-2. URL http://www.ncbi.nlm.nih.gov/pubmed/21076832http://link.springer.com/article/10.1007/s00285-010-0376-2. → pages 9, 10, 22, 33, 50, 51, 59, 60, 61, 78, 82, 113, 115, 116

[51] G.N. Milstein. *Numerical integration of stochastic differential equations*. 1995. ISBN 9789048144877. doi: 10.1007/BF01015322. → pages 10, 50

[52] Roger Grimshaw. *Nonlinear ordinary differential equations*, volume 2. CRC Press, 1991. → pages 10, 51, 55, 57, 125

[53] Thomas G Kurtz. Lectures on stochastic analysis. *Department of Mathematics and Statistics, University of Wisconsin, Madison, WI*, pages 53706–1388, 2001. → pages 10, 52

[54] MJ Stear. Oie manual of diagnostic tests and vaccines for terrestrial animals (mammals, birds and bees) 5th edn. volumes 1 and 2. world organization for animal health 2004. isbn 92 9044 622 6. 140., 2005. → pages 12

[55] R G Webster and W J Bean. Evolution and ecology of influenza A viruses. *Microbiological Reviews*, 56(1):152–179, 1992. URL `http://mmbr.asm.org/content/56/1/152.short`. → pages 12, 13, 15, 21

[56] Ilaria Capua and Dennis J Alexander. Animal and human health implications of avian influenza infections. *Bioscience Reports*, 27(6): 359–372, 2007. → pages 12

[57] Ilaria Capua and Stefano Marangon. Control and prevention of avian influenza in an evolving scenario. *Vaccine*, 25(30):5645–5652, 2007. → pages 12

[58] Centre for Disease Control and Prevention avian influenza a (h7n9) virus. `http://www.cdc.gov/flu/avianflu/h7n9-virus.htm`, 2016. Accessed: 2016-07-07. → pages 12

[59] World Health Organization avian influenza in humans. `http://www.who.int/influenza/human_animal_interface/avian_influenza/en/`, 2016. Accessed: 2016-07-07. → pages

[60] M E E Zowalaty and S A Bustin. Avian influenza: virology, diagnos and surveillance. *Future ...*, pages 1209–1227, 2013. URL `http://www.futuremedicine.com/doi/abs/10.2217/fmb.13.81`. → pages 12

[61] M Martcheva. Avian Flu: Modeling and Implications for Control. *Journal of Biological Systems*, 22(01):151–175, March 2014. ISSN 0218-3390. doi: 10.1142/S0218339014500090. URL `http://www.worldscientific.com/doi/abs/10.1142/S0218339014500090`. → pages 12, 82

[62] Nicole M Bouvier and Peter Palese. The biology of influenza viruses. *Vaccine*, 26:D49–D53, 2008. → pages 12

[63] David E Swayne. *Avian influenza*. John Wiley & Sons, 2009. → pages 12

[64] Chang-Won Lee and Yehia M Saif. Avian influenza virus. *Comparative immunology, microbiology and infectious diseases*, 32(4):301–310, 2009. → pages 12

[65] Ron AM Fouchier, Vincent Munster, Anders Wallensten, Theo M Bestebroer, Sander Herfst, Derek Smith, Guus F Rimmelzwaan, Björn Olsen, and Albert DME Osterhaus. Characterization of a novel influenza a virus hemagglutinin subtype (h16) obtained from black-headed gulls. *Journal of virology*, 79(5):2814–2822, 2005. → pages 12, 13

[66] D J Alexander. A review of avian influenza in different bird species. *Veterinary microbiology*, 74, 2000. URL `http://www.sciencedirect.com/science/article/pii/S0378113500001607`. → pages 13, 15, 21

[67] DE Swayne and DL Suarez. Highly pathogenic avian influenza. *Revue Scientifique et Technique-office International des Epizooties*, 19 (2):463–475, 2000. → pages 13

[68] Christopher S Jennelle, Michelle Carstensen, Erik C Hildebrand, Louis Cornicelli, P Wolf, DA Grear, Hon S Ip, Kaci K Vandalen, and Larissa A Minicucci. Surveillance for highly pathogenic avian influenza virus in wild birds during outbreaks in domestic poultry, minnesota, 2015. *Emerging infectious diseases*, 22(7), 2016. → pages 13

[69] Bethany J Hoye, Vincent J Munster, Hiroshi Nishiura, Marcel Klaassen, and Ron AM Fouchier. Surveillance of wild birds for avian influenza virus. *Emerging infectious diseases*, 16(12):1827–1834, 2010. → pages 13

[70] Kennedy F Shortridge, Nan Nan Zhou, Yi Guan, Peng Gao, Toshihiro Ito, Yoshihiro Kawaoka, Shantha Kodihalli, Scott Krauss, Deborah Markwell, K Gopal Murti, et al. Characterization of avian h5n1 influenza viruses from poultry in hong kong. *Virology*, 252(2):331–342, 1998. → pages 13

[71] Erica Spackman, Dennis A Senne, Sherrill Davison, and David L Suarez. Sequence analysis of recent h7 avian influenza viruses associated with three different outbreaks in commercial poultry in the

united states. *Journal of virology*, 77(24):13399–13402, 2003. → pages 15

[72] Ruben O Donis. Evolution of h5n1 avian influenza viruses in asia. *Emerging infectious diseases*, 11(10), 2005. → pages 13

[73] M Perdue, J Crawford, M Garcia, J Latimer, and D Swayne. Occurrence and possible mechanisms of cleavage-site insertions in the avian influenza hemagglutinin gene. *Avian Diseases*, pages 182–193, 2003. → pages 13

[74] JL Heeney. Zoonotic viral diseases and the frontier of early diagnosis, control and prevention. *Journal of internal medicine*, 260(5):399–408, 2006. → pages 13

[75] Susan J Baigent and John W McCauley. Influenza type a in humans, mammals and birds: determinants of virus virulence, host-range and interspecies transmission. *Bioessays*, 25(7):657–671, 2003. → pages

[76] Rudolf Deibel, Diane E Emord, Ward Dukelow, Virginia S Hinshaw, and John M Wood. Influenza viruses and paramyxoviruses in ducks in the atlantic flyway, 1977-1983, including an h5n2 isolate related to the virulent chicken virus. *Avian Diseases*, pages 970–985, 1985. → pages 13, 19

[77] Linda Widjaja, Scott L Krauss, Richard J Webby, Tao Xie, and Robert G Webster. Matrix gene of influenza a viruses isolated from wild aquatic birds: ecology and emergence of influenza a viruses. *Journal of virology*, 78(16):8771–8779, 2004. → pages 13

[78] World Health Organization avian influenza a (h7n9) virus. `http://www.who.int/influenza/human_animal_interface/influenza_h7n9/en/`, 2016. Accessed: 2016-07-07. → pages 13

[79] VS Hinshaw, RG Webster, and RJ Rodriguez. Influenza a viruses: combinations of hemagglutinin and neuraminidase subtypes isolated from animals and other sources. *Archives of virology*, 67(3):191–201, 1981. → pages 13

[80] Dennis J Alexander. Ecology of avian influenza in domestic birds. *Emergence and control of zoonotic ortho-and paramyxovirus diseases*, pages 25–33, 2001. → pages 13

[81] WB Becker. The isolation and classification of tern virus: influenza virus a/tern/south africa/1961. *Journal of Hygiene*, 64(03):309–320, 1966. → pages 13

[82] DE Stallknecht and SM Shane. Host range of avian influenza virus in free-living birds. *Veterinary research communications*, 12(2-3):125–141, 1988. → pages 13

[83] GB Sharp, Y Kawaoka, SM Wright, B Turner, V Hinshaw, and RG Webster. Wild ducks are the reservoir for only a limited number of influenza a subtypes. *Epidemiology and Infection*, 110(01):161–176, 1993. → pages 13, 21

[84] Yoshihiro Kawaoka, Thomas M Chambers, William L Sladen, and Robert Gwebster. Is the gene pool of influenza viruses in shorebirds and gulls different from that in wild ducks? *Virology*, 163(1):247–250, 1988. → pages 13

[85] B Olsen, V J Munster, and A Wallensten. Global Patterns of Influenza a Virus in Wild Birds. *science*, 312(5772):384–388, 2006. URL `http://www.sciencemag.org/content/312/5772/384.short`. → pages 13, 21

[86] Jeong-Ki Kim, Nicholas J Negovetich, Heather L Forrest, and Robert G Webster. Ducks: the trojan horses of h5n1 influenza. *Influenza and other respiratory viruses*, 3(4):121–128, 2009. → pages 13

[87] DE Stallknecht, MT Kearney, SM Shane, and PJ Zwank. Effects of ph, temperature, and salinity on persistence of avian influenza viruses in water. *Avian diseases*, pages 412–418, 1990. → pages 14, 15

[88] David E Stallknecht, Justin D Brown, and DE Swayne. Ecology of avian influenza in wild birds. *Avian influenza*, 1:43–58, 2008. → pages 14, 15

[89] William B Karesh, Robert A Cook, Elizabeth L Bennett, and James Newcomb. Wildlife trade and global disease emergence. *Emerg Infect Dis*, 11(7):1000–1002, 2005. → pages 14

[90] Kurt D Reed, Jennifer K Meece, James S Henkel, and Sanjay K Shukla. Birds, migration and emerging zoonoses: West nile virus, lyme disease, influenza a and enteropathogens. *Clinical medicine & research*, 1(1):5–12, 2003. → pages 14

[91] HA Westbury, AJ Turner, and L Kovesdy. The pathogenicity of three australian fowl plague viruses for chickens, turkeys and ducks. *Veterinary Microbiology*, 4(3):223–234, 1979. → pages 14

[92] VS Hinshaw, RG Webster, and B Turner. The perpetuation of orthomyxoviruses and paramyxoviruses in canadian waterfowl. *Canadian Journal of Microbiology*, 26(5):622–629, 1980. → pages

[93] DE Stallknecht, SM Shane, MT Kearney, and PJ Zwank. Persistence of avian influenza viruses in water. *Avian diseases*, pages 406–411, 1990. → pages 14, 15, 70

[94] KM Sturm-Ramirez, DJ Hulse-Post, EA Govorkova, J Humberd, P Seiler, P Puthavathana, C Buranathai, TD Nguyen, A Chaisingh, HT Long, et al. Are ducks contributing to the endemicity of highly pathogenic h5n1 influenza virus in asia? *Journal of virology*, 79(17): 11269–11279, 2005. → pages 14

[95] Robert G Webster, M Yakhno, V S Hinshaw, W J Bean, and K C Murti. Intestinal influenza: replication and characterization of influenza viruses in ducks. *Virology*, 84(2):268–278, 1978. → pages 14

[96] DJ Alexander, WH Allan, DG Parsons, and G Parsons. The pathogenicity of four avian influenza viruses for fowls, turkeys and ducks. *Research in veterinary science*, 24(2):242–247, 1978. → pages 14

[97] D J Alexander, G Parsons, and R J Manvell. Experimental assessment of the pathogenicity of eight avian influenza A viruses of H5 subtype for chickens, turkeys, ducks and quail. *Avian pathology : journal of the W.V.P.A*, 15(4):647–662, 1986. ISSN 0307-9457. doi: 10.1080/03079458608436328. → pages 48

[98] O Narayan, G Lang, and BT Rouse. A new influenza a virus infection in turkeys. *Archiv für die gesamte Virusforschung*, 26(1-2):149–165, 1969. → pages

[99] HA Westbury, AJ Turner, and L Amon. Transmissibility of two avian influenza a viruses (h7 n6) between chickens. *Avian Pathology*, 10(4): 481–487, 1981. → pages 14

[100] Patrik Ellström, Neus Latorre-Margalef, Petra Griekspoor, Jonas Waldenström, Jenny Olofsson, John Wahlgren, and Björn Olsen. Sampling for low-pathogenic avian influenza a virus in wild mallard ducks:

oropharyngeal versus cloacal swabbing. *Vaccine*, 26(35):4414–4416, 2008. → pages 14

[101] Justin D Brown, David E Stallknecht, Joan R Beck, David L Suarez, and David E Swayne. Susceptibility of north american ducks and gulls to h5n1 highly pathogenic avian influenza viruses. *Emerg Infect Dis*, 12(11):1663–1670, 2006. → pages 15

[102] David E Stallknecht and Justin D Brown. Wild birds and the epidemiology of avian influenza. *Journal of wildlife diseases*, 43(3), 2007. → pages

[103] Virginia S Hinshaw, RG Webster, and B Turner. Water-borne transmission of influenza a viruses? *Intervirology*, 11(1):66–68, 1979. → pages 15

[104] Scott O Rogers, William T Starmer, and John D Castello. Recycling of pathogenic microbes through survival in ice. *Medical hypotheses*, 63 (5):773–777, 2004. → pages 15

[105] Dany Shoham. Biotic-abiotic mechanisms for long-term preservation and reemergence of influenza type a virus genes. *Progress in medical virology*, 40:178–192, 1993. → pages

[106] Alvin W Smith, Douglas E Skilling, John D Castello, and Scott O Rogers. Ice as a reservoir for pathogenic human viruses: specifically, caliciviruses, influenza viruses, and enteroviruses. *Medical Hypotheses*, 63(4):560–566, 2004. → pages

[107] Gang Zhang, Dany Shoham, David Gilichinsky, Sergei Davydov, John D Castello, and Scott O Rogers. Evidence of influenza a virus rna in siberian lake ice. *Journal of virology*, 80(24):12229–12235, 2006. → pages 15

[108] T Ito, K Okazaki, Y Kawaoka, A Takada, RG Webster, and H Kida. Perpetuation of influenza a viruses in alaskan waterfowl reservoirs. *Archives of virology*, 140(7):1163–1172, 1995. → pages 15

[109] Terrence M Tumpey, David L Suarez, Laura EL Perkins, Dennis A Senne, Jae-gil Lee, Youn-Jeong Lee, In-Pil Mo, Haan-Woo Sung, and David E Swayne. Characterization of a highly pathogenic h5n1 avian influenza a virus isolated from duck meat. *Journal of virology*, 76(12): 6344–6355, 2002. → pages 15

[110] N Kishida, Y Sakoda, N Isoda, K Matsuda, M Eto, Y Sunaga, T Umemura, and H Kida. Pathogenicity of h5 influenza viruses for ducks. *Archives of virology*, 150(7):1383–1392, 2005. → pages 15

[111] Ilaria Capua and Dennis J Alexander. Avian influenza: recent developments. *Avian Pathology*, 33(4):393–404, 2004. → pages 15

[112] Dennis J Alexander. An overview of the epidemiology of avian influenza. *Vaccine*, 25(30):5637–5644, 2007. → pages 16, 17

[113] Blanca Lupiani and Sanjay M Reddy. The history of avian influenza. *Comparative Immunology, Microbiology and Infectious Diseases*, 32 (4):311–323, 2009. → pages 15, 17

[114] RAM Fouchier, VJ Munster, et al. Epidemiology of low pathogenic avian influenza viruses in wild birds. *Revue scientifique et technique*, 28(1):49, 2009. → pages 16

[115] Ian H Brown. Summary of avian influenza activity in europe, asia, and africa, 2006-2009. *Avian diseases*, 54(s1):187–193, 2010. → pages 16

[116] Gerwin Claes, Sylvie Marché, Jeroen Dewulf, Thierry van den Berg, and Bénédicte Lambrecht. An experimental model to analyse the risk of introduction of a duck-originated h5 low-pathogenic avian influenza virus in poultry through close contact and contaminative transmission. *Epidemiology and infection*, 142(09):1836–1847, 2014. → pages 16, 17, 18

[117] World animal health information database detailed country(ies) disease incidence. `http://www.oie.int/wahis_2/public/wahid.php/Diseaseinformation/statusdetail`, 2016. Accessed: 2016-07-07. → pages 16, 17, 18

[118] Dennis J Alexander. Summary of avian influenza activity in europe, asia, africa, and australasia, 2002-2006. *Avian diseases*, 51(s1):161–166, 2007. → pages 16

[119] I Capua, S Marangon, M Dalla Pozza, C Terregino, and G Cattoli. Avian influenza in italy 1997-2001. *Avian diseases*, 47(s3):839–843, 2003. → pages 16

[120] Susan C Trock and John P Huntley. Surveillance and control of avian influenza in the new york live bird markets. *Avian diseases*, 54(s1): 340–344, 2010. → pages 16

[121] C Probst, JM Gethmann, HJ Petermann, J Neudecker, K Jacobsen, and FJ Conraths. Low pathogenic avian influenza h7n7 in domestic poultry in germany in 2011. *Veterinary Record*, pages vetrec–2012, 2012. → pages 16

[122] Laura Campitelli, Concetta Fabiani, Simona Puzelli, Alessandro Fioretti, Emanuela Foni, Alessandra De Marco, Scott Krauss, Robert G Webster, and Isabella Donatelli. H3n2 influenza viruses from domestic chickens in italy: an increasing role for chickens in the ecology of influenza? *Journal of General Virology*, 83(2):413–420, 2002. → pages 17

[123] Yi Peng, Zhi-xun Xie, Jia-bo Liu, Yao-shan Pang, Xian-wen Deng, Zhi-qin Xie, Li-ji Xie, Qing Fan, and Si-si Luo. Epidemiological surveillance of low pathogenic avian influenza virus (lpaiv) from poultry in guangxi province, southern china. *PLoS One*, 8(10):e77132, 2013. → pages 17

[124] PS Chin, E Hoffmann, R Webby, RG Webster, Y Guan, M Peiris, and KF Shortridge. Molecular evolution of h6 influenza viruses from poultry in southeastern china: prevalence of h6n1 influenza viruses possessing seven a/hong kong/156/97 (h5n1)-like genes in poultry. *Journal of virology*, 76(2):507–516, 2002. → pages 17

[125] PR Woolcock, DL Suarez, and D Kuney. Low-pathogenicity avian influenza virus (h6n2) in chickens in california, 2000-02. *Avian diseases*, 47(s3):872–881, 2003. → pages 17

[126] Saad Gharaibeh. Pathogenicity of an avian influenza virus serotype h9n2 in chickens. *Avian diseases*, 52(1):106–110, 2008. → pages 17

[127] DJ Alexander. Report on avian influenza in the eastern hemisphere during 1997–2002. 2009. → pages 17

[128] Hassan Nili and Keramat Asasi. Natural cases and an experimental study of h9n2 avian influenza in commercial broiler chickens of iran. *Avian Pathology*, 31(3):247–252, 2002. → pages 17

[129] Dennis A Senne. Avian influenza in north and south america, 2002-2005. *Avian diseases*, 51(s1):167–173, 2007. → pages 17

[130] George Fleming. *Animal plagues: their history, nature, and prevention*, volume 1. London, Chapman and Hall, 1871. → pages 17

[131] Edoardo Perroncito. *Epizoozia tifoide nei gallinacei*. 1878. → pages 17

[132] DJ Alexander and IH Brown. History of highly pathogenic avian influenza. *Revue scientifique et technique (International Office of Epizootics)*, 28(1):19–38, 2009. → pages 17

[133] WJ Bean, Y Kawaoka, JM Wood, JE Pearson, and RG Webster. Characterization of virulent and avirulent a/chicken/pennsylvania/83 influenza a viruses: potential role of defective interfering rnas in nature. *Journal of Virology*, 54(1):151–160, 1985. → pages 17

[134] T Horimoto, Eduardo Rivera, J Pearson, D Senne, S Krauss, Y Kawaoka, and RG Webster. Origin and molecular changes associated with emergence of a highly pathogenic h5n2 influenza virus in mexico. *Virology*, 213(1):223–230, 1995. → pages 17

[135] Ilaria Capua and Stefano Marangon. The avian influenza epidemic in italy, 19992000: A review. *Avian Pathology*, 29(4):289–294, 2000. → pages 17

[136] David L Suarez, Dennis A Senne, Jill Banks, Ian H Brown, Steve C Essen, Chang-Won Lee, Ruth J Manvell, Christian Mathieu-Benson, Valentina Moreno, Janice C Pedersen, et al. Recombination resulting in virulence shift in avian influenza outbreak, chile. *Emerg Infect Dis*, 10(4):693–699, 2004. → pages 17

[137] John Pasick, Katherine Handel, John Robinson, John Copps, Deidre Ridd, Kevin Hills, Helen Kehler, Colleen Cottam-Birt, James Neufeld, Yohannes Berhane, et al. Intersegmental recombination between the haemagglutinin and matrix genes was responsible for the emergence of a highly pathogenic h7n3 avian influenza virus in british columbia. *Journal of General Virology*, 86(3):727–731, 2005. → pages 17

[138] Guus Koch and Armin RW Elbers. Outdoor ranging of poultry: a major risk factor for the introduction and development of high-pathogenicity avian influenza. *NJAS-Wageningen Journal of Life Sciences*, 54(2):179–194, 2006. → pages 17

[139] Kennedy F Shortridge. Poultry and the influenza h5n1 outbreak in hong kong, 1997: abridged chronology and virus isolation. *Vaccine*, 17:S26–S29, 1999. → pages

[140] LD Sims, TM Ellis, KK Liu, K Dyrting, H Wong, M Peiris, Y Guan, and KF Shortridge. Avian influenza in hong kong 1997-2002. *Avian diseases*, 47(s3):832–838, 2003. → pages

[141] LD Sims, J Domenech, C Benigno, S Kahn, A Kamata, J Lubroth, V Martin, and P Roeder. Origin and evolution of highly pathogenic h5n1 avian influenza in asia. *Veterinary Record*, 157(6):159, 2005. → pages 17

[142] Honglin Chen, GJD Smith, SY Zhang, K Qin, J Wang, KS Li, RG Webster, JSM Peiris, and Y Guan. Avian flu: H5n1 virus outbreak in migratory waterfowl. *Nature*, 436(7048):191–192, 2005. → pages 18

[143] F Brauer, P van der Driessche, and J Wu. *Mathematical Epidemiology: Lecture Notes in Mathematics*. Springer-Verlag Berlin Heidelberg, 2008. ISBN 978-3-540-78910-9. doi: 10.1136/bmj.1.5082.1287-a. → pages 18

[144] JAP Heesterbeek. *Mathematical epidemiology of infectious diseases: model building, analysis and interpretation*, volume 5. John Wiley & Sons, 2000. → pages 18

[145] S Dorjee, Z Poljak, CW Revie, J Bridgland, B McNab, E Leger, and J Sanchez. A review of simulation modelling approaches used for the spread of zoonotic influenza viruses in animal and human populations. *Zoonoses and public health*, 60(6):383–411, 2013. → pages 18

[146] MC de Jong and TJ Hagenaars. Modelling control of avian influenza in poultry: the link with data. *Revue scientifique et technique (International Office of Epizootics)*, 28(1):371–377, 2009. → pages 18

[147] A Ssematimba. *Mechanisms of Avian Influenza virus transmission between farms: combining data collection and mathematical modelling*. Doctoral degree, Wageningen University, 2013. URL `http://www.researchgate.net/publication/235641881_Mechanisms_of_Avian_Influenza_virus_transmission_between_farms_combining_data_collection_and_mathematical_modelling/file/32bfe51238408a38d1.pdf`. → pages 18

[148] Tini Garske, Paul Clarke, and Azra C Ghani. The transmissibility of highly pathogenic avian influenza in commercial poultry in industrialised countries. *PLoS One*, 2(4):e349, 2007. → pages 18

[149] A Mannelli, N Ferre, and S Marangon. Analysis of the 1999–2000 highly pathogenic avian influenza (h7n1) epidemic in the main poultry-production area in northern italy. *Preventive veterinary medicine*, 73 (4):273–285, 2006. → pages 18

[150] Jennifer H McQuiston, Lindsey P Garber, Barbara A Porter-Spalding, John W Hahn, F William Pierson, Sherrilyn H Wainwright, Dennis A Senne, Thomas J Brignole, Bruce L Akey, and Thomas J Holt. Evaluation of risk factors for the spread of low pathogenicity h7n2 avian influenza virus among commercial poultry farms. *Journal of the American Veterinary Medical Association*, 226(5):767–772, 2005. → pages 18

[151] Kieran J Sharkey, Roger G Bowers, Kenton L Morgan, Susan E Robinson, and Robert M Christley. Epidemiological consequences of an incursion of highly pathogenic h5n1 avian influenza into the british poultry flock. *Proceedings of the Royal Society of London B: Biological Sciences*, 275(1630):19–28, 2008. → pages 18

[152] A Nishiguchi, S Kobayashi, T Yamamoto, Y Ouchi, T Sugizaki, and T Tsutsui. Risk factors for the introduction of avian influenza virus into commercial layer chicken farms during the outbreaks caused by a low-pathogenic h5n2 virus in japan in 2005. *Zoonoses and public health*, 54(9-10):337–343, 2007. → pages 18

[153] Marian EH Bos, Michiel Van Boven, Mirjam Nielen, Annemarie Bouma, Armin RW Elbers, Gonnie Nodelijk, Guus Koch, Arjan Stegeman, and Mart CM De Jong. Estimating the day of highly pathogenic avian influenza (h7n7) virus introduction into a poultry flock based on mortality data. *Veterinary research*, 38(3):493–504, 2007. → pages 18

[154] V Guberti, M Scremin, L Busani, L Bonfanti, and C Terregino. A simulation model for low-pathogenicity avian influenza viruses in dabbling ducks in europe. *Avian diseases*, 51(s1):275–278, 2007. → pages

[155] Levan Elbakidze. Modeling of avian influenza mitigation policies within the backyard segment of the poultry sector. *Journal of Agricultural and Resource Economics*, pages 195–211, 2008. → pages

[156] Shingo Iwami, Takafumi Suzuki, and Yasuhiro Takeuchi. Paradox of vaccination: is vaccination really effective against avian flu epidemics? *PLoS One*, 4(3):e4915, 2009. → pages

[157] JA Van der Goot, G Koch, MCM De Jong, and M Van Boven. Quantification of the effect of vaccination on transmission of avian influenza (h7n7) in chickens. *Proceedings of the National Academy of Sciences of the United States of America*, 102(50):18141–18146, 2005. → pages

[158] V Bavinck, A Bouma, M Van Boven, MEH Bos, E Stassen, and JA Stegeman. The role of backyard poultry flocks in the epidemic of highly pathogenic avian influenza virus (h7n7) in the netherlands in 2003. *Preventive veterinary medicine*, 88(4):247–254, 2009. → pages 18

[159] Juan Pablo Aparicio and Mercedes Pascual. Building epidemiological models from r0: an implicit treatment of transmission in networks. *Proceedings of the Royal Society of London B: Biological Sciences*, 274 (1609):505–512, 2007. → pages 18

[160] N M Ferguson, D A T Cummings, S Cauchemez, C Fraser, S Riley, A Meeyai, S Iamsirithaworn, and D S Burke. Strategies for containing an emerging influenza pandemic in Southeast Asia. *Nature*, 437(7056): 209–214, 2005. ISSN 0028-0836. doi: 10.1038/nature04017. → pages 18

[161] Timothy C Germann, Kai Kadau, Ira M Longini, and Catherine A Macken. Mitigation strategies for pandemic influenza in the united states. *Proceedings of the National Academy of Sciences*, 103(15): 5935–5940, 2006. → pages

[162] Rebecca F Grais, J Hugh Ellis, and Gregory E Glass. Assessing the impact of airline travel on the geographic spread of pandemic influenza. *European journal of epidemiology*, 18(11):1065–1072, 2003. → pages 18

[163] Shingo Iwami, Yasuhiro Takeuchi, and Xianning Liu. Avian–human influenza epidemic model. *Mathematical biosciences*, 207(1):1–25, 2007. → pages 18

[164] R Breban, J M Drake, D E Stallknecht, and P Rohani. The role of environmental transmission in recurrent avian influenza epidemics

Supporting Information. *Journal of Experimental Biology*, pages 1–9, 2009. → pages 18, 21, 50

[165] Pejman Rohani, Romulus Breban, David E Stallknecht, and John M Drake. Environmental transmission of low pathogenicity avian influenza viruses and its implications for pathogen invasion. *Proceedings of the National Academy of Sciences*, 106(25):10365–10369, 2009. → pages 18, 21, 47, 83

[166] Scott F Dowell. Seasonal variation in host susceptibility and cycles of certain infectious diseases. *Emerging infectious diseases*, 7(3):369, 2001. → pages 19

[167] JC Downie, V Hinshaw, and WG Laver. The ecology of influenza. isolation of type'a'influenza viruses from australian pelagic birds. *The Australian journal of experimental biology and medical science*, 55(6): 635, 1977. → pages

[168] Andrew W Park and Kathryn Glass. Dynamic patterns of avian and human influenza in east and southeast asia. *The Lancet infectious diseases*, 7(8):543–548, 2007. → pages 19

[169] D Causey and S V Edwards. Ecology of avian influenza virus in birds. *Journal of Infectious Diseases*, 197 Suppl:S29–S33, February 2008. ISSN 0022-1899. doi: 10.1086/524991. URL `http://www.ncbi.nlm.nih.gov/pubmed/18269325http://jid.oxfordjournals.org/content/197/Supplement_1/S29.short`. → pages 19, 70

[170] World Health Organization. Avian influenza in humans. `http://www.who.int/influenza/human_animal_interface/avian_influenza/en/`, 2015. Accessed: 2015-10-26. → pages 21

[171] S Krauss, D Walker, S P Pryor, L Niles, L Chenghong, V S Hinshaw, and R G Webster. Influenza A viruses of migrating wild aquatic birds in North America. *Vector borne and zoonotic diseases (Larchmont, N.Y.)*, 4:177–189, 2004. ISSN 1530-3667. doi: 10.1089/vbz.2004.4.177. → pages 21, 22

[172] J K Kim and N J Negovetich. Ducks: the Trojan horses of H5N1 influenza. *Influenza and other respiratory viruses*, 3(4):121–128, 2009. doi: 10.1111/j.1750-2659.2009.00084.x.

Ducks. URL http://onlinelibrary.wiley.com/doi/10.1111/j.1750-2659.2009.00084.x/full. → pages 21

[173] L Z Garamszegi and A P Møller. Prevalence of avian influenza and host ecology. *Proceedings of the Royal Society B*, 274(1621):2003–2012, August 2007. ISSN 0962-8452. doi: 10.1098/rspb.2007.0124. URL http://www.pubmedcentral.nih.gov/articlerender.fcgi?artid=2275171&tool=pmcentrez&rendertype=abstracthttp://rspb.royalsocietypublishing.org/content/274/1621/2003.short. → pages 21

[174] K A Herrick, F Huettmann, and M A Lindgren. A global model of avian influenza prediction in wild birds: the importance of northern regions. *Veterinary Research*, 44:42, 2013. URL http://www.pubmedcentral.nih.gov/articlerender.fcgi?artid=3687566&tool=pmcentrez&rendertype=abstracthttp://www.biomedcentral.com/content/pdf/1297-9716-44-42.pdf. → pages 21

[175] B Roche and C Lebarbenchon. Water-borne transmission drives avian influenza dynamics in wild birds: the case of the 20052006 epidemics in the Camargue area. *Infection, Genetics and Evolution*, 9(5):800–805, September 2009. ISSN 1567-7257. doi: 10.1016/j.meegid.2009.04.009. URL http://www.ncbi.nlm.nih.gov/pubmed/19379841http://www.sciencedirect.com/science/article/pii/S156713480900077X. → pages 21, 28, 48

[176] C F Clancy, M J A O'Callaghan, and T C Kelly. A multiscale problem arising in a model of avian flu virus in a seabird colony. *Journal of Physics: Conference Series*, 55:45–54, December 2006. ISSN 1742-6588. doi: 10.1088/1742-6596/55/1/004. URL http://stacks.iop.org/1742-6596/55/i=1/a=004?key=crossref.6679b89e39a8072315c8e403dfc665d6. → pages 21

[177] S Danø, P G Sø rensen, and F Hynne. Sustained oscillations in living cells. *Nature*, 402(6759):320–322, 1999. ISSN 0028-0836. doi: 10.1038/46329. → pages 22

[178] T Tomé and M J de Oliveira. Role of noise in population dynamics cycles. *Physical Review E*, 79(6):061128, June 2009. ISSN 1539-3755. doi: 10.1103/PhysRevE.79.

061128. URL http://link.aps.org/doi/10.1103/PhysRevE.79.061128http://pre.aps.org/abstract/PRE/v79/i6/e061128. → pages 22

[179] B Mcnamara. Theory of stochastic resonance. *Physical review A*, 39 (9), 1989. → pages 22

[180] H Gang. *Physical Review Letters*, (6). → pages

[181] M I Dykman and P V E McClintock. What can stochastic resonance do? *Nature*, 391(6665):344, 1998. ISSN 0028-0836. doi: 10.1038/34812. URL http://www.nature.com/nature/journal/v391/n6665/abs/391344a0.html. → pages 22

[182] G E Uhlenbeck and L S Ornstein. On the theory of Brownian motion. *Physical review*, 36(1905), 1930. URL http://journals.aps.org/pr/abstract/10.1103/PhysRev.36.823. → pages 22, 33, 50, 116

[183] J a van der Goot, M C M de Jong, G Koch, and M Van Boven. Comparison of the transmission characteristics of low and high pathogenicity avian influenza A virus (H5N2). *Epidemiology and infection*, 131(2):1003–1013, 2003. ISSN 09502688. doi: 10.1017/S0950268803001067. → pages 32

[184] MATLAB. *version 7.10.0 (R2010a)*. The MathWorks Inc., Natick, Massachusetts, 2010. → pages 35

[185] B Øksendal. *Stochastic differential equations*. 2003. URL http://link.springer.com/content/pdf/10.1007/978-3-642-14394-6_5.pdf. → pages 35

[186] Priscilla E Greenwood, Mark D McDonnell, and Lawrence M Ward. Dynamics of Gamma Bursts in Local Field Potentials. *Neural Computation*, pages 1–30, 2014. ISSN 0899-7667. doi: 10.1162/NECO_a_00688. URL http://dx.doi.org/10.1162/NECO{_}a{_}00688. → pages 41, 47

[187] MS Bartlett. Measles Periodicity and Community Size. *Journal of the Royal Statistical Society. Series A (. . .)*, 120(1):48–70, 1957. URL http://www.jstor.org/stable/2342553. → pages 49

[188] Robert M. May and Roy M. Anderson. Population biology of infectious diseases: Part II, 1979. ISSN 0028-0836. → pages 49

[189] RP Boland, Tobias Galla, and AJ McKane. Limit cycles, complex Floquet multipliers, and intrinsic noise. *Physical Review E*, 79(5): 15, mar 2009. URL http://arxiv.org/abs/0903.5248http://pre.aps.org/abstract/PRE/v79/i5/e051131. → pages 50, 53, 55, 56, 70

[190] Eric W. Weisstein. Mathieu function. From MathWorld—A Wolfram Web Resource, 2016. URL http://mathworld.wolfram.com/MathieuFunction.html. Last visited on 13/4/2012. → pages 51, 67

[191] AJ Black and AJ McKane. Stochastic amplification in an epidemic model with seasonal forcing. *Journal of theoretical biology*, 267(1):85–94, nov 2010. ISSN 1095-8541. doi: 10.1016/j.jtbi.2010.08.014. URL http://www.ncbi.nlm.nih.gov/pubmed/20723547http://www.sciencedirect.com/science/article/pii/S0022519310004236. → pages 54, 55, 56, 72, 79

[192] Elias M Stein and Rami Shakarchi. *Fourier analysis: an introduction*, volume 1. Princeton University Press, 2011. → pages 62

[193] Mathematica. Mathematica 8.0, 2010. → pages 67

[194] DLMF. Mathieu Functions and Hill's Equation. From NIST Digital Library of Mathematical Functions. http://dlmf.nist.gov/, Release 1.0.10 of 2015-08-07. URL http://dlmf.nist.gov/. → pages 67

[195] Milton Abramowitz, Irene A Stegun, et al. Handbook of mathematical functions. *Applied mathematics series*, 55:62, 1966. → pages 67

[196] May Anne Mata, Priscilla Greenwood, and Rebecca Tyson. The role of direct and environmental transmission in stochastic avian flu recurrence. *Paper in submission*, forthcoming. → pages 70, 77

[197] Edward Allen. *Modeling with Itô stochastic differential equations*, volume 22. Springer Science & Business Media, 2007. → pages 81

[198] T G Kurtz. Strong approximation theorems for density dependent Markov chains, 1978. ISSN 03044149. → pages 81

[199] M B Connor. A historical survey of methods of solving cubic equations. 1956. URL http://scholarship.richmond.edu/masters-theses/114/. → pages 122

Appendices

Appendices A

Supplementary materials for Chapter 3

A.1 Derivation of the avian flu SDE system

First, we define the probability of a jump or an increment $\Delta\vec{X}$ as

$$P(\Delta\vec{X} = \boldsymbol{\sigma}_{t+\Delta t} - \boldsymbol{\sigma}_t) = T(\boldsymbol{\sigma}'|\boldsymbol{\sigma})\Delta t.$$

Note that the increments of stochastic processes S_t, I_t and V_t are $\Delta S = S_{t+\Delta t} - S_t$, $\Delta I = I_{t+\Delta t} - I_t$, and $\Delta V = V_{t+\Delta t} - V_t$, respectively. Then, the expected values of the increments given the transition probabilities in Section 3.2.1 are

$$\begin{aligned} E[\Delta S] &= -\left(\beta\frac{S}{N}I + \rho S\frac{V}{N_V}\right)\Delta t + \mu(N - S - I)\Delta t + \mu I\Delta t, \\ E[\Delta I] &= \left(\beta\frac{S}{N}I + \rho S\frac{V}{N_V}\right)\Delta t - \mu I\Delta t - \gamma I\Delta t, \\ E[\Delta V] &= \tau I\Delta t + \delta V\Delta t - \eta V\Delta t. \end{aligned} \tag{A.1}$$

Now, each increment can be expressed as the expected value of the increment plus a sum of centred increments [47]. Hence, we write the increments as:

$$\begin{aligned} \Delta S &= \left(-\beta\frac{S}{N}I - \rho S\frac{V}{N_V} + \mu(N - S - I) + \mu I\right)\Delta t - \Delta Z_1 + \Delta Z_2 + \Delta Z_3, \\ \Delta I &= \left(\beta\frac{S}{N}I + \rho S\frac{V}{N_V} - \mu I - \gamma I\right)\Delta t + \Delta Z_1 - \Delta Z_3 - \Delta Z_4, \\ \Delta V &= (\tau I + \delta V - \eta V)\,\Delta t + \Delta Z_5 - \Delta Z_6. \end{aligned} \tag{A.2}$$

Here the quantities ΔZ_i are conditionally centred Poisson increments with mean zero with conditional variances that are related to the transition rates. The Poisson increment ΔZ_1 corresponding to infection of a susceptible individual has a conditional variance $\left(\beta\frac{S}{N}I + \rho S\frac{V}{N_V}\right)\Delta t$. The

increments ΔZ_2, and ΔZ_3 corresponding to births in susceptible class (or deaths in recovered and infected class) respectively have conditional variances $\mu(N-S-I)\Delta t$, and $\mu I \Delta t$. On the other hand, the Poisson increment ΔZ_4 that corresponds to recovery of an infected individual has a conditional variance equal to $\gamma I \Delta t$. Finally, the two increments corresponding to the replication and decay of viruses ΔZ_5 and ΔZ_6 must have conditional variances $(\tau I + \delta V)\,\Delta t$ and $\eta V \Delta t$, respectively. Divide (A.2) by N and N_V appropriately and take $\Delta t \to 0$ to obtain

$$\begin{aligned} dS &= \left(-\beta \frac{S}{N} I - \rho S \frac{V}{N_V} + \mu(N-S-I) + \mu I\right)\, dt - dZ_1 + dZ_2 + dZ_3, \\ dI &= \left(\beta \frac{S}{N} I + \rho S \frac{V}{N_V} - \mu I - \gamma I\right)\, dt + dZ_1 - dZ_3 - dZ_4, \\ dV &= (\tau I + \delta V - \eta V)\; dt + dZ_5 - dZ_6. \end{aligned} \tag{A.3}$$

Suppose we replace the Poisson increments in (A.2) by multiples of Wiener increments, i.e. $\Delta Z_i \to g_i \Delta W_i$, with same standard deviations as the Poisson increments they replace. By doing the same limiting process $\Delta t \to 0$, we obtain the stochastic differential equations (SDE):

$$\begin{aligned} dS &= \left(-\beta \frac{S}{N} I - \rho S \frac{V}{N_V} + \mu(N-S-I) + \mu I\right)\, dt - g_1 dW_1 + g_2 dW_2 + g_3 dW_3, \\ dI &= \left(\beta \frac{S}{N} I + \rho S \frac{V}{N_V} - \mu I - \gamma I\right)\, dt + g_1 dW_1 - g_3 dW_3 - g_4 dW_4, \\ dV &= (\tau I + \delta V - \eta V)\; dt + g_5 dW_5 - g_6 dW_6, \end{aligned} \tag{A.4}$$

where

$$\begin{aligned} g_1 &= \sqrt{\beta \frac{S}{N} I + \rho S \frac{V}{N_V}}, \qquad g_2 = \sqrt{\mu(N-S-I)}, \qquad g_3 = \sqrt{\mu I}, \\ g_4 &= \sqrt{\gamma I}, \qquad g_5 = \sqrt{\tau I + \delta V}, \qquad \text{and} \qquad g_6 = \sqrt{\eta V}. \end{aligned} \tag{A.5}$$

Furthermore, we can re-write (A.4) by expressing the host and virus populations as proportions rather than absolute numbers, i.e.

$$s = \frac{S}{N}, i = \frac{I}{N}, v = \frac{V}{N_V}, \text{and } k = \frac{N}{N_V}.$$

The corresponding SDEs for the proportions of ducks and virus are then given by (3.2).

The approximation (A.4) is an example of a result of Kurtz [10]. An alternate approach is to use a van Kampen [9] system-size expansion of the Kolmogorov (Master) equation, see e.g. in Baxendale and Greenwood [50].

A.2 Stochastic linearization

In matrix notation, (3.2) can be written as:

$$d\mathbf{x} = \mathbf{F}(\mathbf{x}(t))\ dt + \mathbf{DG}(\mathbf{x}(t))\ d\mathbf{W} \tag{A.6}$$

where $\mathbf{D} = diag(\frac{1}{\sqrt{N}}, \frac{1}{\sqrt{N}}, \frac{1}{\sqrt{N_V}})$, $d\mathbf{W}(t) = (dW_1, dW_2, dW_3, dW_4, dW_5, dW_6)^T$,

and $$\mathbf{G}(\mathbf{x}(t)) = \begin{bmatrix} -G_1 & G_2 & G_3 & 0 & 0 & 0 \\ G_1 & 0 & -G_3 & -G_4 & 0 & 0 \\ 0 & 0 & 0 & 0 & G_5 & -G_6 \end{bmatrix}.$$

Note that $\mathbf{x} = (s, i, v)$ which depends on N and N_V and $\lim_{N,N_V\to\infty} \mathbf{F}(\mathbf{x})$ is a vector whose components are the right-hand side of (3.4). It has been pointed out by Allen et al. [48] that one can construct a stochastic system, which is the same in distribution such that all matrices in the diffusion term of (A.6) are square matrices whose sizes are equal to the dimension of $\mathbf{x}$, i.e. in this case, a matrix $\mathbf{C} \in \mathbb{R}^{3\times 3}$ such that (A.6) would be equivalent in law to the stochastic system

$$d\tilde{\mathbf{x}} = \mathbf{F}(\tilde{\mathbf{x}}(t))\ dt + \mathbf{DC}(\tilde{\mathbf{x}}(t))\ d\tilde{\mathbf{W}}. \tag{A.7}$$

The Wiener processes $\tilde{\mathbf{W}} \in \mathbb{R}^{3\times 1}$ and $\mathbf{W} \in \mathbb{R}^{6\times 1}$ both have independent terms. Moreover, the stochastic processes $\tilde{\mathbf{x}}$ in (A.7) are different from the originally defined stochastic processes found in (A.6) but it can be shown that their stochastic paths are the same. Thus, $\tilde{\mathbf{x}}$ can be replaced by the $\mathbb{R}^3$-valued stochastic process $\mathbf{x}$ that is considered originally. Matrices $\mathbf{G}$ and $\mathbf{C}$ are related through the 3×3 matrix $\mathbf{V}$, where $\mathbf{V} = \mathbf{GG}^\intercal$ and $\mathbf{C} = \mathbf{V}^{1/2}$. An explicit computation of $\mathbf{V}$ confirms that it is the general form for the noise covariance matrix $\mathbf{B}$ that was described in Wang et al. [1]. In other words,

$$\mathbf{V}(\mathbf{x}, t) = \begin{bmatrix} \beta si + \rho sv + \mu(1-s) & -\beta si - \rho sv - \mu i & 0 \\ -\beta si - \rho sv - \mu i & \beta si + \rho sv + (\mu+\gamma)i & 0 \\ 0 & 0 & k\tau i + \delta v + \eta v \end{bmatrix}. \tag{A.8}$$

Letting $N, N_V \to \infty$ so that $s \to \phi_1, i \to \phi_2$, and $v \to \psi$ and $t \to \infty$ we have $\phi_1 \to \phi_1^*, \phi_2 \to \phi_2^*$, and $\psi \to \psi^*$ implies that $\lim_{N,N_V,t\to\infty} \mathbf{V} = \mathbf{B}$ which is a constant matrix whose entries are displayed as follows where $\mathbf{x_{eq}} \equiv (\phi_1 = \phi_1^*, \phi_2 = \phi_2^*, \psi = \psi^*)$, the equilibrium state of the deterministic system:

$$\begin{aligned}
\mathbf{B} &= \begin{bmatrix} B_{11} & B_{12} & 0 \\ B_{21} & B_{22} & 0 \\ 0 & 0 & B_{33} \end{bmatrix}, \qquad \text{where} \\
B_{11} &= \beta\phi_1^*\phi_2^* + \rho\phi_1^*\psi^* + \mu(1-\phi_1^*), \\
B_{12} &= B_{21} = -\beta\phi_1^*\phi_2^* - \rho\phi_1^*\psi^* - \mu\phi_2^*, \\
B_{22} &= \beta\phi_1^*\phi_2^* + \rho\phi_1^*\psi^* + (\mu+\gamma)\phi_2^*, \qquad \text{and} \\
B_{33} &= \kappa\tau\phi_2^* + \delta\psi^* + \eta\psi^*.
\end{aligned} \tag{A.9}$$

It remains to show that the set of Langevin equations obtained by Wang et al. [1] can be constructed from the linear stochastic differential equations (the tilde in (A.7) is dropped for brevity)

$$d\mathbf{x} = \mathbf{F}(\mathbf{x}(t))\ dt + \mathbf{DC}(\mathbf{x}(t))\ d\mathbf{W}. \tag{A.10}$$

Recall that the diagonal matrix $\mathbf{D}$ is given in (A.6) and $\mathbf{C} = \mathbf{V}^{1/2}$ where the entries of $\mathbf{V}$ is described in (A.8). The system (A.10) with the stochastic term generates the deterministic process (3.4), since (A.10) becomes (3.4) as $N, N_V \to \infty$ which means that this term describes the average dynamics of the processes. On the other hand, the second term is referred to as the diffusion term. It represents the variation from the average dynamics, the $\mathcal{O}(N^{-1/2})$ fluctuations of $\mathbf{x}(t)$ away from the deterministic process. The diffusion term prevents a damped system from settling to an equilibrium state.

We linearize (A.10) using the substitution $\mathbf{x}(t) = \mathbf{x_{eq}} + \mathbf{D}\boldsymbol{\xi}(t)$ and obtain

$$\mathbf{D}d\boldsymbol{\xi} = \mathbf{F}(\mathbf{x_{eq}})\ dt + \mathbf{DJ}(\mathbf{x_{eq}})\boldsymbol{\xi}\ dt + \mathbf{DC}(\mathbf{x_{eq}})\ d\mathbf{W}. \tag{A.11}$$

The Jacobian of $\mathbf{F}(\mathbf{x})$ evaluated at $\mathbf{x_{eq}}$ is denoted by $\mathbf{J}(\mathbf{x_{eq}})$. Now, $\mathbf{F}(\mathbf{x_{eq}}) = \mathbf{0}$ and so simplifies (A.11), after pre-multiplying by $\mathbf{D^{-1}}$, to

$$d\boldsymbol{\xi} = \mathbf{J}(\mathbf{x_{eq}})\boldsymbol{\xi}\ dt + \mathbf{C}(\mathbf{x_{eq}})\ d\mathbf{W}. \tag{A.12}$$

Eq. (A.12) is the Langevin (i.e. stochastic) equation in [1](See Eq.6) written in slightly different form. In particular, the two equations would be equivalent if we divide (A.12) by dt and denote $\mathbf{A} = \mathbf{J}(\mathbf{x_{eq}})$ and represent the

diffusion term as $\boldsymbol{\zeta}(t)$, i.e. Gaussian white noise with correlation function $\langle \boldsymbol{\zeta}(t), \boldsymbol{\zeta}(t')^T \rangle = \mathbf{B}\delta(t-t')$. In (3.9), we have $\mathbf{A_0} = \mathbf{J}(\mathbf{x_{eq}})$ and $\mathbf{C_0} = \mathbf{C}(\mathbf{x_{eq}})$.

A.3 Approximate solution for linear diffusion equations in three dimensions

We follow Baxendale and Greenwood [50] to derive the approximate solution for our example where the diffusion processes have values in $\mathbb{R}^3$.

Consider the stochastic system

$$d\boldsymbol{\xi} = \mathbf{A_0}\boldsymbol{\xi}\ dt + \mathbf{C_0}\ d\mathbf{W}, \qquad \boldsymbol{\xi}(t), \mathbf{W}(t) \in \mathbb{R}^3, \mathbf{A_0}, \mathbf{C_0} \in \mathbb{R}^{3\times 3}. \tag{A.13}$$

where,

$$\mathbf{A_0} = \begin{bmatrix} -\beta\phi_2^* - \rho\psi^* - \mu & -\beta\phi_1^* & -\rho\phi_1^* \\ -\beta\phi_2^* & \beta\phi_1^* - \mu - \gamma & \rho\phi_1^* \\ 0 & \kappa\tau & \delta - \eta \end{bmatrix}, \tag{A.14}$$

and

$$\mathbf{C_0} = \begin{bmatrix} \beta\phi_1^*\phi_2^* + \rho\phi_1^*\psi^* + \mu(1-\phi_1^*) & -\beta\phi_1^*\phi_2^* - \rho\phi_1^*\psi^* - \mu\phi_2^* & 0 \\ -\beta\phi_1^*\phi_2^* - \rho\phi_1^*\psi^* - \mu\phi_2^* & \beta\phi_1^*\phi_2^* + \rho\phi_1^*\psi^* + (\mu+\gamma)\phi_2^* & 0 \\ 0 & 0 & \kappa\tau\phi_2^* + \delta\psi^* + \eta\psi^* \end{bmatrix}^{1/2}. \tag{A.15}$$

Here $\mathbf{W}(t)$ contains independent Wiener processes (or Brownian motion).

Suppose that $\mathbf{A_0}$ has eigenvalues $-\zeta$ and $-\lambda \pm i\omega$ for $\zeta, \lambda, \omega \in \mathbb{R}^+$. One can find a matrix $\mathbf{Q} \in \mathbb{R}^{3\times 3}$ such that

$$\mathbf{Q}^{-1}\mathbf{A_0}\mathbf{Q} = \mathbf{\Lambda} \equiv \begin{bmatrix} -\zeta & 0 & 0 \\ 0 & -\lambda & \omega \\ 0 & -\omega & -\lambda \end{bmatrix}. \tag{A.16}$$

The matrix $\mathbf{\Lambda}$ is called the real block diagonal form of the eigenvalue matrix of $\mathbf{A_0}$ so it follows that $\mathbf{Q}$ is the real block diagonal form of the associated matrix of eigenvectors. By pre-multiplying (A.13) with $\mathbf{Q}^{-1}$ and using the substitution $\mathbf{y}(t) = \mathbf{Q}^{-1}\boldsymbol{\xi}(t)$,we have

$$d\mathbf{y} = \mathbf{\Lambda}\mathbf{y}\ dt + \mathbf{Q}^{-1}\mathbf{C_0}\ d\mathbf{W}. \tag{A.17}$$

Let $\mathbf{\Sigma} = \mathbf{Q}^{-1}\mathbf{C_0}$ and denote $\mathbf{\Sigma}_{\bullet j}$ and $\mathbf{\Sigma}_{i\bullet}$ as its jth column vector and ith row vector, respectively. With $\mathbf{y} = [y_1, y_2, y_3]^\intercal$, we write (A.17) as

$$dy_1 = -\zeta y_1\ dt + \mathbf{\Sigma}_{1\bullet}\ d\mathbf{W}, \tag{A.18a}$$

$$d\tilde{\mathbf{y}} = \tilde{\mathbf{\Lambda}}\tilde{\mathbf{y}}\ dt + \tilde{\mathbf{\Sigma}}\ d\mathbf{W}, \tag{A.18b}$$

where $\tilde{\mathbf{y}} = [y_2, y_3]^\intercal$, $\tilde{\mathbf{\Lambda}} = \begin{bmatrix} -\lambda & \omega \\ -\omega & -\lambda \end{bmatrix}$, and $\tilde{\mathbf{\Sigma}} = [\mathbf{\Sigma}_{2\bullet}, \mathbf{\Sigma}_{3\bullet}]^\intercal$.
Now, using the result of [48], we find that the SDE (A.18a) is equivalent to

$$dy_1 = -\zeta y_1 \, dt + \sigma_1 \, dW_1, \tag{A.19}$$

where $\sigma_1^2 = \mathbf{\Sigma_{1\bullet}} \mathbf{\Sigma_{1\bullet}^\intercal}$ is the variance of the stationary distribution of $y_1(t)$ and $W_1(t)$ is a one-dimensional Wiener process. It is apparent that (A.19) describes an Ornstein-Uhlenbeck process [182] in one dimension with a stationary variance $\sigma_1^2/2\zeta$. The square-root of this stationary variance corresponds to the standard deviation typically observed in the process $y_1(t)$.

On the other hand, (A.18b) is equivalent to:

$$d\tilde{\mathbf{y}} = \tilde{\mathbf{\Lambda}}\tilde{\mathbf{y}} \, dt + \tilde{\mathbf{C}} \, d\tilde{\mathbf{W}}, \tag{A.20}$$

where $\tilde{\mathbf{C}} = (\tilde{\mathbf{\Sigma}}\tilde{\mathbf{\Sigma}}^\intercal)^{1/2}$ and $\tilde{\mathbf{W}}(t)$ is a two-dimensional Wiener process. The approximate solution of (A.20) is related to a two-dimensional Ornstein-Uhlenbeck process as proven by Baxendale and Greenwood [50]. The approximation is reasonable under the assumption that $\lambda \ll \omega$. Thus, if it is assumed that $\lambda \ll \omega$ then by the theorem of Baxendale and Greenwood [50], the approximate solution for $\tilde{\mathbf{y}}$ is:

$$\tilde{\mathbf{y}} \approx \tilde{\mathbf{y}}^{\mathbf{app}} = \frac{\tilde{\sigma}}{\sqrt{\lambda}} \mathbf{R}_{-\omega t} \mathbf{S}_{\lambda t}, \tag{A.21}$$

where

$$\tilde{\sigma}^2 = \frac{1}{2} Tr(\tilde{\mathbf{C}}\tilde{\mathbf{C}}^\intercal). \tag{A.22}$$

Thus,

$$\begin{aligned} \boldsymbol{\xi} \approx \boldsymbol{\xi}^{app} \equiv \mathbf{Q}\mathbf{y}^{app} &= y_1 \mathbf{Q_{\bullet 1}} + y_2^{app} \mathbf{Q_{\bullet 2}} + y_3^{app} \mathbf{Q_{\bullet 3}} \\ &= y_1 \mathbf{Q_{\bullet 1}} + [\mathbf{Q_{\bullet 2}}, \mathbf{Q_{\bullet 3}}] \tilde{\mathbf{y}}^{\mathbf{app}}. \end{aligned} \tag{A.23}$$

More precisely,

$$\boldsymbol{\xi}^{app}(t) = y_1(t) \mathbf{Q_{\bullet 1}} + \frac{\tilde{\sigma}}{\sqrt{\lambda}} [\mathbf{Q_{\bullet 2}}, \mathbf{Q_{\bullet 3}}] \mathbf{R}_{-\omega t} \mathbf{S}_{\lambda t}. \tag{A.24}$$

Now, we know that in polar coordinates

$$\mathbf{R}_{-\omega t} \mathbf{S}_{\lambda t} = \begin{bmatrix} \cos \omega t & \sin \omega t \\ -\sin \omega t & \cos \omega t \end{bmatrix} \begin{bmatrix} S_1(\lambda t) \\ S_2(\lambda t) \end{bmatrix} = \begin{bmatrix} S_1(\lambda t) \cos \omega t + S_2(\lambda t) \sin \omega t \\ -S_1(\lambda t) \sin \omega t + S_2(\lambda t) \cos \omega t \end{bmatrix}. \tag{A.25}$$

Using the formula $x\cos\theta + y\sin\theta = z\cos(\theta - \varphi)$ where $z = |x+iy|$ and $\varphi = \arg(x+iy)$ for $x, y \in \mathbb{R}$ and $i = \sqrt{-1}$, we then write $S_1(\lambda t) = z(\lambda t)\cos\varphi(\lambda t)$ and $S_2(\lambda t) = z(\lambda t)\sin\varphi(\lambda t)$ with $z(\lambda t) = \sqrt{S_1^2 + S_2^2} \equiv |\mathbf{S}(\lambda t)|$ and $\varphi(\lambda t) = \tan^{-1}(S_2/S_1)$ to obtain

$$\mathbf{R}_{-\omega t}\mathbf{S}_{\lambda t} = z(\lambda t)\begin{bmatrix}\cos\left(\varphi(\lambda t) - \omega t\right)\\ \sin\left(\varphi(\lambda t) - \omega t\right)\end{bmatrix} \equiv |\mathbf{S}(\lambda t)|\begin{bmatrix}\cos\left(\varphi_{\lambda t} - \omega t\right)\\ \sin\left(\varphi_{\lambda t} - \omega t\right)\end{bmatrix}. \quad \text{(A.26)}$$

Applying (A.26) to the second term of (A.24) yields

$$\begin{bmatrix}\xi_1^{app}(t)\\ \xi_2^{app}(t)\\ \xi_3^{app}(t)\end{bmatrix} = y_1(t)\begin{bmatrix}q_{11}\\ q_{21}\\ q_{31}\end{bmatrix} + \frac{\tilde{\sigma}}{\sqrt{\lambda}}|\mathbf{S}(\lambda t)|\begin{bmatrix}q_{12}\cos\left(\varphi_{\lambda t} - \omega t\right) + q_{13}\sin\left(\varphi_{\lambda t} - \omega t\right)\\ q_{22}\cos\left(\varphi_{\lambda t} - \omega t\right) + q_{23}\sin\left(\varphi_{\lambda t} - \omega t\right)\\ q_{32}\cos\left(\varphi_{\lambda t} - \omega t\right) + q_{33}\sin\left(\varphi_{\lambda t} - \omega t\right)\end{bmatrix}, \quad \text{(A.27)}$$

where $\mathbf{Q} = [q_{ij}]$.

We define $q_{i2} = r_i\cos\theta_i$ and $q_{i3} = r_i\sin\theta_i$ where $r_i = \sqrt{q_{i2}^2 + q_{i3}^2}$ and $\theta_i = \tan^{-1}(q_{13}/q_{12})$ so that the approximate fluctuation of each component takes the form:

$$\xi_i^{app}(t) = q_{i1}y_1(t) + \frac{\tilde{\sigma}}{\sqrt{\lambda}}|\mathbf{S}(\lambda t)|r_i\cos(\varphi_{\lambda t} - \omega t - \theta_i). \quad \text{(A.28)}$$

The polar form of the approximation reveals that each model component fluctuates according to a combination of a univariate and bi-variate OU processes. The first term of the approximation contains a one-dimensional OU process weighted by a scalar determined from the transformation matrix $\mathbf{Q}$ while the second term contains the two-dimensional OU process that varies slowly and λt is a quantity that influences the radius and phase of the circular path. The stationary variance of $\xi_i^{app}(t)$ is the sum of the stationary variance of each term in (A.28). This means that the long-term variance of a fluctuation is

$$\frac{q_{i1}^2\sigma_1^2}{2\zeta} + r_i^2\frac{\tilde{\sigma}^2}{\lambda} \quad \text{(A.29)}$$

Hence, the typical magnitude of $\xi_i^{app}(t)$, i.e. stationary standard deviation, is

$$SSD_i = \sqrt{\frac{q_{i1}^2\sigma_1^2}{2\zeta} + r_i^2\frac{\tilde{\sigma}^2}{\lambda}}. \quad \text{(A.30)}$$

Note that the fluctuation of each component i has a constant phase shift θ_i, which is useful in computing phase differences between disease components.

A.4 Additional insight from the approximation on the interaction of disease components

In Section 3.4.1, we showed that for the given set of avian flu parameter values, the system exhibits noise-sustained oscillations which can be viewed as a sum of two processes given by (3.25): (i) a process proportional to the one-dimensional OU process and (ii) a process proportional to the product of a rotation matrix and a standard OU process.

We describe here, using (3.13), the behaviour of the sample path in three-dimensional space. The first term of (3.13) means that sample path behaves as an Ornstein-Uhlenbeck process $y_1(t)$ that travels along the axis that points to the direction of $\mathbf{Q}_{\bullet\mathbf{1}}$, i.e. the eigenvector associated to $-\zeta$. In addition, the second term of (3.13) implies that the sample path cycles on the subspace spanned by the last two column vectors of the transformation matrix $\mathbf{Q}$, i.e. eigenvectors of the eigenvalues $-\lambda \pm i\omega$. This subspace contains a plane whose equation (see (A.35) in Appendix A.5 for general formulation), for our chosen set of parameters, is given by:

$$\xi_S - 19.376\xi_I + 0.5814\xi_V = 0. \tag{A.31}$$

Figure A.1 shows the plane (A.31) and a realization of the stochastic simulation of (3.25). In Figure A.1(a), we observe that the sample path lies chiefly on or near the plane (A.31). However, if we neglect the first term of (3.25), the dynamics of the fluctuations lie entirely on this plane (see Figure A.1(b)). Thus, the portion of the sample path that departs from the plane is clearly due to the one-dimensional OU process whereas the second term constrains the sample path to move within the plane.

From (3.25), we know that the stationary standard deviation of $y_1(t)$ is 1.63 which is small compared to the constant $\tilde{\sigma}/\sqrt{\lambda} = 10.21$ that appears in the second term of the equation. Therefore, we can neglect the first term of (3.25) and show that avian flu epidemics cycle on the plane (A.31). This can be achieved mathematically when the magnitude of the real eigenvalue ζ is larger than λ, which means that the approximate process approaches the hyperplane in fast manner.

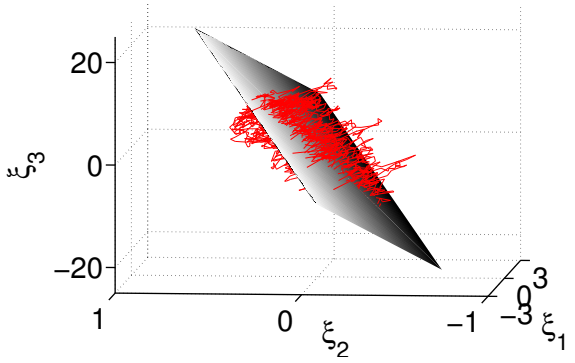

(a)

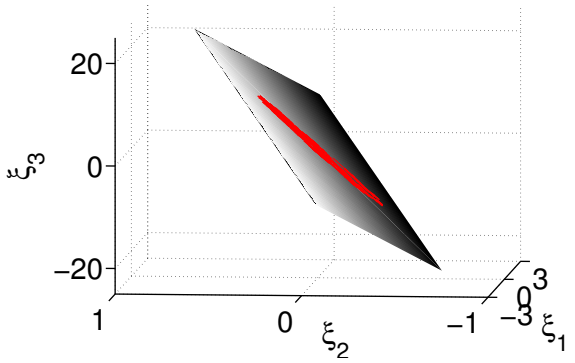

(b)

Figure A.1: (Colour online) A sample path of the approximate fluctuations given by (3.25) when the first term is (a) not set to zero and (b) set to zero. The grey region is the plane (A.31) that lies in the subspace spanned by the eigenvectors of $-0.3091 \pm 0.8377i$.

In Figure A.2, we compute the magnitude ζ over combinations of β and ρ values and found that the epidemic cycles occur primarily in the hyperplane when β is below 100 and ρ is high, i.e. where ζ is larger than λ.

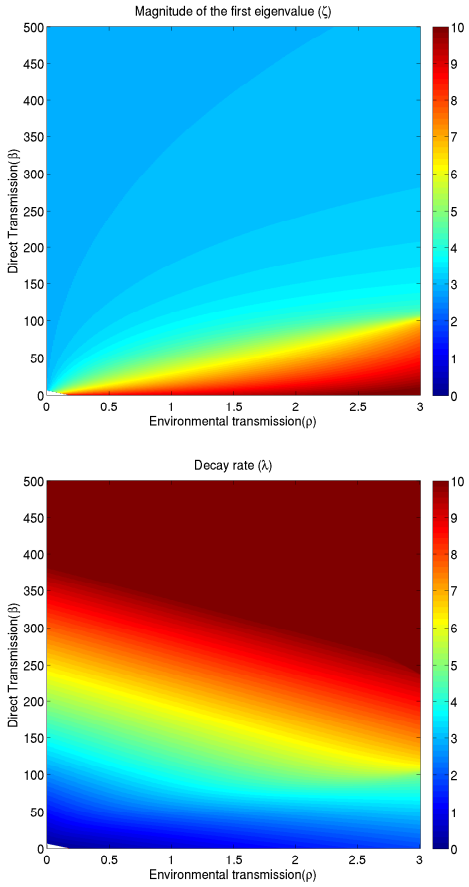

Figure A.2: (Colour online) Plot of ζ (left panel) and λ (right panel) as functions of β and ρ. The white region is where $R_0 < 1$, i.e. noise-sustained oscillations cannot be observed here. Default parameter values are in Table 3.1.

The fact that avian flu dynamics could primarily occur in the plane suggest that under certain conditions for each transmission route, one can project the avian flu system (3.9) onto the plane (A.31) and so simplify the analysis. For instance, using the equation of the plane, we can write one component in terms of the other and convert the three-dimensional linear avian flu SDE system (3.9) into a two-dimensional one. The possibility of modelling recurrent avian flu epidemics as stochastic system in two dimensions must therefore be explored.

A.5 The subspace where the cycling takes place

For the case when the stationary standard deviation (s.s.d.) of the second term is very large compared to the s.s.d. of the first term in our approximation, the first term of (A.24) is negligible and we expect the stochastic path to primarily lie in a plane, i.e. a subspace of $\mathbb{R}^3$, spanned by the last two column vectors of $\mathbf{Q}$ ($\mathbf{Q_{\bullet 2}}$ and $\mathbf{Q_{\bullet 3}}$). Here we show a general way for computing the equation of this plane.
The sample path defined by the fluctuations $\xi_i(t)$ is centred at $(0,0,0)$ and so the equation of the plane should take the form:

$$a_1\xi_1 + a_2\xi_2 + a_3\xi_3 = 0 \tag{A.32}$$

We know that the vectors $\mathbf{Q_{\bullet 2}}$ and $\mathbf{Q_{\bullet 3}}$ span the plane, hence must satisfy (A.32).Therefore,

$$[a_1, a_2, a_3] \cdot [\mathbf{Q_{\bullet 2}}, \mathbf{Q_{\bullet 3}}] = \mathbf{0}. \tag{A.33}$$

By Gaussian elimination or by manipulating the explicit form of the linear system, we can eliminate a_3 in (A.33) and a little algebra turns (A.33) into a simpler equation,

$$\det(\mathbf{M_1})a_1 + \det(\mathbf{M_2})a_2 = 0 \qquad \text{where} \qquad \mathbf{M_1} = \begin{bmatrix} q_{12} & q_{13} \\ q_{32} & q_{33} \end{bmatrix} \text{ and } \mathbf{M_2} = \begin{bmatrix} q_{22} & q_{23} \\ q_{32} & q_{33} \end{bmatrix}. \tag{A.34}$$

Now we require $\det(\mathbf{M_2}) \neq 0$ so that $a_2 = -\dfrac{\det(\mathbf{M_1})}{\det(\mathbf{M_2})}a_1$, which gives $a_3 = \dfrac{a_1}{q_{32}}\left(\dfrac{\det(\mathbf{M_1})}{\det(\mathbf{M_2})}q_{22} - q_{12}\right)$. Therefore, assuming that $a_1 \neq 0$, the desired equation of the plane is

$$\xi_1 - \frac{\det(\mathbf{M_1})}{\det(\mathbf{M_2})}\xi_2 + \frac{1}{q_{32}}\left(\frac{\det(\mathbf{M_1})}{\det(\mathbf{M_2})}q_{22} - q_{12}\right)\xi_3 = 0. \tag{A.35}$$

A.6 Derivation of the explicit form of the mean-field eigenvalues

Our starting point is the Jacobian evaluated at the stable endemic equilibrium point [1], i.e.,

$$\mathbf{J}(\mathbf{x_{eq}}) = \begin{bmatrix} -\beta\phi_2^* - \rho\psi^* - \mu & -\beta\phi_1^* & -\rho\phi_1^* \\ -\beta\phi_2^* & \beta\phi_1^* - \mu - \gamma & \rho\phi_1^* \\ 0 & \kappa\tau & \delta - \eta \end{bmatrix}, \tag{A.36}$$

where $\phi_1^* = \dfrac{1}{\mathcal{R}_0}$, $\phi_2^* = \dfrac{\mu}{\mu+\gamma}\left(1-\dfrac{1}{\mathcal{R}_0}\right)$, and $\psi^* = \dfrac{\kappa\mu\tau}{(\eta-\delta)(\mu+\gamma)}\left(1-\dfrac{1}{\mathcal{R}_0}\right)$ for the basic reproduction number

$$\mathcal{R}_0 = \frac{\beta}{\mu+\gamma} + \frac{\kappa\rho\tau}{(\eta-\delta)(\mu+\gamma)}.$$

The condition $\mathcal{R}_0 > 1$ must be satisfied for the non-trivial steady-state $\mathbf{x_{eq}} = (\phi_1^*, \phi_2^*, \psi^*)$ to exist.

The eigenvalues of $\mathbf{J}(\mathbf{x_{eq}})$ determine the local dynamics of the deterministic SIR-V system close to the non-trivial equilibrium point $\mathbf{x_{eq}}$. Now, denote the eigenvalues of $\mathbf{J}(\mathbf{x_{eq}})$ as ν. It follows that $|\mathbf{J}(\mathbf{x_e q}) - \nu I| = 0$ gives rise to a cubic polynomial of the form

$$\nu^3 - a\nu^2 - b\nu - c = 0, \tag{A.37}$$

where:

$$\begin{aligned} a &= (\delta-\eta) - \mu\mathcal{R}_0 - \gamma - \mu + \beta/\mathcal{R}_0 \\ b &= -\mu(\eta-\delta+\gamma+\mu)\mathcal{R}_0 + \mu\beta/\mathcal{R}_0 \\ c &= -\mu(\eta-\delta)(\gamma+\mu)(\mathcal{R}_0-1). \end{aligned} \tag{A.38}$$

Equations (A.37) and (A.38) in fact appeared in the Appendix section of [1], where it was proven that the endemic equilibrium is stable. Now, substitute $\nu = y + \dfrac{a}{3}$ to yield the normal form transformation,

$$y^3 + py + q = 0 \qquad \text{where} \qquad p = \frac{1}{3}(-a^2 - 3b) \text{ and } q = \frac{1}{27}(-2a^3 - 9ab - 27c). \tag{A.39}$$

This method is also known as Vieta's subsitution [199]. Equation (A.39) has been well-studied and has known solutions in general form:

$$\begin{aligned} y_1 &= Y_+ + Y_-, \\ y_2 &= -\frac{1}{2}(Y_+ + Y_-) + i\frac{\sqrt{3}}{2}(Y_+ - Y_-), \\ y_3 &= -\frac{1}{2}(Y_+ + Y_-) - i\frac{\sqrt{3}}{2}(Y_+ - Y_-), \end{aligned} \tag{A.40}$$

where: $Y_\pm = \left(-\dfrac{q}{2} \pm \sqrt{\dfrac{q^2}{4} + \dfrac{p^3}{27}}\right)^{1/3}$ and $i = \sqrt{-1}$.

We are interested in the case when all three roots exist with two of them being complex conjugates. This is satisfied by assuming that $\dfrac{q^2}{4} + \dfrac{p^3}{27} > 0$.

By back substitution, the solutions of (A.37) are:

$$\begin{aligned}
\nu_1 &= Y_+ + Y_- + \frac{a}{3}, \\
\nu_2 &= -\frac{1}{2}(Y_+ + Y_-) + \frac{a}{3} + i\frac{\sqrt{3}}{2}(Y_+ - Y_-), \\
\nu_3 &= -\frac{1}{2}(Y_+ + Y_-) + \frac{a}{3} - i\frac{\sqrt{3}}{2}(Y_+ - Y_-).
\end{aligned} \tag{A.41}$$

The eigenvalues ν_2 and ν_3 are conjugate pairs whose real part is negative as confirmed by Wang et al. [1]. The magnitude of the real and imaginary part corresponds to the decay rate λ and the intrinsic frequency ω, respectively, of the deterministic system linearized at the endemic equilibrium state. Therefore,

$$\begin{aligned}
\lambda &= \left| -\frac{1}{2}(Y_+ + Y_-) + \frac{a}{3} \right|, \\
\omega &= \left| \frac{\sqrt{3}}{2}(Y_+ - Y_-) \right|.
\end{aligned} \tag{A.42}$$

Using avian flu parameters in Table 3.1, we can write λ and ω in terms of β and ρ, as follows:

$$\begin{aligned}
\lambda(\rho,\beta) \approx \Big| &- 2.9 - 0.0172\beta - 0.5945\rho + \frac{\beta}{0.5172\beta + 17.84\rho} \\
&- 0.5\left(\sqrt[3]{\mathsf{F}(\rho,\beta) + \mathsf{G}(\rho\beta)} + \sqrt[3]{\mathsf{F}(\rho,\beta) - \mathsf{G}(\rho,\beta)} \right) \Big|,
\end{aligned} \tag{A.43}$$

$$\omega(\rho,\beta) \approx \frac{\sqrt{3}}{2} \Big| - \sqrt[3]{\mathsf{F}(\rho,\beta) + \mathsf{G}(\rho,\beta)} + \sqrt[3]{\mathsf{F}(\rho,\beta) - \mathsf{G}(\rho,\beta)} \Big|, \tag{A.44}$$

where

$$\begin{aligned}
\mathsf{F}(\rho,\beta) &= \frac{-0.5P_1(\rho,\beta)}{(0.1724\beta + 5.945\rho)^3}, \\
\mathsf{G}(\rho,\beta) &= 0.56\sqrt{\frac{81P_1(\rho,\beta)^2}{(0.1724\beta + 5.945\rho)^6} + \frac{12P_2(\rho,\beta)^3}{(0.1724\beta + 5.945\rho)^6}}, \\
P_1(\rho,\beta) &= \sum_{i=0}^{6}\sum_{j=0}^{6} \mathsf{M}_{i+1,j+1}\beta^i\rho^j, \\
P_2(\rho,\beta) &= \sum_{i=0}^{6}\sum_{j=0}^{6} \mathsf{N}_{i+1,j+1}\beta^i\rho^j.
\end{aligned} \tag{A.45}$$

Here

$$\mathsf{M} = \begin{bmatrix} 0 & 0 & 0 & 9190 & 3152 & -646 & 88.3 \\ 0 & 0 & 236 & 311 & -119 & 15.4 & 0 \\ 0 & 1.39 & 13.5 & -8.33 & 1.11 & 0 & 0 \\ -0.008 & 0.306 & -0.284 & 0.043 & 0 & 0 & 0 \\ 0.003 & -0.005 & 0.001 & 0 & 0 & 0 & 0 \\ 0 & 0 & 0 & 0 & 0 & 0 & 0 \\ 0 & 0 & 0 & 0 & 0 & 0 & 0 \end{bmatrix} \tag{A.46}$$

and

$$\mathsf{N} = \begin{bmatrix} 0 & 0 & -892 & 183 & -37.5 & 0 & 0 \\ 0 & -19 & 23 & -4.35 & 0 & 0 & 0 \\ -0.135 & 0.871 & -0.189 & 0 & 0 & 0 & 0 \\ 0.01 & -0.004 & 0 & 0 & 0 & 0 & 0 \\ 0 & 0 & 0 & 0 & 0 & 0 & 0 \\ 0 & 0 & 0 & 0 & 0 & 0 & 0 \\ 0 & 0 & 0 & 0 & 0 & 0 & 0 \end{bmatrix}. \tag{A.47}$$

Additionally, the first eigenvalue $\nu_1 < 0$ (eigenvalue with largest negative real part) and so the decay rate of the OU process $y_1(t)$ in (3.13) is $\zeta = |\nu_1|$.

Appendices B

Supplementary materials for Chapter 4

B.1 Floquet Theory

We present here the formal statement of the theory preceded by definitions of essential terminologies [52]. One can refer to the notes of Dr. Michael J. Ward for examples and detailed discussion of the theory (see `http://www.emba.uvm.edu/~jxyang/teaching/Floquet_theory_Ward.pdf`).

Definition B.1 (Principal fundamental matrix)**.** Let $\boldsymbol{x}^1(t), ..., \boldsymbol{x}^n(t)$ be n linearly independent solutions of

$$\dot{\mathbf{x}}(t) = \mathbf{A}(t)\mathbf{x}(t). \tag{B.1}$$

The $n \times n$ matrix $\mathbf{X}(t) = \left[\boldsymbol{x}^1(t) \cdots \boldsymbol{x}^n(t)\right]$ is a fundamental matrix solution of (B.1) if $\dot{\mathbf{X}} = \mathbf{A}\mathbf{X}$ for a given $\mathbf{X}(t_0)$. Moreover, if $\mathbf{X}(t_0) = I$ then $\mathbf{X}(t) \equiv \mathbf{X}_0$ is the principal fundamental matrix.

Definition B.2 (Floquet multipliers and exponents)**.** For $t \in [0, T]$, define $\mathbf{B} = \mathbf{X}^{-1}(0)\mathbf{X}(T)$, e.g. $\mathbf{B} = \mathbf{X}_0(T)$. The eigenvalues $\rho_1, \ldots, \rho_n$ of $\mathbf{B}$ are called the Floquet multipliers of $\dot{\mathbf{X}}(t) = \mathbf{A}(t)\mathbf{X}(t)$ or equivalently, of (B.1). The Floquet exponents are $\mu_1, \ldots, \mu_n$ satisfying $\rho_j = e^{\mu_j T}$. Note that $\rho_j, \mu_j \in \mathbb{C}$.

Theorem B.3 (Floquet theory)**.** *Let ρ be a Floquet multiplier for* (B.1) *and let μ be the corresponding Floquet exponent so that $\rho = e^{\mu T}$. Then there exists a solution $\boldsymbol{x}(t)$ of* (B.1) *such that $\boldsymbol{x}(t + T) = \rho\boldsymbol{x}(t)$ for all t. Further, there exists an n-dimensional T-periodic function $\boldsymbol{p}(t)$ such that $\boldsymbol{x}(t) = e^{\mu t}\boldsymbol{p}(t)$.*

Analogous to the interpretation of the eigenvalues in continuous- or discrete-time systems with $\mathbf{A}(t) = \mathbf{A}_0$ a constant matrix, the long-time behaviour of the solutions to (B.1) can be predicted using both the Floquet exponents μ_j and multipliers ρ_j. Below we enumerate the possible solution behaviours:

1. If $Re(\mu_j) < 0$, or equivalently $|\rho_j| < 1$, for all j, then $\mathbf{x}(t) \to 0$ as $t \to \infty$.
2. If $Re(\mu_j) > 0$, or equivalently $|\rho_j| > 1$, for some j, then $\mathbf{x}(t) \to \infty$ as $t \to \infty$.
3. If $Re(\mu_j) = 0$, or equivalently $|\rho_j| = 1$, for some j, then we have a pseudo-periodic solution.

In application, Floquet exponents are used to describe the growth rate of various perturbations over a cycle on the average

Corollary B.4 (Lyapunov transformation)**.** *Under the transformation* $\boldsymbol{x}(t) = P(t)\boldsymbol{y}(t)$*, which is invertible and periodic, the periodic system given by* (B.1) *yields a time-invariant system.*

B.2 Itô formula for multi-dimensional process

Theorem B.5. *Suppose a multi-dimensional process* $\boldsymbol{X}$ *satisfies*

$$d\boldsymbol{X} = \boldsymbol{u}\ dt + V d\boldsymbol{W},$$

where $\boldsymbol{X} \in \mathbb{R}^n, \boldsymbol{u} \in \mathbb{R}^n, V \in \mathbb{R}^{n\times n}, \boldsymbol{W} \in \mathbb{R}^n$*. Let* $\boldsymbol{Y}(t) = (g_1(t, \boldsymbol{X}(t)), \ldots, g_p(t, \boldsymbol{X})(t))$*. Then the process* $\boldsymbol{Y}(t)$ *satisfies*

$$dY_k(t) = \frac{\partial g_k}{\partial t}(t, \boldsymbol{X})\ dt + \sum_i \frac{\partial g_k}{\partial x_i}(t, \boldsymbol{X})\ dX_i + \frac{1}{2}\sum_{i,j} \frac{\partial^2 g_k}{\partial x_i \partial x_j}(t, \boldsymbol{X})\ d\langle X_i, X_j\rangle,$$

where $\langle X_i, X_j\rangle$ *denotes the bracket process. When the SDEs* $d\boldsymbol{X} = \boldsymbol{u}\ dt + V d\boldsymbol{W}$ *is linear in* $\boldsymbol{X}$*, the last term in the Itô formula above vanishes since* $\dfrac{\partial^2 g_k}{\partial x_i \partial x_j} = 0$*.*